

Article

Optimization of a benzoylpiperidine class identifies a highly potent and selective reversible monoacylglycerol lipase (MAGL) inhibitor

Carlotta Granchi, Margherita Lapillo, Sandra Glasmacher, Giulia Bononi, Cristina Licari, Giulio Poli, Maguie el Boustani, Isabella Caligiuri, Flavio Rizzolio, Jürg Gertsch, Marco Macchia, Filippo Minutolo, Tiziano Tuccinardi, and Andrea Chicca

J. Med. Chem., **Just Accepted Manuscript** • DOI: 10.1021/acs.jmedchem.8b01483 • Publication Date (Web): 04 Feb 2019

Downloaded from <http://pubs.acs.org> on February 5, 2019

Just Accepted

“Just Accepted” manuscripts have been peer-reviewed and accepted for publication. They are posted online prior to technical editing, formatting for publication and author proofing. The American Chemical Society provides “Just Accepted” as a service to the research community to expedite the dissemination of scientific material as soon as possible after acceptance. “Just Accepted” manuscripts appear in full in PDF format accompanied by an HTML abstract. “Just Accepted” manuscripts have been fully peer reviewed, but should not be considered the official version of record. They are citable by the Digital Object Identifier (DOI®). “Just Accepted” is an optional service offered to authors. Therefore, the “Just Accepted” Web site may not include all articles that will be published in the journal. After a manuscript is technically edited and formatted, it will be removed from the “Just Accepted” Web site and published as an ASAP article. Note that technical editing may introduce minor changes to the manuscript text and/or graphics which could affect content, and all legal disclaimers and ethical guidelines that apply to the journal pertain. ACS cannot be held responsible for errors or consequences arising from the use of information contained in these “Just Accepted” manuscripts.

1
2
3
4
5
6
7
8
9
10
11
12
13
14
15
16
17
18
19
20
21
22
23
24
25
26
27
28
29
30
31
32
33
34
35
36
37
38
39
40
41
42
43
44
45
46
47
48
49
50
51
52
53
54
55
56
57
58
59
60

Optimization of a benzoylpiperidine class identifies a highly potent and selective reversible monoacylglycerol lipase (MAGL) inhibitor

Carlotta Granchi^a, Margherita Lapillo^a, Sandra Glasmacher^b, Giulia Bononi^a, Cristina Licari^a, Giulio Poli^a, Maguie el Boustani^{c,d}, Isabella Caligiuri^c, Flavio Rizzolio^{c,e}, Jürg Gertsch^b, Marco Macchia^a, Filippo Minutolo^a, Tiziano Tuccinardi^{a,}, Andrea Chicca^b*

^a Department of Pharmacy, University of Pisa, Via Bonanno 6, 56126 Pisa, Italy.

^b Institute of Biochemistry and Molecular Medicine, NCCR TransCure, University of Bern, CH-3012 Bern, Switzerland.

^c Pathology Unit, Department of Molecular Biology and Translational Research, National Cancer Institute and Center for Molecular Biomedicine, 33081 Aviano (PN), Italy.

^d Doctoral School in Molecular Biomedicine, University of Trieste, 34100 Trieste, Italy.

^e Department of Molecular Sciences and Nanosystems, Ca' Foscari University, 30123 Venezia, Italy.

* Corresponding author.

E-mail address: tiziano.tuccinardi@unipi.it

ABSTRACT

Monoacylglycerol lipase (MAGL) is the enzyme degrading the endocannabinoid 2-arachidonoylglycerol and it is involved in several physiological and pathological processes. The therapeutic potential of MAGL is linked to several diseases, including cancer. The development of MAGL inhibitors has been greatly limited by the side effects associated with the prolonged MAGL

1
2
3 inactivation. Importantly, it could be preferable to use reversible MAGL inhibitors *in vivo*, but
4
5 nowadays only few reversible compounds have been developed. In the present study, structural
6
7 optimization of a previously developed class of MAGL inhibitors led to the identification of
8
9 compound **23**, which proved to be a very potent reversible MAGL inhibitor ($IC_{50} = 80$ nM), selective
10
11 for MAGL over the other main components of the endocannabinoid system, endowed of a promising
12
13 antiproliferative activity in a series of cancer cell lines and able to block MAGL both in cell-based as
14
15 well as *in vivo* assays.
16
17
18
19
20
21
22

23 INTRODUCTION

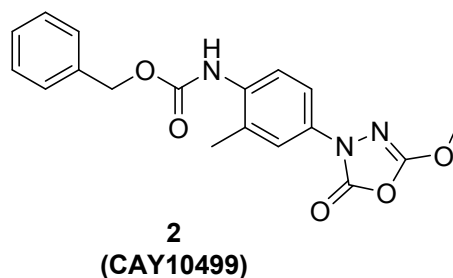
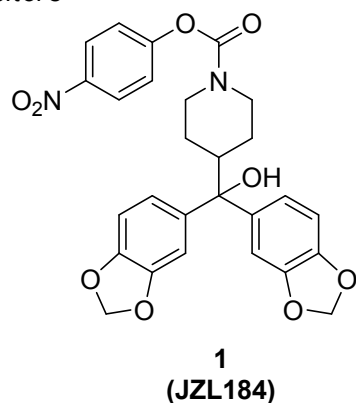
24
25
26 The endocannabinoids system (ECS) is an endogenous system involved in many physiological and
27
28 pathological processes. ECS is composed of two seven-transmembrane G protein-coupled receptors
29
30 named cannabinoid receptors type 1 and type 2 (CB1, CB2),^{1,2} a class of lipid signaling molecules
31
32 called endocannabinoids (eCBs) and several biosynthetic and degrading enzymes that are involved
33
34 in the production and transformation of these molecules. CB1 receptors are mainly expressed in the
35
36 brain where they regulate the release of neurotransmitters from pre-synaptic neurons, whereas CB2
37
38 receptors are principally expressed in immune cells. Anandamide (AEA) and 2-arachidonoylglycerol
39
40 (2-AG) are the two most abundant and well-studied eCBs,³ which are biosynthesized on-demand
41
42 from phospholipid precursors in the plasma membrane and released into the extracellular milieu.⁴
43
44 After activating cannabinoid receptors, eCBs are transported into the cytoplasm via facilitated
45
46 diffusion mediated by a putative endocannabinoid membrane transporter^{5,6} and degraded by specific
47
48 enzymes. AEA is hydrolyzed by fatty acid amide hydrolase (FAAH) in arachidonic acid and
49
50 ethanolamine, whereas 2-AG is hydrolyzed into arachidonic acid and glycerol by monoacylglycerol
51
52 lipase (MAGL) and α/β hydrolase-6 and -12 (ABHD6 and ABHD12). MAGL is the main degrading
53
54 enzyme for 2-AG and it is responsible for approximately 85% of 2-AG hydrolysis in the brain, with
55
56 a minor contribution of ABHD6 and ABHD12.^{7,8} Several studies indicate the therapeutic potential of
57
58
59
60

1
2
3 selective FAAH and MAGL inhibitors in several disease models of inflammation, pain, anxiety and
4 other neuroinflammatory diseases.^{9–16} The inhibition of eCBs degradation represents a promising
5 pharmacological strategy to activate the ECS limiting the potential side effects associated with direct
6
7
8
9
10 receptor agonists.^{7,17,18}

11
12 Many MAGL inhibitors were published¹⁹ and patented²⁰ and some representative compounds are
13 reported in Figure 1; however, most MAGL inhibitors reported to date in the literature are
14 characterized by an irreversible binding mode. The irreversible mechanism of action shown by these
15 inhibitors hampered their subsequent clinical development, since chronic administration of
16 irreversible inhibitors, as well as genetic deletion of MAGL, provokes many negative effects *in vivo*.
17
18
19
20
21
22
23 However, there are some recent noteworthy examples of irreversible inhibitors, endowed with a good
24 pharmacokinetic profile and highly effective in reducing inflammation *in vivo*.^{21,22} In some
25 experimental studies reported in literature, sustained inactivation of MAGL by irreversible inhibition
26 led to a loss of the therapeutic effects and a cross-tolerance to CB1 agonists in mice, accompanied by
27
28
29
30
31
32
33 physical dependence. Moreover, prolonged MAGL inhibition provokes marked changes in some
34 brain regions, such as CB1 receptor downregulation and desensitization, together with a reduction of
35 the endocannabinoid-mediated synaptic plasticity. These effects are due to chronic MAGL
36
37
38
39
40
41
42
43
44
45
46
47
48
49
50
51
52
53
54
55
56
57
58
59
60
60 inactivation in the central nervous system, provoking the maintenance of elevated 2-AG levels, which
continuously activate and thus desensitize CB1 receptors in the brain, since this enzyme has a great
impact on the brain ECS.²³ These just mentioned effects were observed *in vivo* by administration of
irreversible inhibitors such as compound **1** (JZL184, 4-nitrophenyl-4-[bis(1,3-benzodioxol-5-
yl)(hydroxy)methyl]piperidine-1-carboxylate, Figure 1), which is a very potent carbamate-based
MAGL inhibitor.²⁴ Moreover, compound **2** (CAY10499, benzyl(4-(5-methoxy-2-oxo-1,3,4-
oxadiazol-3(2*H*)-yl)-2-methylphenyl)carbamate, Figure 1) is a widely known irreversible MAGL
inhibitor, used in many experimental studies concerning MAGL inhibition.²⁵ Despite the variety of
irreversible MAGL inhibitors, at present their use is mainly limited as experimental tools in many
studies. To the best of our knowledge, only a few reversible MAGL inhibitors are known and some

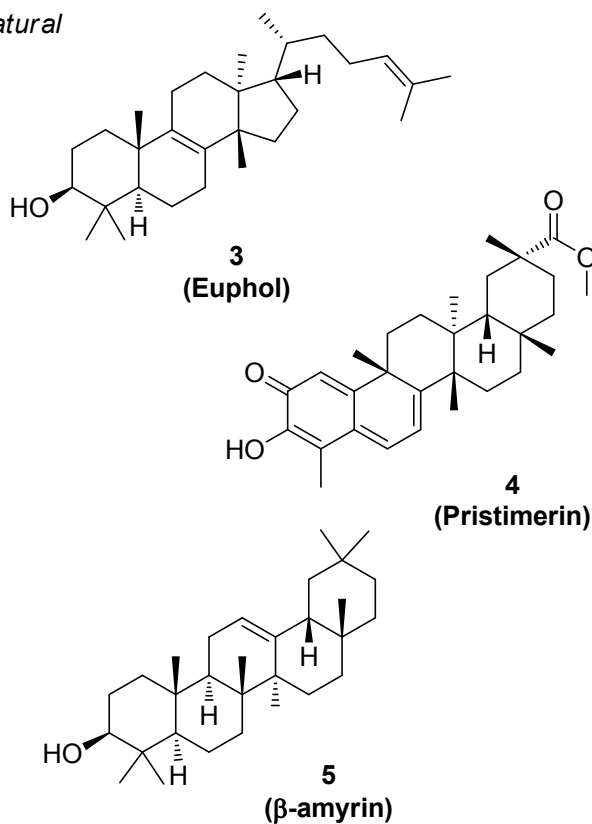
1
2
3 examples are reported in Figure 1. For example, natural terpenoids Euphol (compound **3**, Figure 1)
4
5 and Pristimerin (compound **4**, Figure 1) were found to be potent MAGL inhibitors *in vitro* (IC₅₀ values
6
7 in the nanomolar range), although they were not selective, acting also on other targets different from
8
9 MAGL.^{26–28} Natural triterpenoid β-amyrin **5** (Figure 1) is a MAGL inhibitor structurally related to,
10
11 although less potent than, Pristimerin and Euphol, but it also inhibits other enzymes that hydrolyse 2-
12
13 AG, such as ABHDs.²⁹ In 2014, benzo[*d*][1,3]dioxol-5-ylmethyl 6-phenylhexanoate **6** (Figure 1) was
14
15 reported by Hernández-Torres *et al.* as a potent, reversible and selective MAGL inhibitor. This
16
17 compound was able to alleviate the clinical progression and the symptoms of a multiple sclerosis
18
19 mouse model, without inducing catalepsy or other motor impairments, which were instead previously
20
21 observed after the administration of irreversible MAGL inhibitors.³⁰ More recent examples of
22
23 reversible MAGL inhibitors include derivative **7** (JZP-361, Figure 1), a nanomolar MAGL inhibitor
24
25 that was characterized by a dual action, since it showed an anti-histaminergic activity, due to its high
26
27 structural similarity to Loratadine, a histamine H₁ receptor antagonist.³¹ Very recently, reversible
28
29 MAGL inhibitor 1,5-diphenylpyrazole-3-carboxamide **8** (Figure 1) was reported to exert
30
31 antiproliferative effects in cancer cell lines and to relieve the neuropathic hypersensitivity induced *in*
32
33 *vivo* by oxaliplatin.³² Moreover, compound **9** (Figure 2) is a benzoylpiperidine-based reversible
34
35 MAGL inhibitor developed by our group in 2016 and it has been used as the starting point for the
36
37 chemical optimization of the class of compounds reported in this paper.
38
39
40
41
42
43
44
45
46
47
48
49
50
51
52
53
54
55
56
57
58
59
60

Irreversible inhibitors



Reversible inhibitors

Natural



Synthetic

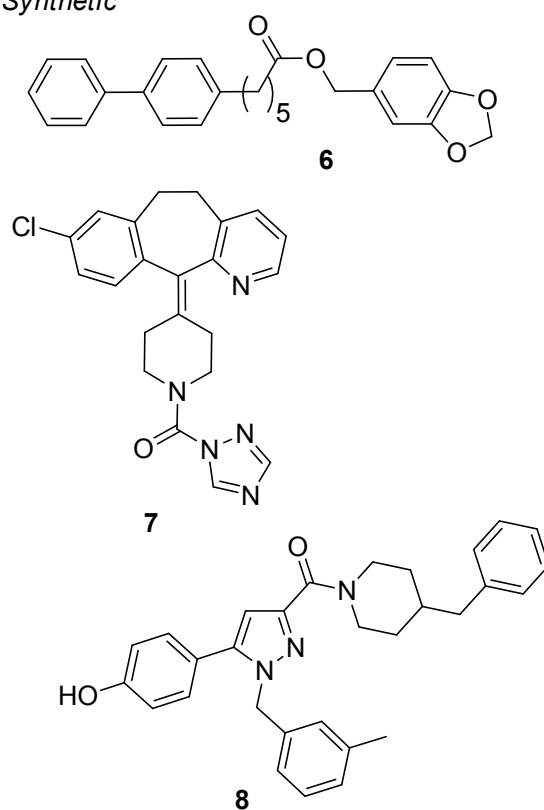


Figure 1. Structures of some of the most important known MAGL inhibitors.

RESULTS AND DISCUSSION

Design. In 2016, our group published the discovery of a chemical class of reversible MAGL inhibitors, based on a benzoylpiperidine scaffold, and within this class compound **9** (Figure 2) was

1
2
3 identified as the most potent inhibitor, showing an IC_{50} value of 0.84 μ M, thus representing one of
4
5 the first example of potent and selective reversible MAGL inhibitor.³³ The significant improvement
6
7 of the inhibitory potency of this compound with respect to the other synthesized compounds is
8
9 supposed to be due to a strategic hydrogen bond network established between the *meta*-hydroxyl
10
11 group on the amidic phenyl ring of compound **9**, which replaces a structural water molecule observed
12
13 in many MAGL X-ray structures, and a couple of active site residues (E53 and H272). Starting from
14
15 this consideration, we were intrigued by the possibility to increase the acidity of the phenolic hydroxyl
16
17 group of compound **9**, in order to strengthen the established hydrogen bonds and thus potentially lead
18
19 to an increase in the inhibitory activity. At the same time, we took into account that this part of the
20
21 molecule is located into a small pocket of the protein, where some polar residues are present, as
22
23 suggested by modeling studies. Therefore, the insertion of bulky groups in the amidic phenyl ring is
24
25 discouraged in order to avoid steric clashes and maintain the same binding disposition observed for
26
27 compound **9**. On these bases, we started to modify compound **9** by adding halogen atoms (iodine,
28
29 bromine, chlorine and fluorine atoms) in all the possible substitution positions of the amidic phenyl
30
31 ring, due to their electron withdrawing properties and at the same time their different dimensions
32
33 (Figure 2, panel A). This modification gave rise to compounds **10a-d**, **11a-d**, **12a-d** and **13a-d** (Figure
34
35 2, panel B) where iodine, bromine, chlorine and fluorine were inserted in the two possible *ortho*
36
37 positions, in the *meta* or in the *para* positions with respect the phenolic hydroxyl group, still
38
39 maintaining the 4-chlorobenzoylpiperidine portion on the other side of the molecule fixed. Regarding
40
41 this last portion of compound **9**, molecular modeling studies suggested that the benzoyl moiety is
42
43 directed toward the open cavity of the protein, pointing at the lipophilic channel of the enzyme (Figure
44
45 2, panel A). This consideration was confirmed by the good inhibition activity shown by a previously
46
47 obtained analogue of **9**, where the *p*-Cl atom in the benzoyl ring was replaced by a second phenyl
48
49 ring, which showed a 2-fold increase of inhibitory activity.³³ As an additional structural investigation,
50
51 in the present work we have explored the possibility to fill the wide open enzymatic cavity, where the
52
53 benzoyl part of compound **9** is located, with suitable groups. This purpose was achieved by removing
54
55
56
57
58
59
60

1
2
3 the chlorine atom from the benzoyl moiety (compound **14**, Figure 2, panel B) or replacing it with
4
5 alkyl groups of different dimensions, such as methyl, ethyl, *n*-propyl, *i*-propyl or *n*-butyl (compounds
6
7 **15-19**, Figure 2, panel B). Then, in order to verify whether this region preferentially hosts lipophilic
8
9 groups, the *p*-Cl-phenyl was also replaced by more polar fragments, such as a phenolic ring, a
10
11 benzodioxane and a 4-phenyl-morpholine moiety (compounds **20-22**, Figure 2, panel B).

12
13
14 Finally, we investigated the combinations of chemical modifications on both sides of the scaffold,
15
16 such as: 1) the presence of a fluorine atom in *para* position to the phenolic hydroxyl group or to the
17
18 amide carbonyl moiety, as in compounds **11d** and **13d**, respectively; 2) the presence of a *i*-propyl or
19
20 *n*-butyl chain on the benzoyl ring, as in compounds **18** and **19**, respectively. The resulting compounds
21
22 **23-26** (Figure 3) maintained the same central benzoylpiperidine scaffold and derived from the
23
24 combination of different substituents in the two terminal portions of the parent compound **9** and they
25
26 were synthesized accordingly.
27
28
29
30
31
32
33
34
35
36
37
38
39
40
41
42
43
44
45
46
47
48
49
50
51
52
53
54
55
56
57
58
59
60

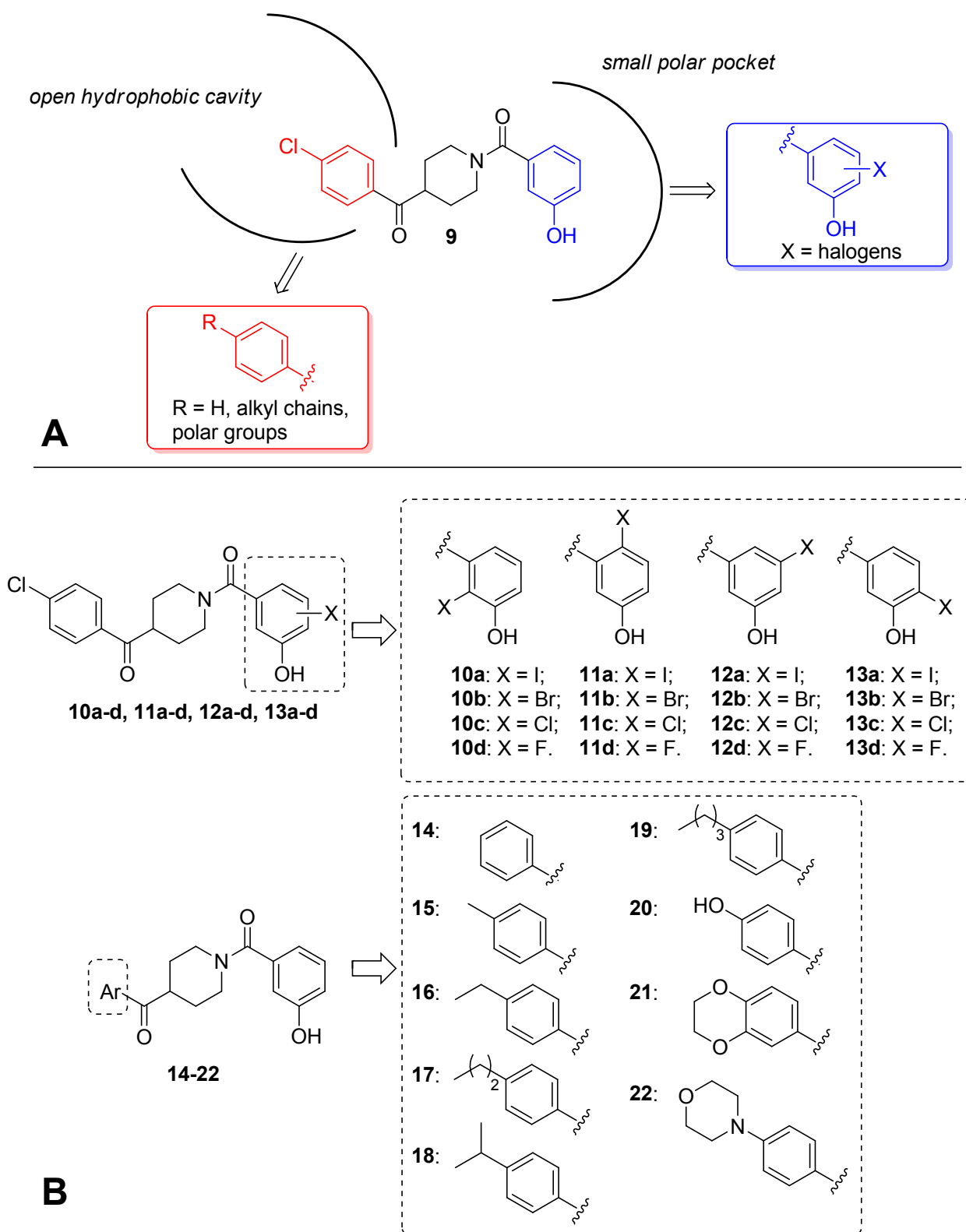


Figure 2. Design of new benzoylpiperidine derivatives. Upper panel (A): previously published starting compound **9** and its schematic location in the MAGL binding site: planned modifications of

the benzoyl part (in red) and the amidic moiety (in blue). Lower panel (B): newly synthesized compounds, modified in the amidic (**10a-d**, **11a-d**, **12a-d**, **13a-d**) and in the benzoyl (**14-22**) portions.

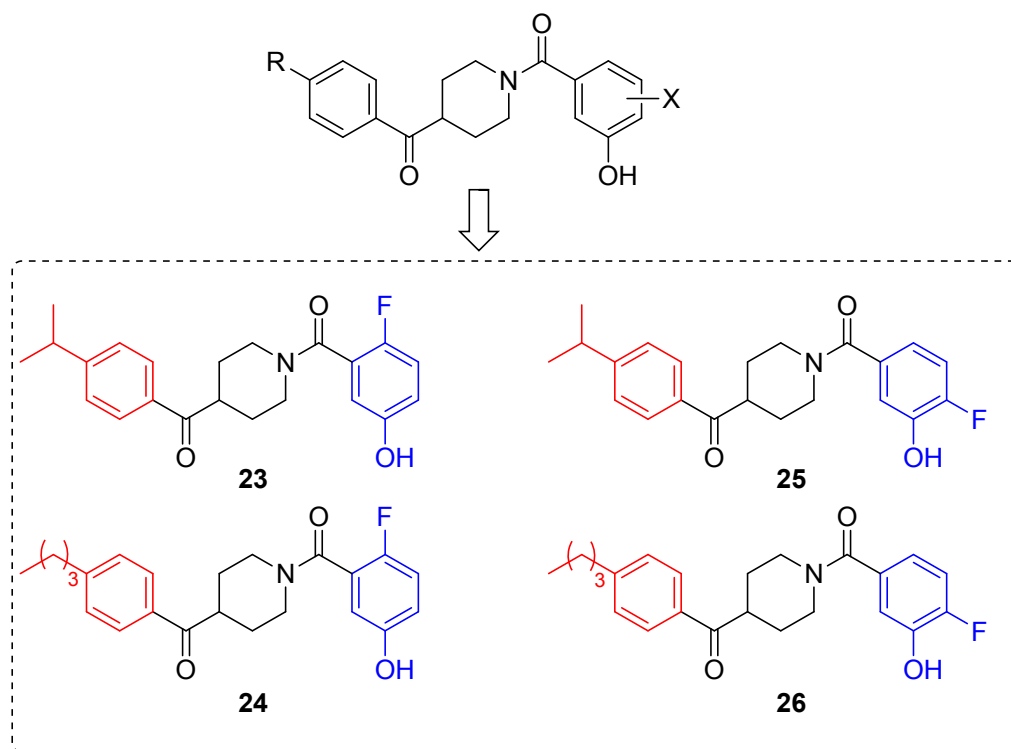
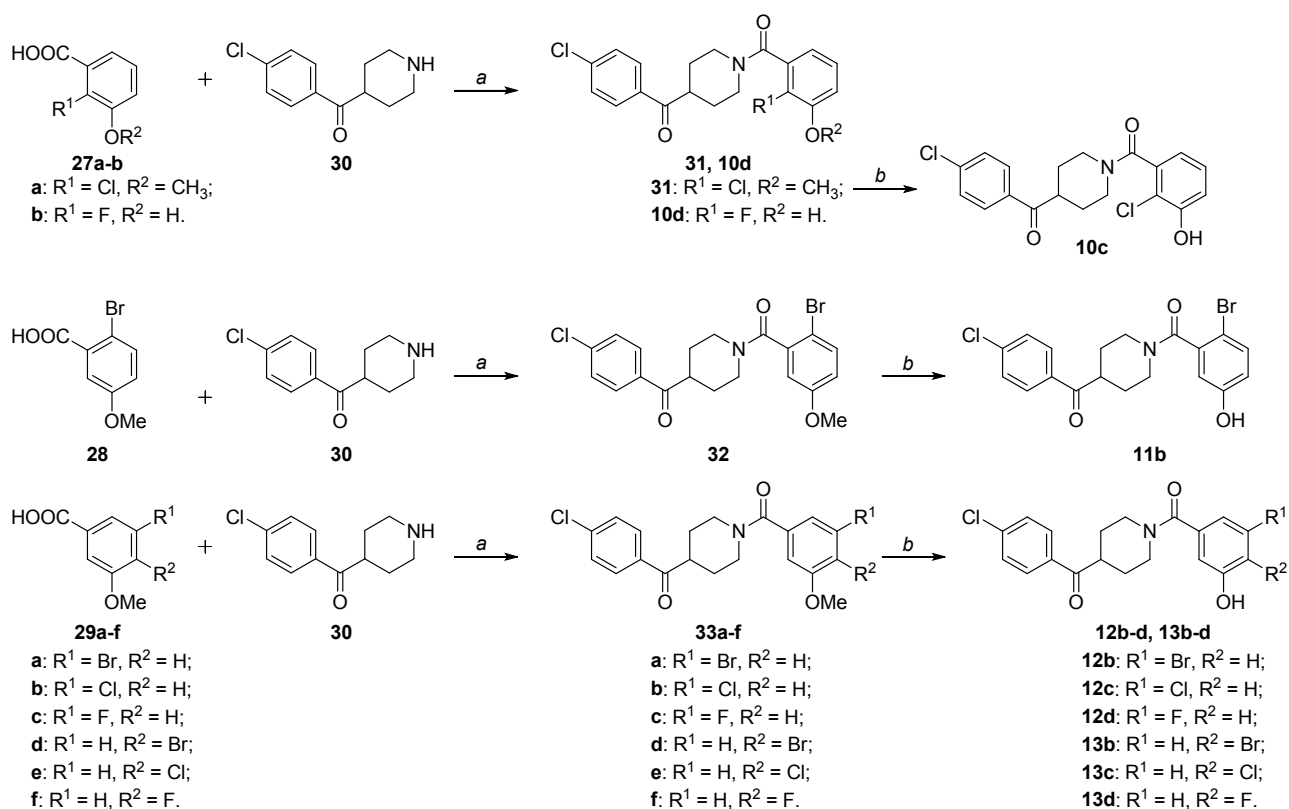


Figure 3. Design of new benzoylpiperidine derivatives: compounds **23-26** resulting from the combination of the best structural motifs present in compounds **10-22**.

Chemistry. For the synthesis of halogenated compounds, in most cases the starting halogenated carboxylic acids were commercially available and, therefore, they were directly submitted to the amidic condensation with the appropriate amine, as shown in Scheme 1. Basically, halogenated 3-methoxy-benzoic acids **27a**, **28** and **29a-f** were reacted with commercially available 4-(4-chlorobenzoyl)piperidine **30** in the presence of 1-[bis(dimethylamino)methylene]-1*H*-1,2,3-triazolo[4,5-*b*]pyridinium 3-oxid hexafluorophosphate (HATU) as the condensing agent, DIPEA as the base and dry *N,N*-dimethylformamide as the solvent, as previously reported,^{33,34} to obtain the corresponding amidic derivatives **31**, **32** and **33a-f** (Scheme 1). Finally, the methoxy groups of these

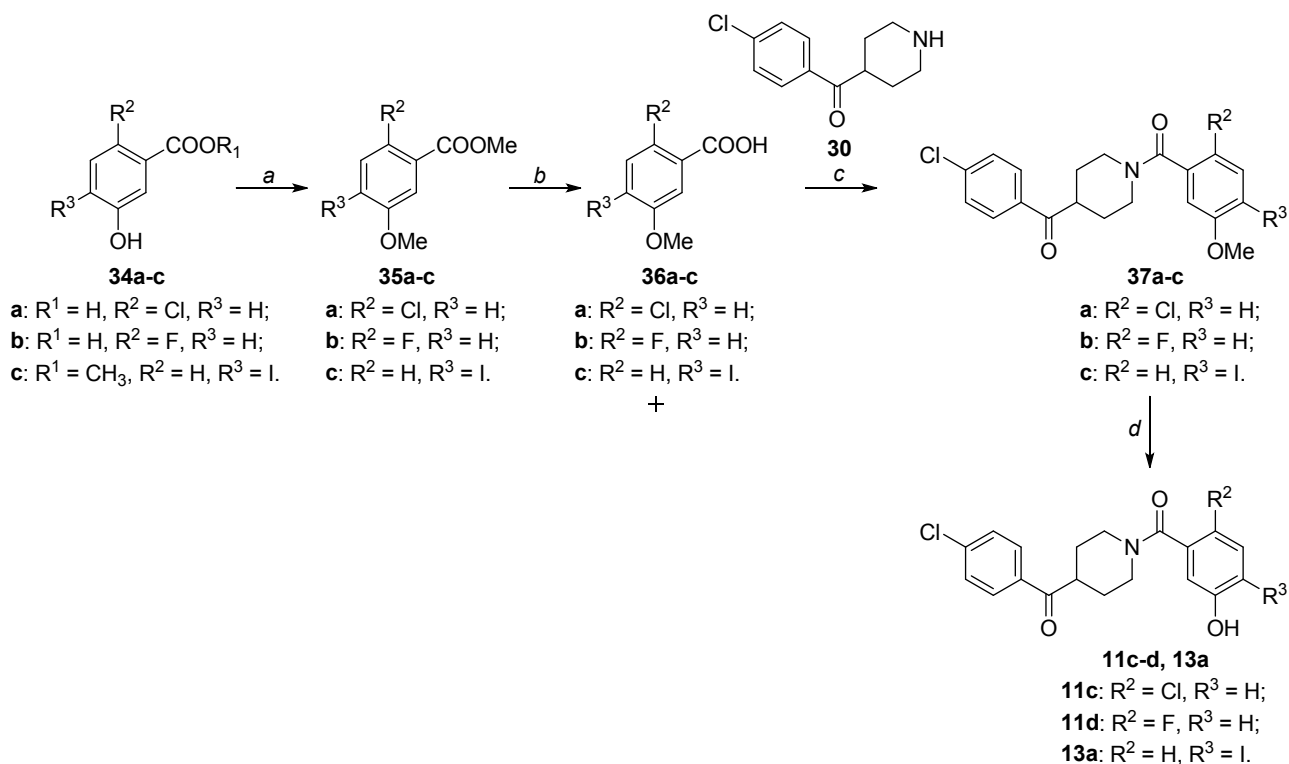
intermediates were deprotected with boron tribromide to yield the final hydroxy-substituted compounds **10c**, **11b**, **12b-d** and **13b-d**. Just one case differs from the commonly adopted synthetic strategy, since we directly used the halogenated benzoic acid bearing the free phenolic group, in order to skip the last deprotection step. 2-Fluoro-3-hydroxybenzoic acid **27b** and piperidine derivative **30** straightforwardly furnished the final product **10d** (Scheme 1). However, the purification of this compound from the impurities formed in the reaction was not straightforward, finally resulting in a low reaction yield (23%). We believe that this problem was mainly due to the presence of a free phenolic OH group in precursor **27b**. Therefore, we slightly modified the synthetic strategy for the preparation of the other compounds of this series, by generally using the appropriate methoxylated benzoic acid in the amidic condensation reaction.



Scheme 1. Synthesis of halogenated derivatives **10c-d**, **11b**, **12b-d**, **13b-d**.

Reagents and conditions: (a) HATU, DIPEA, dry DMF, RT, 2-6.5 h [23-77%]; (b) 1M BBr₃, dry CH₂Cl₂, -10 to 0 °C, then RT, 1.5-4 h [40-81%].

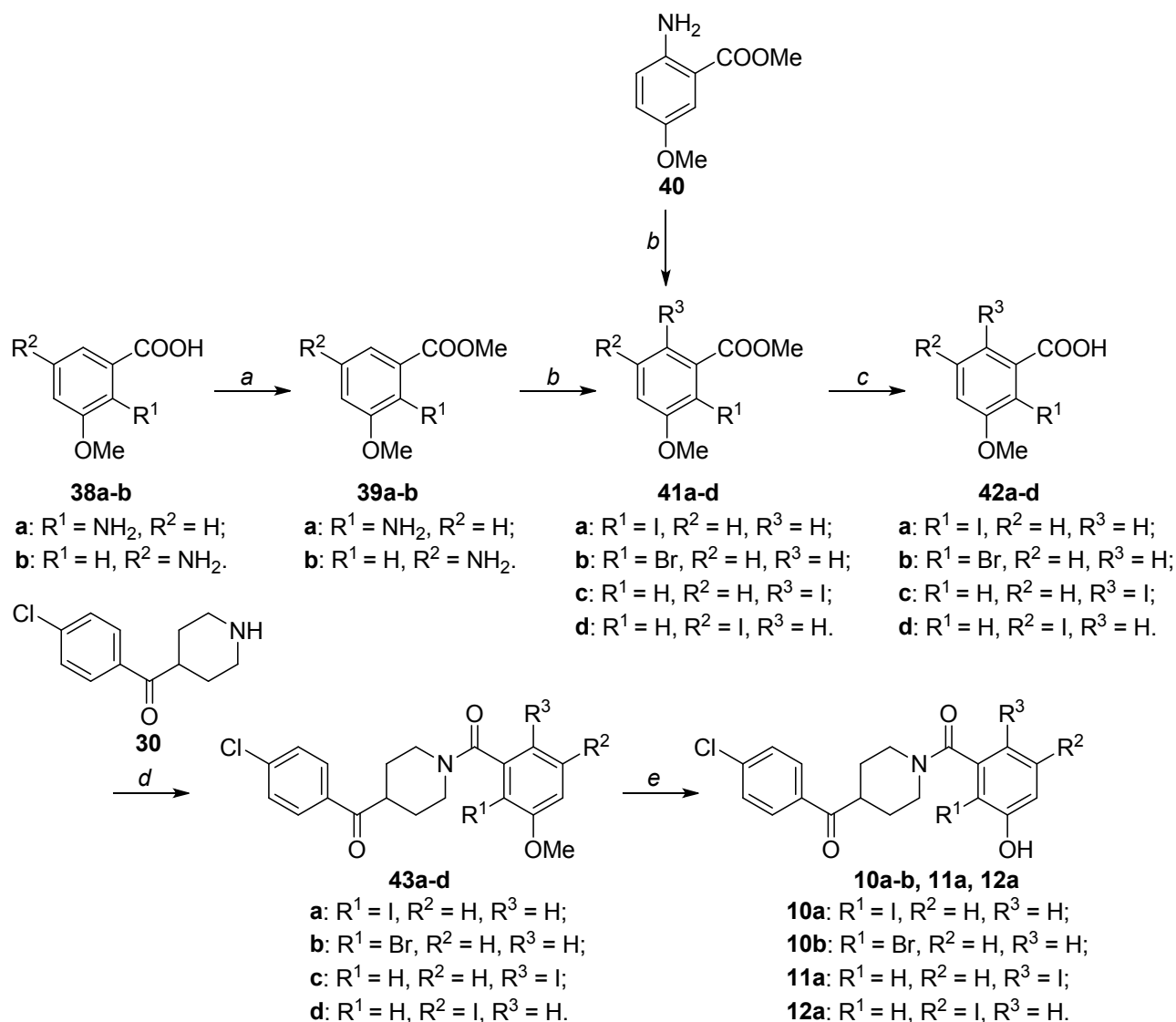
In details, considering the just mentioned problems encountered with the amide formation starting from a hydroxy-substituted benzoic acid, and that in some cases benzoic acids or methyl benzoates bearing free phenolic hydroxyl groups were the only commercially available starting materials, we methylated the phenolic derivatives **34a-c** with methyl iodide by using potassium carbonate in DMF (Scheme 2). Under these conditions, both the carboxylic acid (if present, such as in compounds **34a,b**) and the hydroxyl groups were methylated and consequently, methoxylated methyl benzoates **35a-c** were hydrolyzed under aqueous basic conditions in order to obtain the free acids **36a-c**. At this point, the previously adopted reaction conditions were followed, which consisted in the amide condensation with compound **30** and the subsequent BBr₃-promoted deprotection of intermediates **37a-c** to obtain final compounds **11c-d** and **13a** (Scheme 2).



Scheme 2. Synthesis of halogenated derivatives **11c-d**, **13a**.

1
2
3 *Reagents and conditions:* (a) MeI, K₂CO₃, DMF, RT, 24 h [79-99%]; (b) aq. 2N LiOH, THF/MeOH
4
5 1:1 v/v, RT, overnight [95-99%]; (c) HATU, DIPEA, dry DMF, RT, 3-5 h [39-75%]; (d) 1M BBr₃,
6
7 dry CH₂Cl₂, -10 to 0 °C, then RT, 1.5-7 h [33-88%].
8
9

10
11
12 An appropriate aniline derivative was used as the starting material instead of the halogenated
13
14 precursor, when the latter was not commercially available. Hence, amino-substituted benzoic acids
15
16 **38a-b** (Scheme 3) were converted to the corresponding methyl esters **39a-b** by refluxing them with
17
18 thionyl chloride in methanol. Compounds **39a-b** and commercially available methyl-2-amino-5-
19
20 methoxybenzoate **40** were reacted in a Sandmeyer reaction with the appropriate source of nucleophile
21
22 (copper (I) bromide for compound **41b** or potassium iodide for compounds **41a, c, d**) to obtain
23
24 halogenated compounds **41a-d**. Methyl esters **41a-d** were hydrolyzed to benzoic acids **42a-d**, which
25
26 were then condensed with 4-(4-chlorobenzoyl)piperidine **30** to get amides **43a-d**. The final *O*-
27
28 demethylation reaction furnished the last groups of halogenated benzoylpiperidine derivatives **10a-**
29
30
31
32
33 **b, 11a and 12a** (Scheme 3).
34
35
36
37
38
39
40
41
42
43
44
45
46
47
48
49
50
51
52
53
54
55
56
57
58
59
60

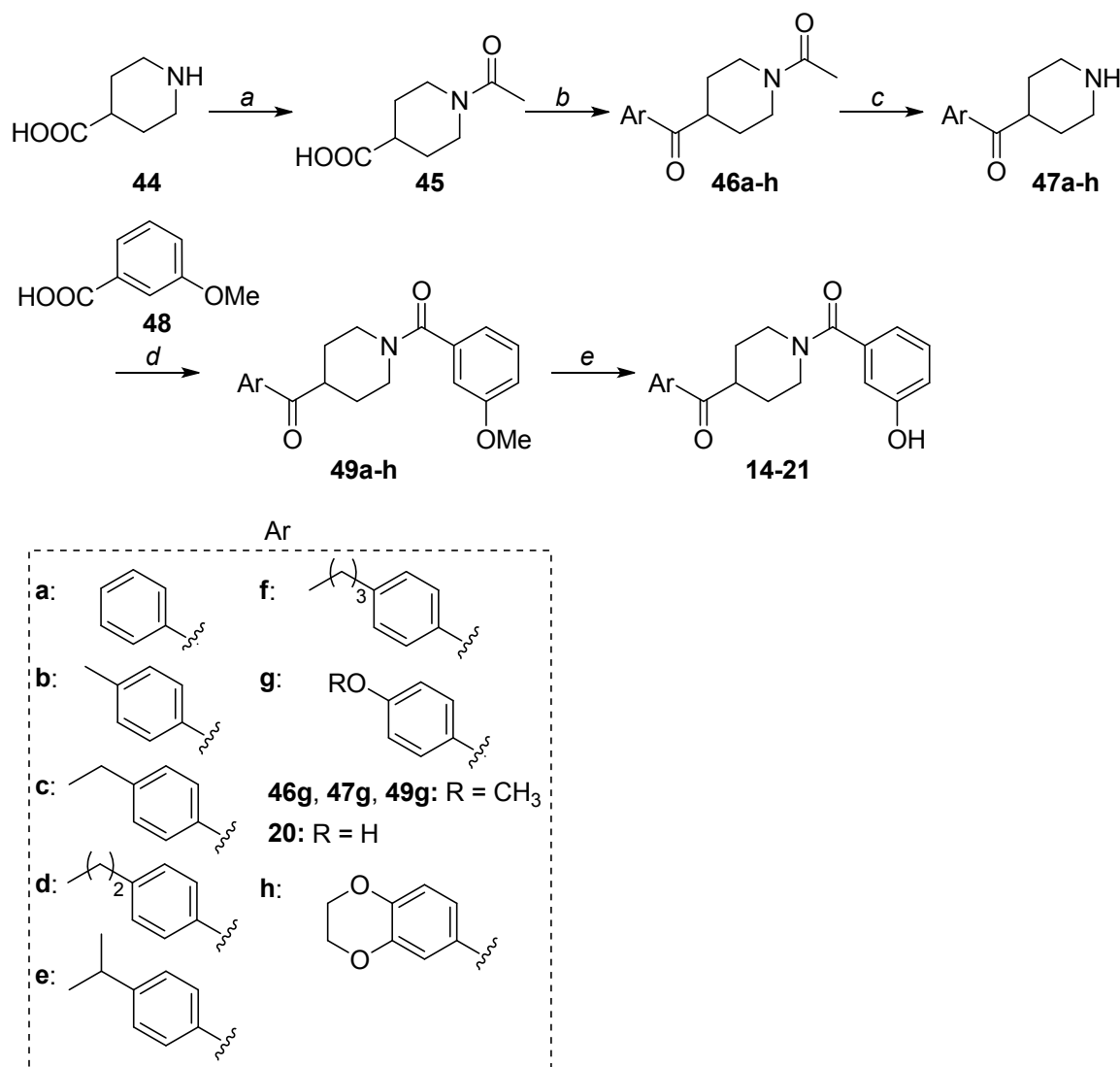


Scheme 3. Synthesis of halogenated derivatives **10a-b**, **11a**, **12a**.

Reagents and conditions: (a) SOCl_2 , MeOH, reflux, 3-24 h [**39a**: 69%, **39b**: 97%]; (b) if $R = \text{I}$ (**41a**, **c**, **d**): KI, NaNO_2 , H_2SO_4 , H_2O , -5 °C to RT, 1-3 h; if $R = \text{Br}$ (**41b**): CuBr, HBr 48%, NaNO_2 , H_2O , dioxane, -5 °C to RT, then 110 °C, 5 h [25-78%]; (c) aq. 2N LiOH, THF/MeOH 1:1 v/v, RT, overnight [64-99%]; (d) HATU, DIPEA, dry DMF, RT, 3-5 h [43-60%]; (e) 1M BBr_3 , dry CH_2Cl_2 , -10 to 0 °C, then RT, 1.5-4.5 h [24-94%].

Compounds **14-21** bearing different aromatic groups in the place of the *para*-chlorobenzoyl ring of the previous series of derivatives were obtained according to the synthetic pathway outlined in Scheme 4. Commercially available isonipecotic acid **44** was acetylated on the piperidine nitrogen

1
2
3 atom by using acetic anhydride in pyridine to obtain compound **45**, which was then converted to the
4
5 corresponding acyl chloride by refluxing it with thionyl chloride in dichloroethane, and then reacted
6
7 in a Friedel-Crafts reaction with the appropriate aromatic moiety, in the presence of aluminum
8
9 chloride in dichloroethane. The aromatic systems utilized in this step were either a simple benzene
10
11 ring (**46a**) or mono-substituted aromatic rings with alkyl chains of increasing length, such as toluene
12
13 (**46b**), ethylbenzene (**46c**), *n*-propylbenzene (**46d**), cumene (**46e**) or *n*-butylbenzene (**46f**). More polar
14
15 groups were also inserted, such as an anisole (**46g**) and a benzo-1,4-dioxane moiety (**46h**). After the
16
17 different functionalization of the piperidine portion, hydrolysis under aqueous basic conditions and
18
19 heating removed the acetyl group, thus making the piperidine nitrogen atom free to react with 3-
20
21 methoxybenzoic acid **48** to get the corresponding amides **49a-h**. The final demethylation step
22
23 afforded compounds **14-21**; in particular, it should be noticed that the two antipodal methoxy groups
24
25 of compound **20**, one in *meta* position of the amidic phenyl ring and the other in *para* position of the
26
27 benzoyl ring, were both converted to free hydroxyls.
28
29
30
31
32
33
34
35
36
37
38
39
40
41
42
43
44
45
46
47
48
49
50
51
52
53
54
55
56
57
58
59
60



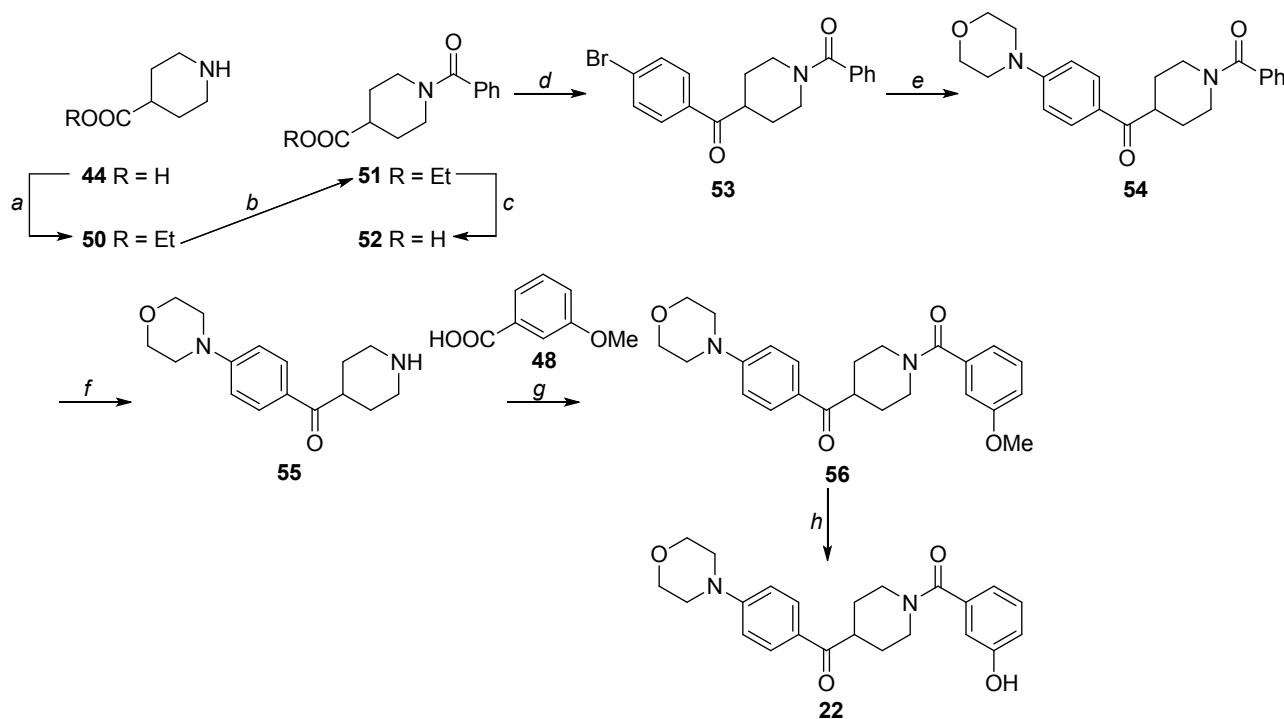
Scheme 4. Synthesis of aryl-substituted derivatives **14-21**.

Reagents and conditions: (a) Ac_2O , pyridine, $140\text{ }^\circ\text{C}$, 2 h [85%]; (b) *i.* SOCl_2 , dry 1,2-DCE, $60\text{ }^\circ\text{C}$, 4 h; *ii.* appropriate aromatic system, AlCl_3 , dry 1,2-DCE, $90\text{ }^\circ\text{C}$, overnight [43-76%]; (c) NaOH 1N, EtOH, $90\text{ }^\circ\text{C}$, overnight [66-95%]; (d) HATU, DIPEA, dry DMF, RT, 2-3 h [33-97%]; (e) 1M BBr_3 , dry CH_2Cl_2 , -10 to $0\text{ }^\circ\text{C}$, then RT, 1-2.5 h [43-76%].

Slight synthetic modifications were used for the preparation of morpholine-substituted derivative **22** (Scheme 5), when compared to the procedure used for the synthesis of compounds **14-21**. The piperidine nitrogen atom of isonipecotic acid **44** was protected by benzoylation and then its acyl chloride was reacted with bromobenzene in a Friedel-Crafts reaction to obtain compound **53**. This

1
2
3
4
5
6
7
8
9
10
11
12
13
14
15
16
17
18
19
20
21
22
23
24
25
26
27
28
29
30
31
32
33
34
35
36
37
38
39
40
41
42
43
44
45
46
47
48
49
50
51
52
53
54
55
56
57
58
59
60

bromo-derivative was subjected to a C-N coupling reaction with morpholine in the presence of tris(dibenzylideneacetone)dipalladium as the catalyst and XPhos as the ligand, by using potassium phosphate as the base under heating conditions, in order to replace the bromine atom with the morpholine ring. The protection of the piperidine nitrogen with a benzoyl group instead of the previous acetyl moiety was due to the harsh conditions in which this intermediate was subjected during the coupling reaction: our intent was to avoid the unwanted hydrolysis of the protecting amide group by using a quite resistant protecting group such as the benzoyl instead of the acetyl. Once the benzamide group was removed by basic hydrolysis for prolonged times, piperidine **55** was condensed with 3-methoxybenzoic acid **48** and finally the methoxy group was converted to the free phenolic OH to give final compound **22** (Scheme 5).

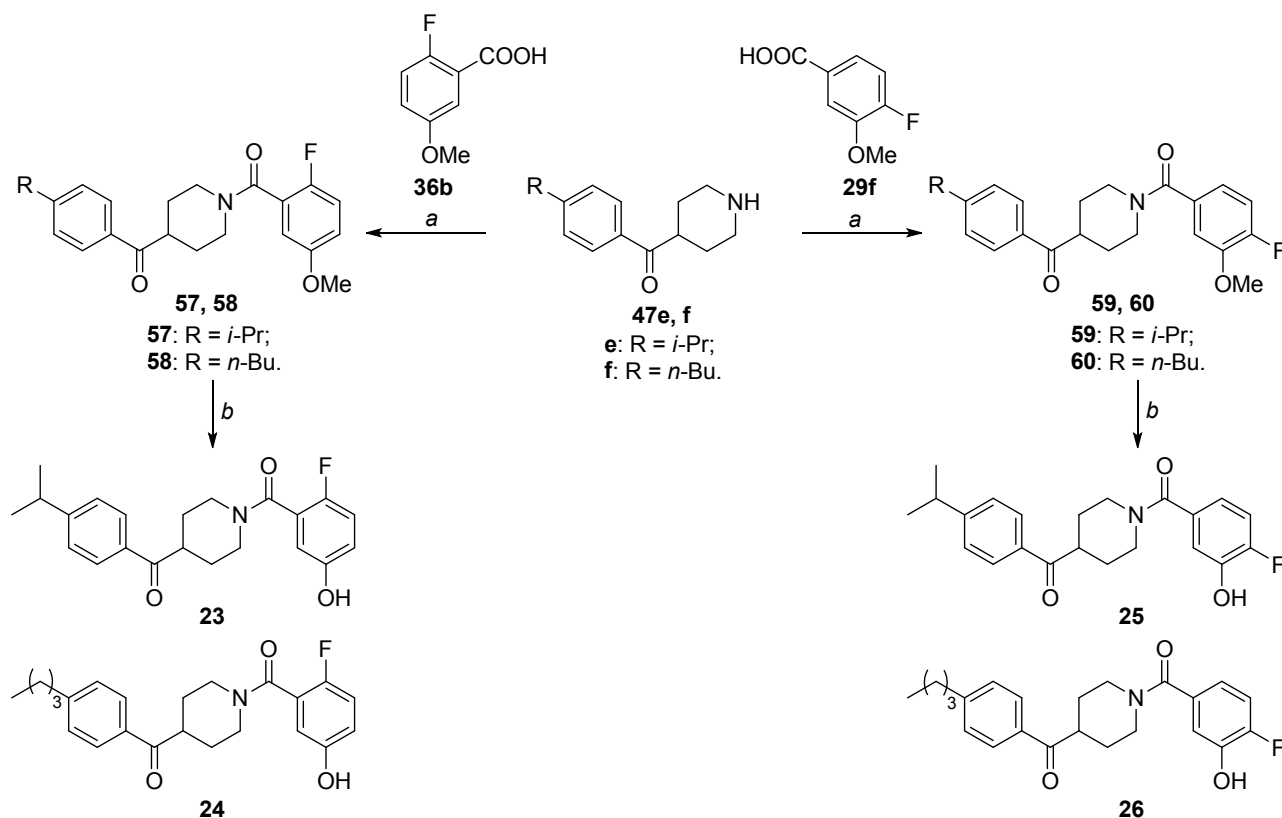


Scheme 5. Synthesis of derivative morpholine-substituted derivative **22**.

Reagents and conditions: (a) SOCl₂, EtOH, reflux, 3 h [74%]; (b) benzoyl chloride, Et₃N, dry DCM, RT, overnight [93%]; (c) NaOH, EtOH/H₂O, RT, overnight [99%]; (d) i. SOCl₂, dry 1,2-DCE, 60 °C, 4 h; ii. PhBr, AlCl₃, dry 1,2-DCE, 90 °C, overnight [43%]; (e) morpholine, Pd₂(dba)₃, XPhos, K₃PO₄,

toluene, 100 °C, 20 h [63%]; (f) NaOH 1N, EtOH, 95 °C, overnight [72%]; (g) HATU, DIPEA, dry DMF, RT, 3 h [99%]; (h) 1M BBr₃, dry CH₂Cl₂, -10 to 0 °C, then RT, 1.5 h [27%].

Finally, we combined the structural portions that gave the best results in enzymatic assays (see below): the *i*-propyl and *n*-butyl chains were favored as substituents in the benzoyl ring and *o*-/*p*-F-phenolic portions were chosen in the other terminal benzamide portion. Therefore, amines **47e** and **47f**, which were prepared as displayed in Scheme 4, were reacted either with benzoic acids **36b**, synthesized as outlined in Scheme 2, or with commercially available compound **29f** (Scheme 1), since it was observed that a fluorine atom in *para* to the phenolic hydroxyl group on the amidic phenyl ring or to the amide carbonyl group was beneficial for MAGL inhibition potency. The corresponding amides (**57**, **58** and **59**, **60**) were converted to the final compounds by BBr₃-promoted demethylation of the methoxy groups, to give compounds **23-26** (Scheme 6).



Scheme 6. Synthesis of compounds **23-26**.

1
2
3 *Reagents and conditions:* (a) HATU, DIPEA, dry DMF, RT, 3 h [86-93%]; (b) 1M BBr₃, dry CH₂Cl₂,
4
5 -10 to 0 °C, then RT, 1-1.5 h [17-87%].
6
7
8
9

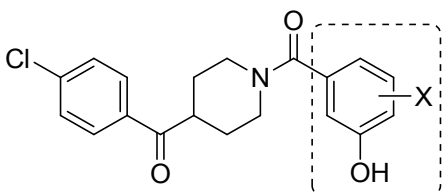
10 Analysis of ¹H and ¹³C-NMR spectra of some of these benzoylpiperidine derivatives confirmed the
11 presence of two rotational conformers generated by the hindered rotation around the C-C bond
12 between the amidic phenyl ring and the carbonyl group nearby, as previously observed by us for
13 similar compounds.³³ The splitting of ¹H and ¹³C-NMR signals was observed for compounds bearing
14 bulkier halogen atoms in the *ortho* position to the amidic carbonyl group, such as I (**10a** and **11a**), Br
15 (**10b** and **11b**) and Cl (**10c** and **11c**). Conversely, the presence of a smaller fluorine atom in the same
16 position, as in compounds **10d** and **11d**, led to the presence of a unique species detected by NMR,
17 and this fact may be explained by considering the smaller size of the fluorine atom, which allows a
18 free rotation around the above-mentioned C-C bond.
19
20
21
22
23
24
25
26
27
28
29
30
31
32
33

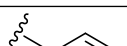
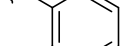
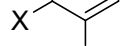
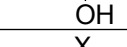
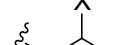
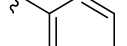
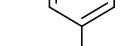
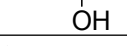
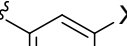
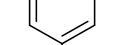
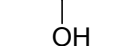
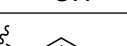
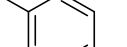
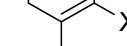
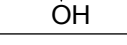
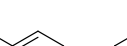
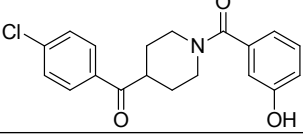
34 **Enzymatic assays and molecular modeling.** The newly synthesized compounds were evaluated for
35 their inhibition potency in human MAGL by using an enzymatic assay in which 4-nitrophenylacetate
36 was used as the substrate and the absorbance values relative to the amount of the formed product 4-
37 nitrophenol were measured at 405 nm. The IC₅₀ values obtained for the new series of compounds
38 were compared with those of two reference inhibitors: the previously published (4-(4-
39 chlorobenzoyl)piperidin-1-yl)(3-hydroxyphenyl)methanone (**9**), which represents the parent
40 compound of this new class of derivatives, and the irreversible MAGL inhibitor CAY10499 (**2**),
41 which is one of the most potent MAGL inhibitors present in literature. The MAGL inhibition activity
42 data for the first series of compounds, halogenated derivatives **10a-d**, **11a-d**, **12a-d** and **13a-d**, are
43 reported in Table 1. It is evident that the presence of the halogen atom in the *meta* or *ortho* position
44 to both the amidic carbonyl moiety and the phenolic hydroxyl group (**12a-d** and **10a-d**, respectively)
45 was not satisfactory for the MAGL inhibitory activity, because the IC₅₀ values of these compounds
46
47
48
49
50
51
52
53
54
55
56
57
58
59
60

1
2
3 were only in the micromolar range. In particular, they were greater than 1 μM for compounds **12a-d**
4
5 and even greater than 5 μM for compounds **10a-d**, thus resulting to be less active than original
6
7 compound **9**. On the contrary, the other two substitution positions led to very positive effects in some
8
9 cases. In fact, the shift of the halogen atom to the *para* position to either the amidic carbonyl moiety
10
11 (**13a-d**) or the phenolic hydroxyl group (**11a-d**) generally produced more potent inhibitors and
12
13 highlighted a possible trend: the inhibitory activity increased in parallel with the electron withdrawing
14
15 property of the halogen present in the molecule, since it gradually increased going from iodine- (**11a**,
16
17 **13a**) to bromine- (**11b**, **13b**), chlorine- (**11c**, **13c**) and fluorine- (**11d**, **13d**) substituted compounds. In
18
19 particular, in the series of compounds **11a-d**, iodine and bromine led to IC_{50} values in the range of
20
21 2.4-2.5 μM , but when the halogen atom was a chlorine the activity of the resulting compound **11c**
22
23 increased (IC_{50} value of 960 nM). This effect was even more pronounced in the presence of a fluorine
24
25 atom, such as in compound **11d**, whose IC_{50} value was of 240 nM, thus reaching a higher inhibition
26
27 potency than that of parent compound **9**. Similarly, in the series **13a-d** we observed an evident
28
29 improvement by passing from iodine ($\text{IC}_{50} = 1.3 \mu\text{M}$) to bromine and chlorine ($\text{IC}_{50} = 457$ and 424
30
31 nM, respectively) and finally reaching the best inhibition activity in this group of halogenated
32
33 benzoylpiperidines with the insertion of a fluorine atom in *para* to the amidic carbonyl group in
34
35 compound **13d**, which showed an IC_{50} value of 389 nM (Table 1). The above-mentioned MAGL
36
37 inhibition improvement given by fluorine atom in two specific positions of the amidic phenyl ring
38
39 may rely on the small size and the powerful electron withdrawing property of fluorine. This atom is
40
41 an isoster of hydrogen, but additionally it increases the acidity of the neighboring phenolic OH,
42
43 stabilizing the anionic form, the phenoxide, thus leading to a highly polarized hydroxyl and,
44
45 consequently, to the formation of stronger hydrogen bonds involving this group. The negative charge
46
47 on the phenoxide can be delocalized on the carbons in *para* or *ortho* positions, that correspond to the
48
49 same carbon atoms where the fluorine atom is bound (compounds **11d** and **13d**), thus contributing to
50
51 a further stabilization of the charge. On the contrary, considering the two possible *ortho* positions to
52
53 the phenolic OH, the one in which F is in the middle between the carbonyl and the phenolic OH leads
54
55
56
57
58
59
60

to negative results for the inhibition activity (compound **10d**). This effect could be rationalized by considering that the steric bulk in compound **10d** induces a plausible block of rotation around the adjacent C-C bond, thus preventing an ideal approach of the hydroxyl group to the protein residues involved in the hydrogen bond network.

Table 1. *In vitro* inhibitory activity on MAGL (IC_{50} , nM)^a of halogenated derivatives **10a-d**, **11a-d**, **12a-d**, **13a-d**.

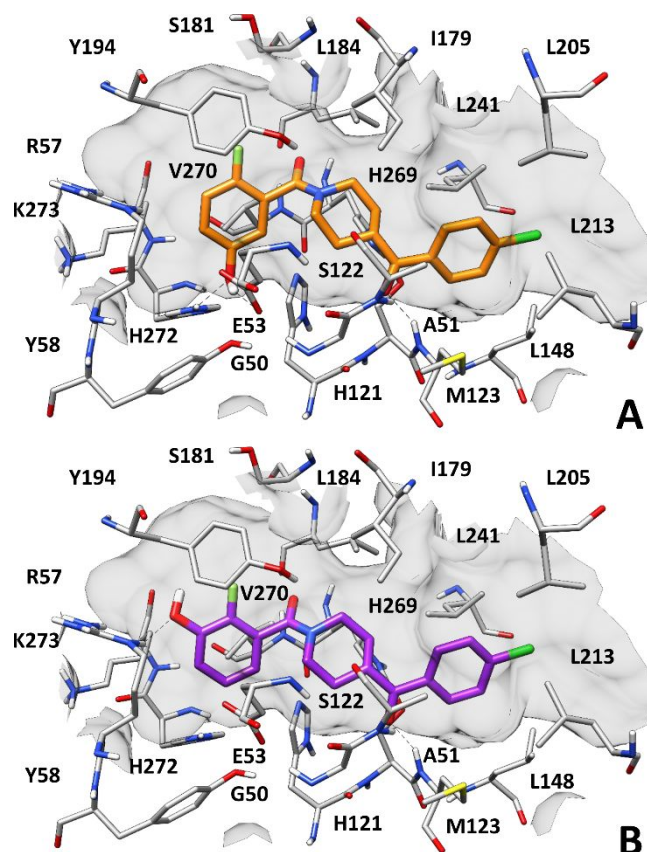


Compounds	X	IC_{50} (nM)
10		5300 ± 200
		8200 ± 300
		8700 ± 500
		12300 ± 600
11		2500 ± 400
		2400 ± 300
		960 ± 50
		240 ± 26
12		1400 ± 200
		1300 ± 200
		1100 ± 100
		1300 ± 200
13		1300 ± 100
		457 ± 6
		424 ± 46
		389 ± 15
9		840 ± 40
CAY10499		134 ± 15
JZL184		49.3 ± 3.9
KML29		3.0 ± 0.1

^a Enzymatic values are the mean of three or more independent experiments, performed in duplicate.

1
2
3 With the aim of investigating the effect of the introduction of halogen atoms in different positions of
4 the amidic phenyl ring of the benzoylpiperidine derivatives, the compounds showing the most
5 interesting structure-activity relationship (SAR) have been analyzed through molecular modeling
6 studies, thus evaluating their binding mode within MAGL and the impact of their different
7 substitution pattern on the ligand-protein interactions. In particular, compounds **11d** and **10d**,
8 presenting the highest and lowest MAGL inhibitory activity, respectively, among the halogenated
9 derivatives, were subjected to a robust docking procedure (see the Experimental section for details),
10 which further confirmed the reliability of the binding mode already predicted for the parent inhibitor
11 **9**. In fact, these two ligands shared a very similar disposition within the protein, with the 4-
12 chlorobenzoyl moiety directed toward the entrance of the catalytic site and showing lipophilic
13 interactions with L148, L205, L213 and L241 already observed for compound **9**.³³ Moreover, the
14 carbonyl oxygen of **10d** and **11d** forms H-bonds with the backbone nitrogen of A51 and M123. The
15 fluorophenol ring of the ligands is placed within the small pocket of the enzyme binding site,
16 sandwiched between Y194 and V270 that form lipophilic interactions with the inhibitors (Figure 4).
17 Interestingly, the docking calculations suggested that only compound **11d** was able to form the H-
18 bond network with E53 and H272 through its hydroxyl group, as predicted for the parent compound
19 **9**. In fact, the fluorophenol ring of compound **10d** was predicted to be about 180° rotated with respect
20 to that of **11d**, with the hydroxyl group pointing toward the inner side of the binding site cavity, far
21 from both E53 and H272. In this orientation, the hydroxyl group can only form an H-bond with the
22 side chain of R57 (Figure 4B). This difference in the binding mode predicted for the two derivatives
23 might be ascribed to the steric hindrance that would occur between the fluorine atom and the central
24 piperidine core of **10d** if its fluorophenol ring assumed the opposite orientation in order to place the
25 OH group in close proximity to the E53/H272 pair. Moreover, a repulsive electrostatic interaction
26 between the highly electronegative fluorine atom and the close carboxylic group of E53 would need
27 to be overcome for allowing the formation of the H-bond between E53 and the ligand hydroxyl group.
28 Such steric and electrostatic factors could make this binding mode energetically unfavorable for **10d**,

1
2
3 compared to that displayed in Figure 4B. Therefore, the consequential loss of the H-bond network
4
5 with E53 and H272 could explain the drop of activity observed for compound **10d** with respect to
6
7 **11d**.
8
9



40 **Figure 4.** Docking results of compounds **11d** (A) and **10d** (B) into MAGL (PDB code 3PE6).
41
42
43
44

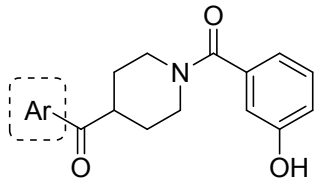
45 In order to analyze the binding modes proposed for the two compounds from an energetic point of
46 view, the predicted **11d**-MAGL and **10d**-MAGL complexes were further studied through a 101 ns
47 molecular dynamics (MD) simulation protocol followed by ligand-protein binding energy evaluations
48 performed using the Molecular Mechanics-Generalized Born Surface Area (MM-GBSA) method (see
49 the Experimental section for details). The MD studies confirmed the reliability of the predicted
50 binding modes, as both compounds maintained their disposition within MAGL catalytic site during
51 the simulations. The last 80 ns of MD simulation were employed to estimate the binding free energies
52
53
54
55
56
57
58
59
60

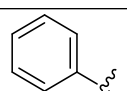
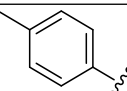
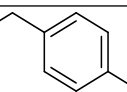
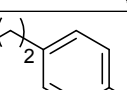
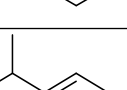
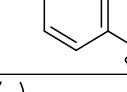
1
2
3 associated with the two ligand-protein complexes. The results of the energetic evaluations were found
4
5 to be consistent with the experimental activities of the compounds and further confirmed the
6
7 reliability of the predicted ligand binding modes. In fact, the ligand-protein binding energy calculated
8
9 for compound **11d** (-61.3 kcal/mol) exceeded of about 11 kcal/mol the binding energy predicted for
10
11 **10d** (-50.4 kcal/mol), in agreement with the remarkably higher MAGL inhibition activity of **11d**
12
13 compared to **10d** (Table S1). The whole computational protocol including docking, MD simulations
14
15 and binding free energy evaluations was then employed to evaluate and analyze the binding mode of
16
17 compound **13d**, which showed an IC₅₀ value for MAGL inhibition considerably close to that
18
19 determined for compound **11d**. As expected, compound **13d** showed a binding disposition very
20
21 similar to that predicted for **11d**, consistently with the very similar activity of the two compounds. In
22
23 particular, compound **13d** was able to form the H-bond network with E53 and H272 through its
24
25 hydroxyl group (Figure S1). In agreement with the experimental data, free energy evaluations
26
27 performed on MAGL in complex with **13d** predicted a ligand-protein binding energy of -61.0
28
29 kcal/mol, comparable to that calculated for the **11d**-MAGL complex, thus supporting the reliability
30
31 of the binding mode predicted for the *p*-fluoro derivative **13d**.
32
33
34
35
36
37

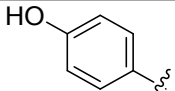
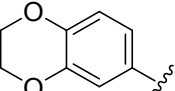
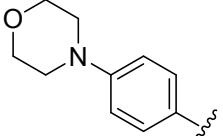
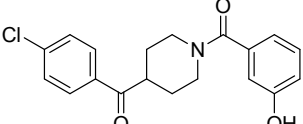
38 The inhibition activity results obtained for compounds **14-22**, which are variously substituted on the
39
40 ketone part of the scaffold, are reported in Table 2. The removal of the chlorine atom of compound **9**
41
42 led to compound **14**, possessing an unsubstituted benzoyl ring, but this modification was not
43
44 beneficial for the inhibition activity on MAGL, resulting in an IC₅₀ value of about 2.2 μM. On the
45
46 other hand, the insertion of alkyl groups of increasing dimensions – going from a methyl group
47
48 (compound **15**) to a *n*-butyl chain (compound **19**) – generated a progressive improvement of the
49
50 inhibitory activity. However, this behavior was subjected to a sort of “plateau”: after an initial
51
52 decrease of the IC₅₀ values from methyl, to ethyl and *n*-propyl chain of compounds **15**, **16** and **17**
53
54 (IC₅₀ = 368, 194 and 162 nM, respectively), the best results were reached by *i*-propyl (**18**) and *n*-butyl
55
56 (**19**)-substituted compounds that showed nearly the same IC₅₀ values (138 and 136 nM, respectively),
57
58
59
60

thus indicating a limit in the increase of the activity induced by the increase of the dimension of the alkyl chain. Moreover, it is worth noting that compounds **18** and **19** were not only more potent than parent compound **9**, but their IC_{50} values were comparable to that of irreversible inhibitor **CAY10499** and were only about 3-fold less active than **JZL184**. With regards to compound **KML29**,³⁵ it was about 46-fold more active than compounds **18** and **19**. The presence of polar groups in the place of the aliphatic chains, such as a phenol (**20**), a benzodioxane (**21**) or a morpholine ring (**22**), was detrimental for the enzyme inhibition activity of the resulted compound, which raised to values in the micromolar range (in the range of 1-10 μ M), thus suggesting that the insertion of polar moieties in this position is strongly disadvantageous for MAGL inhibition.

Table 2. *In vitro* inhibitory activity on MAGL (IC_{50} , nM)^a of compounds **14-22**.



Compounds		IC_{50} (nM)
14		2200 ± 200
15		368 ± 25
16		194 ± 19
17		162 ± 5
18		138 ± 9
19		136 ± 9

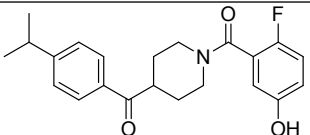
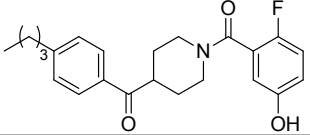
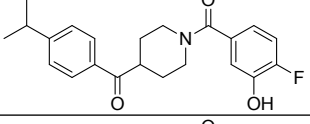
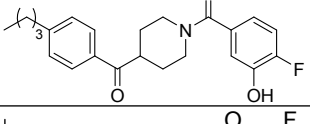
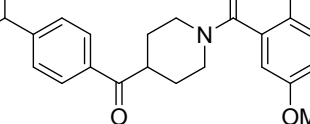
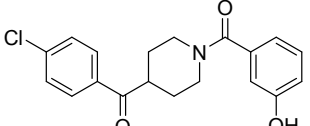
20		10200 ± 1100
21		1000 ± 100
22		5000 ± 900
9		840 ± 40

^a Enzymatic values are the mean of three or more independent experiments, performed in duplicate.

Considering the inhibitory activities of the compounds belonging to the two previous series of MAGL inhibitors (Table 1 and 2), we selected the more potent inhibitors with the aim of combining the best structural modifications in new molecules. Therefore, the presence of a fluorine atom in *para* position to the amidic carbonyl group (compound **13d**) or to the phenolic hydroxyl group (compound **11d**), as well as the insertion of a *n*-butyl (compound **19**) or *i*-propyl (compound **18**) chain on the ketone-type benzoyl ring were the most promising modifications, which were therefore combined to obtain “hybrid” compounds **23-26** (Table 3). These new four compounds showed IC₅₀ values in the nanomolar range, which were comparable to, or even better than, those of the original compounds which inspired their design. In fact, compounds **25** and **26** (IC₅₀ = 110 and 262 nM, respectively), bearing a common *p*-F,*m*-OH-benzamido motif, were more active than their simpler analogue **13d** (IC₅₀ = 389 nM). However, **26** was less potent than its *n*-butyl-substituted non-fluorinated analogue **19** (IC₅₀ values of 262 and 136 nM, respectively), whereas the inhibition potency of **25** was quite similar to that of its *i*-propyl-substituted non-fluorinated analogue **18** (IC₅₀ values of 110 and 138 nM, respectively). The strongest synergistic effect was observed in compounds **23** and **24**, which both shared a common *o*-F,*m*-OH-benzamido portion. In fact, **23** and **24** gave IC₅₀ values of 80 and 74 nM, respectively, thus being remarkably more active than their close analogues **11d**, **18** and **19**. These

two new compounds were also found to be more potent than both reference compounds **9** and **2**. Therefore, **23** and **24** currently represent the most active benzoylpiperidine-based MAGL inhibitors.

Table 3. *In vitro* inhibitory activity on MAGL (IC₅₀, nM)^a of compounds **23-26**, **57**.

Compounds	IC ₅₀ (nM)
23 	80 ± 12
24 	74 ± 1
25 	110 ± 8
26 	262 ± 26
57 	2600 ± 400
9 	840 ± 40

^a Enzymatic values are the mean of three or more independent experiments, performed in duplicate.

Finally, in order to confirm the importance of the phenolic hydroxyl group, which was maintained fixed in all synthesized derivatives, we tested the methoxylated precursor of compound **23**, compound **57** (Scheme 6, Table 3). The decrease of activity of compound **57** was evident, since it displayed an IC₅₀ value of 2.6 μM, compared to its analogue **23** with the free OH (IC₅₀ = 80 nM), thus confirming that the hydroxyl group is essential for the interaction with MAGL, as previously suggested by modeling studies.³³ In order to have information about the lipophilic properties of the herein reported

1
2
3 compounds, an evaluation of the $\log P$ has been carried out. Table S2 shows the consensus $\log P$ values
4
5 obtained through the Chemicalize tool. None of the analyzed compounds showed a $\log P$ value higher
6
7 than five and, furthermore, no evident correlation between $\log P$ and activity of the different
8
9 compounds was observed; in fact, by plotting the $\log P$ values against the measured pIC_{50} values of
10
11 the ligands a correlation (R^2) lower than 0.2 was obtained. In order to confirm the hypothesized
12
13 reversible mechanism of inhibition, the effects of dilution and preincubation on the inhibitory activity
14
15 of compound **23** were evaluated. In the presence of an irreversible mechanism of inhibition, the
16
17 potency should not decrease after dilution, whereas for a reversible inhibition, the potency level
18
19 should be strongly reduced after dilution.³⁶ Therefore, the inhibition produced by incubation with a
20
21 4000 nM concentration of **23** was measured after a 40X dilution and compared to the potency
22
23 observed by a 4000 nM and a 100 nM of compound **23**. The results showed in Figure 5A supported
24
25 a reversible mechanism of inhibition, since the inhibition produced by 100 nM of this compound was
26
27 similar to that obtained after a 40X dilution and was considerably lower than that produced by the
28
29 same compound at a concentration of 4000 nM. As a second assay, the inhibition activity of **23** was
30
31 measured at different preincubation times with MAGL. Compound **23** was preincubated with the
32
33 enzyme for 0, 30 and 60 min before adding the substrate to start the enzymatic reaction. An
34
35 irreversible inhibition should produce a higher potency after longer incubation times, whereas a
36
37 reversible inhibitor should produce a constant inhibition potency over all the different incubation
38
39 times. As shown in Figure 5B, this test agreed with the reversible property of **23**, as it showed a very
40
41 similar activity for the three different incubation times.
42
43
44
45
46
47
48
49
50
51
52
53
54
55
56
57
58
59
60

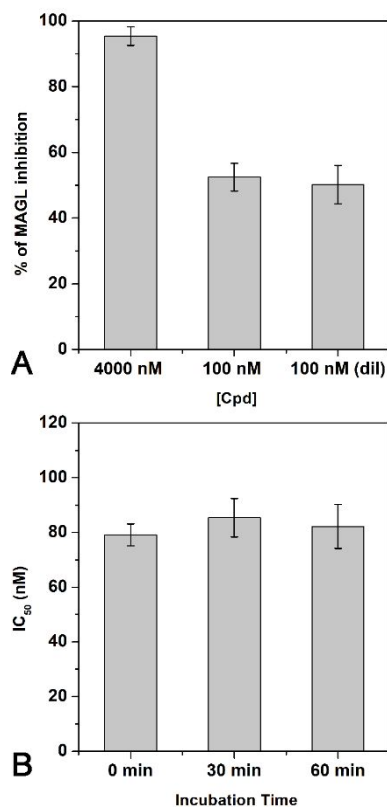
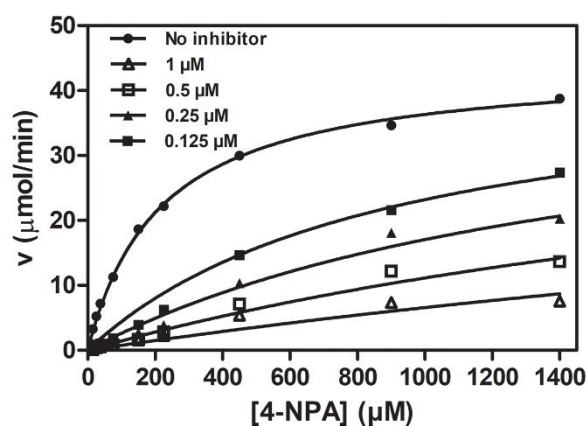


Figure 5. Analysis of the mechanism of MAGL inhibition by compound **23**-MAGL inhibition analysis. A) Dilution assay: the first two columns indicate the inhibition percentage of compound **23** at a concentration of 4000 nM and 100 nM. The third column indicates the inhibition percentage of compound **23** after dilution (final concentration = 100 nM). B) IC₅₀ (nM) values of **23** at different preincubation times with MAGL (0 min, 30 min and 60 min).

Once we verified the reversible mechanism of inhibition of compound **23**, its mode of inhibition was then evaluated by measuring Michaelis–Menten kinetics at various inhibitor concentrations. The dataset was plotted as substrate concentration *versus* enzyme activity and analyzed by applying the mixed-model inhibition fit of GraphPad Prism 5.0, which includes competitive, uncompetitive, and noncompetitive inhibition terms. This model evaluates the V_{\max} , K_m and the α parameter, which is indicative of the inhibition mechanism. When α corresponds to one, the inhibitor does not alter the binding of the substrate to the enzyme, and the mixed-model can be considered as a noncompetitive

1
2
3 inhibition. When α is a very large value, the inhibitor interaction prevents the substrate binding and
4
5 the mixed-model corresponds to a competitive inhibition. Finally, when α is a very small value, the
6
7 binding of the inhibitor increases the binding of the substrate and the mixed model corresponds to an
8
9 uncompetitive model. Kinetic studies indicate for **23** a K_i value of 39 ± 4 nM and an α value greater
10
11 than 10000, thus supporting a competitive behavior for this compound (Figure 6).
12
13
14
15
16
17
18
19

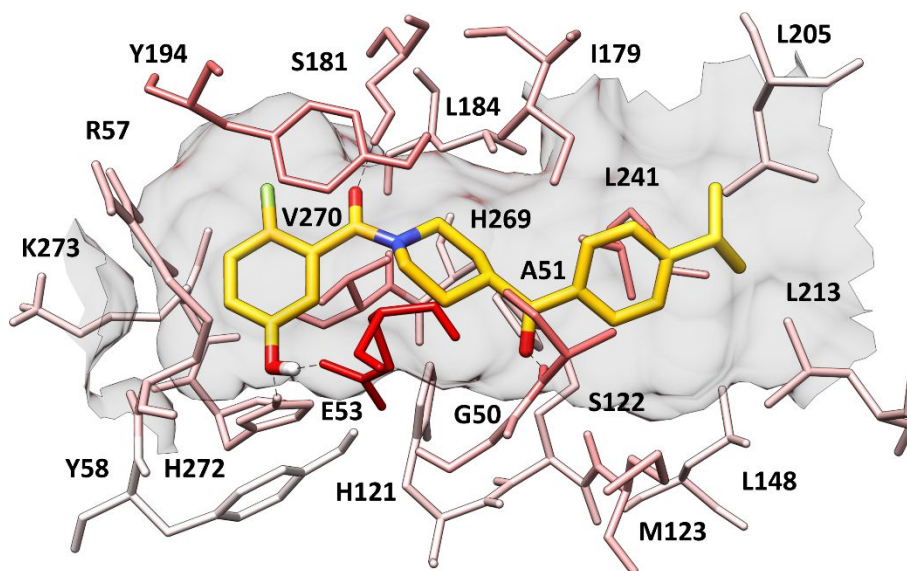


20
21
22
23
24
25
26
27
28
29
30
31
32
33
34 **Figure 6.** Inhibition of the activity of MAGL and competitive nature of compound **23** ($K_i = 39 \pm 4$
35 nM, $\alpha > 10000$). 4-NPA = 4-nitrophenylacetate.
36
37
38
39
40
41

42
43 The binding mode of the most promising derivative of the series compound **23**, which showed the
44
45 best activity in the cell-based assay and selectivity profile (see also following sections), was studied
46
47 through the same robust docking procedure applied on **10d**, **11d** and **13d**. As expected, the predicted
48
49 disposition of compound **23** within MAGL catalytic site, as well as its H-bond interactions with the
50
51 binding site residues (Figure 7), were highly similar to those predicted for compound **11d**. The
52
53 predicted MAGL-**23** complex was further studied through the same MD simulation protocol applied
54
55 on the other derivatives, in order to evaluate the reliability of the predicted ligand-protein interactions
56
57 (see the Experimental section for details). The ligand was found to maintain its binding disposition
58
59 with remarkable stability during the whole simulation, showing an average root-mean-square
60

1
2
3 deviation (RMSD) from its initial coordinates about 1.4 Å (Figure S2 in the Supporting Information).
4
5 The H-bond analysis revealed very stable H-bonds with A51 and E53, which were kept for more than
6
7 95% of the whole MD simulation, and a strong H-bond with H272 maintained for about 80% of the
8
9 MD. Moreover, in agreement with the results obtained for compound **9**, compound **23** only partially
10
11 maintained the interaction with M123 in favor of an additional H-bond with S181 that was formed
12
13 for almost 90% of the MD (Table S3 in the Supporting Information). A deeper analysis of the ligand-
14
15 protein interactions was then carried out with the aim of identifying which residues play a key role
16
17 for the ligand inhibitory potency, thus providing a better interpretation of SAR data. For this purpose,
18
19 the MM-GBSA approach was used to perform binding free energy evaluations with pairwise per-
20
21 residue energy decomposition, thus calculating the contribution to the ligand binding affinity of each
22
23 single amino acid constituting the MAGL catalytic site located in the surroundings of the ligand in
24
25 its predicted binding mode.^{37,38} This analysis, which was performed on the last 80 ns of MD
26
27 simulation, highlighted E53 as a fundamental residue for the activity of the ligand (Figure 7), since
28
29 the free energy contribute of the single **23**-E53 interaction corresponds to -9.6 kcal/mol out of an
30
31 overall binding energy of -64.9 kcal/mol. These data further confirmed the importance of the
32
33 hydroxyl group for the inhibitory potency of compound **23** and its analogues, in agreement with the
34
35 experimental results herein reported. Other residues that mostly contribute to the total interaction
36
37 energy were found to be A51 and Y194 (-4.6 kcal/mol), as well as L241 (around -4.0 kcal/mol): in
38
39 fact, A51 forms a particularly stable H-bond with the carbonyl oxygen of the ligand (Table S3), the
40
41 aromatic portion of Y194 shows a π - π stacking with the ligand benzamide moiety, whereas the side
42
43 chain of L241 establishes extensive hydrophobic interactions with both the phenyl and the isopropyl
44
45 group of the ligand oriented toward the solvent exposed region of the binding site. Finally, among the
46
47 other residues showing a considerable impact on ligand-protein binding affinity we found other
48
49 hydrophobic residues, such as I179 and V270, as well as polar residues S181 and H272, which form
50
51 strong H-bonds with the inhibitor and appeared as key amino acids for the inhibitory potency of this
52
53 series of compounds. Interestingly, none of the protein residues surrounding the ligand showed an
54
55
56
57
58
59
60

1
2
3 unfavorable contribute to the ligand-protein binding energy in the free energy decomposition
4 calculation. The prediction of the pK_a value for the phenolic oxygen ($pK_a = 8.6$) confirmed that at
5
6 physiological pH the undissociated form is the most prevalent (97.7% of the total population) with
7
8 respect to the deprotonated one (2.3% of the total population).
9
10
11
12
13
14



15
16
17
18
19
20
21
22
23
24
25
26
27
28
29
30
31
32
33
34
35
36
37
38
39
40
41
42
43
44
45
46
47
48
49
50
51
52
53
54
55
56
57
58
59
60
Figure 7. Minimized average structure of **23** within MAGL catalytic site. The residues are colored on the basis of their contribute to the ligand-protein binding affinity (red = highest, white = lowest) (PDB code 3PE6).

Finally, in order to verify the possible inhibition of cytochrome P450 (CYP) enzymes, compound **23** was analyzed by means of the CypRules prediction online server, which is able to predict the potential inhibition properties of ligands against CYP1A2, CYP2D6, CYP2C19, CYP2C9 and CYP3A4 that account for 90% of the xenobiotic and drug metabolism in human body.³⁹ From this prediction analysis the compound did not show to potentially inhibit any of the analyzed cytochromes. With regards to the main most probable atomic site of the molecule that will be modified during CYP-mediated metabolism, the analysis carried out by using the Xenosite prediction tool suggests that the isopropyl fragment is the most susceptible group to CYP-modifications (see Figure S3).⁴⁰

Selectivity. Compounds **23-26** were further profiled for their selectivity towards the other components of the ECS. As shown in Table 4, at 10 μM none of the compounds significantly bound to CB1 and CB2 receptors or inhibited ABHD6 and ABHD12. The most potent MAGL inhibitors **23** and **24** did not significantly inhibit FAAH activity at 10 μM , whereas **25** and **26** blocked AEA hydrolysis catalyzed by this enzyme with IC_{50} values of 1.0 ± 0.5 and 3.2 ± 0.6 μM , respectively (Table 4).

Table 4. Pharmacological characterization of compounds **23-26** towards the other components of the ECS. Data represent IC_{50} values (μM , mean \pm SD) and the % of receptor binding/enzyme inhibition at the concentration of 10 μM (in brackets).

Compound	IC_{50} values (μM , mean \pm SD)				
	CB1	CB2	FAAH	ABHD6	ABHD12
23	> 10 (4%)	> 10 (30%)	> 10 (18%)	> 10 (0%)	> 10 (21%)
24	> 10 (15%)	> 10 (13%)	> 10 (30%)	> 10 (0%)	> 10 (20%)
25	> 10 (9%)	> 10 (17%)	1.0 ± 0.5	> 10 (11%)	> 10 (12%)
26	> 10 (14%)	> 10 (24%)	3.2 ± 0.6	> 10 (16%)	> 10 (18%)

Cell-based assays of MAGL inhibition. In order to confirm the MAGL inhibition of **23** and **24** in a physiological system, we tested the compounds in the intact human monocytic cell line U937. As shown in Figure 8, both compounds inhibited [^3H]2-oleoyl glycerol (2-OG) hydrolysis in a concentration dependent manner. As expected, the inhibition of [^3H]glycerol formation (closed circles, solid line) is mirrored by the accumulation of non-hydrolyzed [^3H]2-OG (open circles, dotted line).

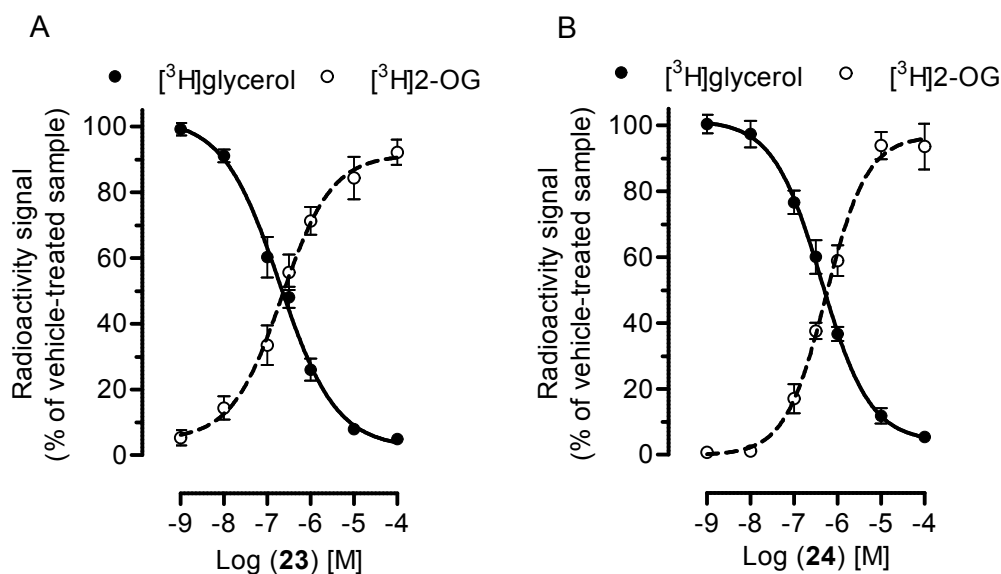


Figure 8. Concentration-dependent inhibition of $[^3\text{H}]2\text{-OG}$ hydrolysis in intact U937 cells. Compound (A) **23** and (B) **24** were co-incubated with 1.0×10^6 cells and then $10 \mu\text{M}$ of 2-OG with a 0.5 nM of $[^3\text{H}]2\text{-OG}$ as tracer was added to the cells. After 5 min of incubation at $37 \text{ }^\circ\text{C}$, cells were centrifuged and the supernatants were extracted with a 1:1 mixture of CHCl_3 :methanol. The radioactivity associated with the aqueous phase is associated with $[^3\text{H}]$ glycerol formation (closed circles, solid line), while the organic phase is associated with $[^3\text{H}]2\text{-OG}$ (open circles, dotted line).

In intact U937 cells, the IC_{50} value of compound **23** was approximately double ($193 \pm 41 \text{ nM}$) than that measured in the purified MAGL assay ($80 \pm 12 \text{ nM}$), while for compound **24** the IC_{50} value was approximately 6-times higher ($431 \pm 64 \text{ nM}$ vs. $74 \pm 1.0 \text{ nM}$). The lower potency observed for compound **24** in intact cells may depend on a suboptimal crossing of the plasma membrane or a potential interaction of the compound with other cellular components, thus reducing the actual concentration at the site of action (i.e. MAGL). On the basis of all these results, we decided to discard compound **24** focusing our attention on compound **23**: both compounds showed a similar inhibition potency on the isolated MAGL enzyme with compound **24** that showed a slightly higher activity (although the standard deviations measured for both compounds in enzymatic assays make them highly comparable). The selectivity assays suggested that both compounds are almost inactive against

1
2
3 CB1 and CB2 receptors FAAH, ABHD6 and ABHD12; however, the cell-based assays of MAGL
4 inhibition clearly support the hypothesis that compound **23** is the best candidate as it shows an about
5 two-fold higher potency with respect to **24**.
6
7
8
9

10 **Activity-based protein profiling experiments.** With the aim of assessing the effect of a reversible
11 MAGL inhibition *in vivo*, we first performed competitive activity-based protein profiling (ABPP)
12 experiments for compound **23** using mouse brain membrane preparations. ABPP is a functional
13 proteomic technology, which exploits chemical probes that react with mechanistically related classes
14 of enzymes.⁴¹ TAMRA-fluorophosphonate (TAMRA-FP) is used to visualize serine hydrolases
15 which includes the major eCB degrading enzymes.⁴² An important advantage of ABPP relative to
16 other approaches is that it can detect changes in activity of very low-abundance enzymes in highly
17 complex samples and can simultaneously assess the potency and selectivity of an inhibitor towards
18 the entire family of serine hydrolases in a specific tissue.
19
20
21
22
23
24
25
26
27
28
29

30 As shown in Figure 9, compound **23** inhibited MAGL in a concentration dependent manner (Figure
31 9, doublet band 3 and 4, and Table 5, MAGL migrates as double band in the ABPP),⁴³ without
32 affecting other serine hydrolases in particular FAAH (Figure 9, band 1) and ABHD6 (Figure 9, band
33 5) up to 50 μM , indicating a high selectivity of compound **23** in mouse brain preparations.
34
35
36
37
38
39
40 Unfortunately, we were not able to confirm the selectivity of **23** versus ABHD12 in ABPP assays
41 because we could not clearly visualize the band associated with this serine hydrolase (approx. 46
42 kDa) possibly due to low expression/activity of the enzyme and the experimental conditions.
43
44
45
46
47
48
49
50
51
52
53
54
55
56
57
58
59
60

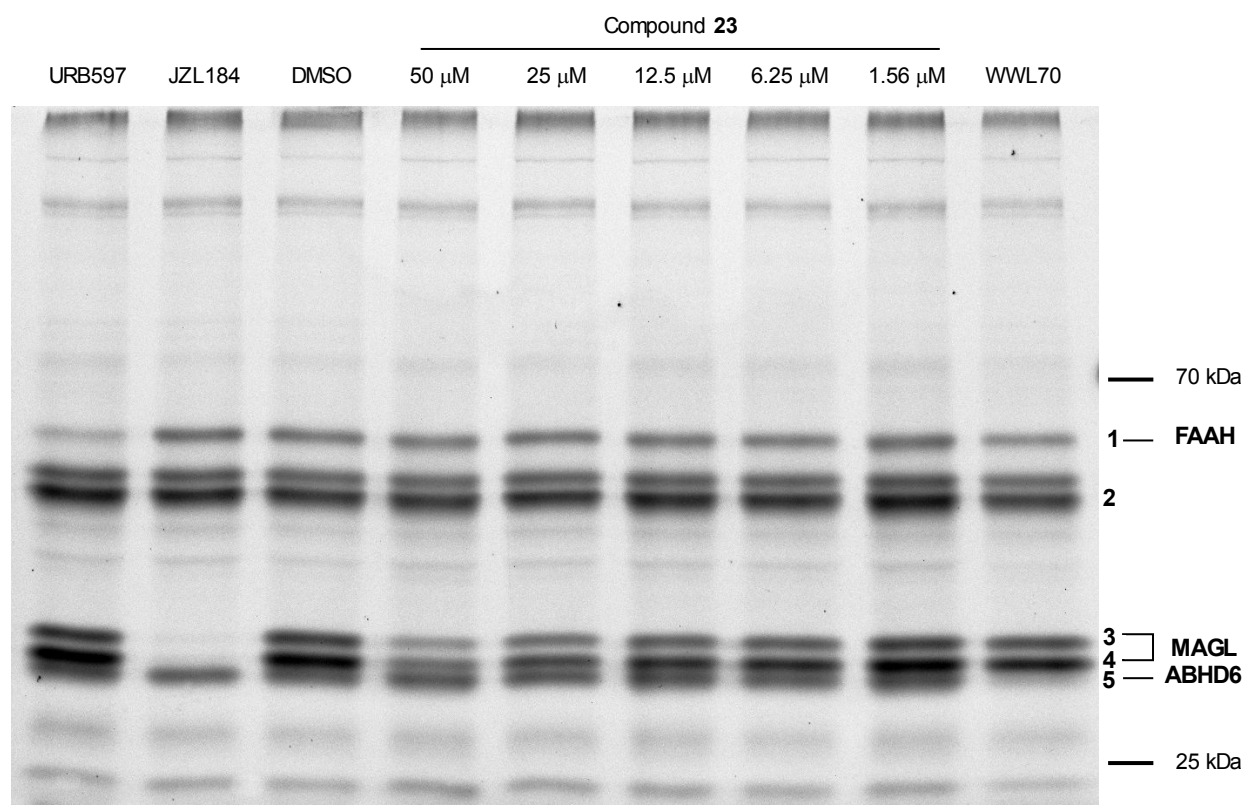


Figure 9. ABPP fluorescent screen of mouse brain membrane (MBM, 2 mg/mL) preparations with TAMRA-Fluorophosphonate serine hydrolase probe (TAMRA-FP). The MBM proteome was preincubated for 25 min with either DMSO, URB597 (4 μM), JZL184 (1 μM), WWL70 (10 μM) or compound **23** at different concentrations (50 μM, 25 μM, 12.5 μM, 6.25 μM, 1.56 μM) followed by 5 min labeling with TAMRA-FP (125 nM final concentration). Band 1 = FAAH, band 2 = used as a reference band for quantification, band 3 and 4 = doublet of MAGL, band 5 = ABHD6.

The quantification of the fluorescent bands confirmed a concentration dependent MAGL inhibition without showing any inhibition of FAAH and ABHD6 up to 50 μM (Table 5).

Table 5. Enzyme activity of FAAH, MAGL and ABHD6 calculated by quantifying of the intensity of band and expressed as % of vehicle control. The gels were analyzed using the software ImageJ and the quantification of band intensity was performed by normalizing the values obtained for FAAH

(band 1) MAGL (bands 3 and 4) and ABHD6 (band 5) with the reference band (2). The intensities were compared to DMSO sample, which reflects 100% of enzyme activity. Data are an average of three independent gels.

Enzyme	URB597	JZL184	WWL70	Compound 23				
	4 μ M	1 μ M	10 μ M	50 μ M	25 μ M	12.5 μ M	6.25 μ M	1.56 μ M
FAAH	49	102	102	105	103	101	98	92
MAGL	92	9	95	47	60	68	78	94
ABHD6	96	116	50	123	116	112	103	90

Mouse membrane assays of MAGL inhibition. In order to further characterize the inhibition of MAGL activity in a functional assay, we tested compound **23** in mouse brain membrane preparations. As shown in Figure S4, compound **23** inhibited 2-OG hydrolysis in a concentration-dependent manner with an IC_{50} value of $2.1 \pm 0.2 \mu$ M, in line with the data observed in ABPP experiments in the same biological matrix.

Antiproliferative assays. Compound **23** was also selected for further *in vitro* experiments to evaluate its antiproliferative potency against cancer cells. Compound CAY10499 (**2**) was used as the reference compound. Due to the key role that MAGL plays in the tumor progression of breast, colon and ovarian cancer, five tumor cell lines were chosen: human breast MDA-MB-231, colorectal HCT116 and ovarian CAOV3, OVCAR3 and SKOV3 cancer cells (Table 6).⁴⁴ Therefore, the antiproliferative activity of the two compounds was tested against these five cell lines, together with the noncancerous human fibroblast lung cells MRC5 (Table 6).⁴⁴ Derivative **23** produced an appreciable inhibition of cell viability in all the tested cancer cell lines, with IC_{50} values ranging from 7.9 to 57 μ M. With respect to the covalent reference inhibitor **CAY10499**, the compound showed a more potent cytotoxic activity on HCT116, MDA-MB-231, CAOV3 and SKOV3, whereas the proliferation of the OVCAR3 tumor cells was similarly affected by the two compounds. Furthermore, both compounds proved to

be inactive against MRC5 ($IC_{50} > 100 \mu\text{M}$). We cannot exclude that the antiproliferative effects of compound **23** are not mediated by the inhibition of MAGL; however, we can exclude that these effects are mediated by the other main proteins of the ECS, as this compound showed a selectivity higher than 100-fold against the CB1 and CB2 receptors, FAAH, ABHD6 and ABHD12.

Table 6. Cell growth inhibitory activities (IC_{50} values) of **CAY10499** and compound **23**.

Compound	IC_{50} (μM , mean \pm SD)					
	HCT116	MDA-MB-231	CAOV3	OVCAR3	SKOV3	MRC5
CAY10499	42 \pm 2	89 \pm 4	92 \pm 5	50 \pm 3	34 \pm 3	> 100
23	21 \pm 1	7.9 \pm 1.2	25 \pm 3	57 \pm 2	15 \pm 2	> 100

In Vivo Experiments. In order to evaluate the ability of compound **23** to inhibit MAGL *in vivo*, we injected this compound to C57BL6 mice and quantified the levels of 2-AG and other related lipids in brain and plasma after 1 h and 2 h. The results showed that 2-AG levels were significantly increased in plasma (after 1 h and 2 h by 55%, Figure 10A) and in brain (after 1 h by 30%, Figure 10C). In agreement with the selectivity over FAAH observed in cellular system and mouse brain homogenates (ABPP experiments), compound **23** did not show any modification of AEA levels in plasma (Figure 10B) and brain (Figure 10D). Similarly, compound **23** did not significantly alter arachidonic acid and prostaglandin levels in plasma and brain as compared to vehicle (Figure S5 in the Supporting Information).

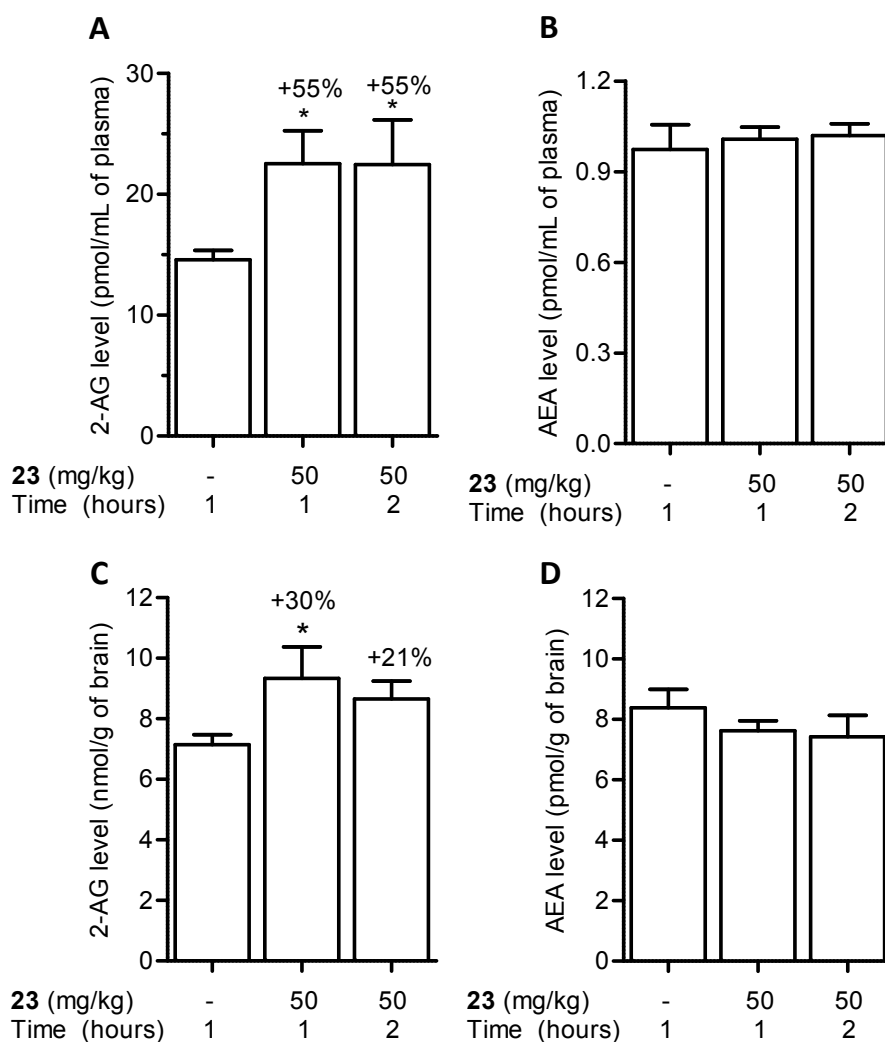


Figure 10. Quantification of 2-AG and AEA levels in plasma (A and B) and in brain (C and D) of C57BL6 mice treated with compound **23** at the dose of 50 mg/kg (i.p.). The animals were sacrificed after 1 h and 2 h post-injection. Male C57BL6 mice, 8-10 weeks old, n= 5-15. Data show mean \pm SE. Statistical analysis was performed with one-way ANOVA followed by Tukey post-hoc test. * $p < 0.05$ versus vehicle.

CONCLUSIONS

In the present work, starting from (4-(4-chlorobenzoyl)piperidin-1-yl)(3-hydroxyphenyl)methanone (**9**), a structural optimization has been performed leading to the identification of compound **23**, which

1
2
3 displayed a high MAGL inhibition activity with an IC₅₀ value of 80 nM and a reversible mode of
4
5 action, as well as a high selectivity for MAGL vs. CB1, CB2, FAAH, ABHD6 and ABHD12 (IC₅₀
6
7 value > 10 μM in all cases). This reversible inhibitor was also tested in intact human monocytic cell
8
9 line U937, where it inhibited 2-OG hydrolysis, with an IC₅₀ value of 193 nM. Furthermore, **23** showed
10
11 antiproliferative activities in human breast MDA-MB-231, colorectal HCT116 and ovarian CAOV3,
12
13 OVCAR3 and SKOV3 cancer cells at micromolar concentrations. Finally, after intraperitoneal
14
15 injection into C57BL6 mice, compound **23** induced a significant increase of 2-AG levels in brain and
16
17 plasma confirming its MAGL inhibition *in vivo*. These preliminary *in vivo* studies suggest that the
18
19 effects of this compound could be further explored. In particular, a wide *in silico* and *in vitro* ADME
20
21 evaluation will be developed and, in case of potential problems, compound's modifications supported
22
23 by molecular modeling will be carried out to maintain the potency and selectivity and to overcome
24
25 any potential ADME problems. Taken together these results suggest that, to the best of our
26
27 knowledge, compound **23** is one of the most active and selective MAGL reversible inhibitors so far
28
29 reported in literature and may thus open new perspectives to study the therapeutic potential of
30
31 reversible MAGL inhibition. The biological characterization of reversible MAGL inhibition *in vivo*
32
33 will be addressed in a future work focused on the pharmacology of this new class of compounds.
34
35 Compound **23** is the most potent inhibitor of this series, but it may need to be further optimized to
36
37 become a lead candidate for drug development.
38
39
40
41
42
43
44
45
46
47

48 **EXPERIMENTAL SECTION**

49
50 **1. Synthesis. General Procedures and Materials.** All solvents and chemicals were used as
51
52 purchased without further purification. Chromatographic separations were performed on silica gel
53
54 columns by flash chromatography (Kieselgel 40, 0.040–0.063 mm; Merck). Reactions were followed
55
56 by thin layer chromatography (TLC) on Merck aluminum silica gel (60 F254) sheets that were
57
58 visualized under a UV lamp. Evaporation was performed *in vacuo* (rotating evaporator). Sodium
59
60

1
2
3 sulfate was always used as the drying agent. Proton (^1H) and carbon (^{13}C) NMR spectra were obtained
4
5 with a Bruker Avance III 400 MHz spectrometer using the indicated deuterated solvents. Chemical
6
7 shifts are given in parts per million (ppm) (δ relative to residual solvent peak for ^1H and ^{13}C). ^1H -
8
9 NMR spectra are reported in this order: multiplicity and number of protons. Standard abbreviation
10
11 indicating the multiplicity were used as follows: s = singlet, d = doublet, dd = doublet of doublets,
12
13 ddd = doublet of doublet of doublets, t = triplet, tt = triplet of triplets, dt = doublet of triplets, td =
14
15 triplet of doublets, q = quartet, quint = quintet, sext = sextet, sept = septet, m = multiplet, bm = broad
16
17 multiplet and bs = broad signal. HPLC analysis was used to determine purity: all target compounds
18
19 (i.e., assessed in biological assays) were $\geq 95\%$ pure by HPLC, as confirmed via UV detection ($\lambda =$
20
21 254 nm). Analytical reversed-phase HPLC was conducted using a Kinetex EVO C18 column (5 μm ,
22
23 150 \times 4.6 mm, Phenomenex, Inc.); eluent A, water; eluent B, CH_3CN ; after 5 min. at 25% B, a
24
25 gradient was formed from 25% to 75% of B in 5 min and held at 75% of B for 10 min; flow rate was
26
27 1 mL/min. HPLC analyses were performed at 254 nm. Elemental analysis was used to further
28
29 characterize the final compounds; analytical results are within $\pm 0.4\%$ of the theoretical value. Yields
30
31 refer to isolated and purified products derived from non-optimized procedures. Compound **2** was
32
33 purchased from Cayman Chemical and compound **9** was synthesized as previously reported.³³
34
35
36
37
38
39

40 **1.1. General procedure for the synthesis of amide derivatives 10d, 31, 32, 33a-f, 37a-c, 43a-d,**
41
42 **49a-h, 56-60.** HATU (1.05 equiv) was added to a solution of the appropriate benzoic acid (1 equiv)
43
44 in dry DMF (2.1 mL), then DIPEA (4 equiv) was added dropwise. The resulting mixture was stirred
45
46 at room temperature for 30 min and then 4-(4-chlorobenzoyl)piperidine **30** or substituted piperidines
47
48 **47a-h, 55** (100 mg, 1 equiv) was added and left under stirring at room temperature until consumption
49
50 of starting material (TLC). After this time, the residue was diluted with water and extracted with
51
52 EtOAc. The organic layer was repeatedly washed with brine, dried over Na_2SO_4 and the solvent was
53
54 removed under reduced pressure. The residue was purified with a flash column chromatography
55
56 (silica gel, appropriate mixture of *n*-hexane/ethyl acetate) or with a preparative TLC (only for
57
58
59
60

1
2
3 compound **10d**, mixture CHCl₃/MeOH) and pure fractions containing the desired compound were
4
5 evaporated to dryness affording the amides.
6

7
8 **1.2. General procedure for the synthesis of *O*-deprotected benzoylpiperidines **10a-c**, **11a-d**, **12a-****

9
10 **d**, **13a-d**, **14-26**. A solution of pure *O*-methylated amides (0.23 mmol) in anhydrous CH₂Cl₂ (2.7 mL)
11
12 was cooled to -10 °C and treated dropwise with a 1.0 M solution of BBr₃ in CH₂Cl₂ (0.73 mL) under
13
14 argon. The mixture was left under stirring at the same temperature for 5 min and then at 0 °C for 1 h
15
16 and finally at RT until starting material was consumed (TLC). For compound **20**, further 0.36 mL
17
18 BBr₃ were added. The mixture was then diluted with water and extracted with ethyl acetate. The
19
20 organic phase was washed with brine, dried and concentrated. The crude product was purified by
21
22 flash chromatography over silica gel. Elution with *n*-hexane/EtOAc mixtures afforded the desired
23
24 compounds.
25
26
27

28
29 **1.3. General procedure for the synthesis of methyl 3-methoxybenzoates **35a-c****. A solution of

30
31 phenolic derivatives **34a-c** (300 mg, 1 equiv) in 6 mL of DMF was treated with anhydrous K₂CO₃
32
33 (2.2 equiv) and iodomethane (3 equiv) and the reaction mixture was stirred at room temperature for
34
35 24 h. The mixture was diluted with water and extracted into ethyl acetate. The organic extract was
36
37 repeatedly washed with brine, and the organic solvent was removed under vacuum on a rotary
38
39 evaporator. The crude product afforded the pure desired compounds **35a-c**, that were used in the next
40
41 step without further purification.
42
43

44
45 **1.4. General procedure for the synthesis of 3-methoxybenzoic acids **36a-c**, **42a-d****. Methyl esters

46
47 **35a-c** (200 mg) were dissolved in a 1:1 v/v mixture of THF/methanol (7 mL) and treated with 2.1 mL
48
49 of 2 N aqueous solution of LiOH. The reaction was stirred overnight, then the solvents were
50
51 evaporated, and the residue was treated with 1 N aqueous HCl and extracted with EtOAc. The organic
52
53 phase was dried and evaporated to afford the pure desired carboxylic acid derivatives.
54
55

56
57 **1.5. General procedure for the synthesis of methyl 3-methoxybenzoates **39a-b****. Under argon

58
59 atmosphere, thionyl chloride (2.5 equiv) was added dropwise to a solution of commercially available
60
benzoic acids **38a-b** (400 mg, 1 equiv) in dry methanol (17 mL) cooled in an ice bath and then the

1
2
3 mixture was refluxed at 80 °C until starting material was not more present (TLC). The reaction
4
5 mixture was cooled to room temperature and then carefully diluted with water and ethyl acetate and
6
7 the organic phase was washed with saturated aqueous NaHCO₃ solution. The organic layer was dried
8
9 over Na₂SO₄ and concentrated. Pure methyl esters **39a-b** were obtained and used in the next step
10
11 without any further purification.
12
13

14 **1.6. General procedure for the synthesis of iodinated derivatives 41a, c, d.** To a solution of **39a-**
15 **b**, commercially available methyl 2-amino-5-methoxybenzoate **40** (200 mg, 1 equiv) in H₂SO₄ (0.2
16
17 mL) and water (1.5 mL) cooled to -5 °C, a solution of sodium nitrite (1.05 equiv) in water (1.1 mL)
18
19 was added dropwise. The mixture was stirred for 30 min, then a solution of potassium iodide (1.5 eq)
20
21 in water (1.1 mL) was added dropwise. The reaction was stirred for 1-3 h at room temperature and
22
23 then extracted with EtOAc. The combined organic extracts were washed with saturated aqueous
24
25 Na₂S₂O₃, dried with anhydrous Na₂SO₄, filtered and concentrated. The crude product was purified by
26
27 flash column chromatography to obtain the title compounds.
28
29
30
31
32

33 **1.7. General procedure for the synthesis of compounds 46a-h, 53.** To a cooled suspension of 1-
34
35 acetylpiperidine-4-carboxylic acid **45** or 1-benzoylpiperidine-4-carboxylic acid **52** (500 mg, 1 equiv)
36
37 in 2.7 mL of anhydrous 1,2-dichloroethane was slowly added SOCl₂ (2.3 equiv). The mixture was
38
39 stirred at 60 °C for 4 h (the mixture turned from white to orange) and then evaporated under vacuum.
40
41 Under argon atmosphere, the residue acyl chloride was dissolved in 2.2 mL of anhydrous 1,2-
42
43 dichloroethane, then the reddish solution was cooled and AlCl₃ (2 equiv) was slowly added. Finally,
44
45 a solution of the aromatic reagent (1 equiv; benzene, toluene, ethylbenzene, *n*-propylbenzene,
46
47 cumene, *n*-butylbenzene, anisole, benzo-1,4-dioxane or bromobenzene) in anhydrous 1,2-
48
49 dichloroethane (1.3 mL) was added dropwise. The mixture was stirred at 90 °C overnight. The
50
51 solution was cooled to room temperature and poured into ice. The water layer was extracted with
52
53 EtOAc, the combined organic phase was washed with brine, dried over anhydrous sodium sulfate and
54
55 concentrated in vacuo. The residue was purified by silica gel chromatography using appropriate *n*-
56
57 hexane/EtOAc mixtures.
58
59
60

1.8. General procedure for the synthesis of piperidine derivatives 47a-h and 55. To a solution of *N*-acetylated intermediates **46a-h** or *N*-benzoylated intermediate **54** (400 mg) in 17 mL of EtOH, 1 N aqueous solution of NaOH was added (17 mL). The reaction mixture was heated at 90 °C (for **47a-h**) or 95 °C (for **55**) overnight. The solution was cooled to room temperature, then concentrated under reduced pressure, diluted with water and extracted with EtOAc. The organic layer was washed with brine, dried over Na₂SO₄ and concentrated to dryness to obtain the pure desired compounds **47a-h**, **55** that were used in the next step without further purification.

(4-(4-Chlorobenzoyl)piperidin-1-yl)(3-hydroxy-2-iodophenyl)methanone (10a). Light grey solid; 94% yield from **43a**, eluent *n*-hexane/EtOAc 1:1. ¹H-NMR (acetone-*d*₆; asterisk denotes isomer peaks) δ (ppm): 1.52-2.02 (m, 4H), 2.98-3.08 (m, 1H), 3.16-3.33 (m, 1H), 3.41-3.53 (m, 1H), 3.74-3.84 (m, 1H), 4.64-4.72 (m, 1H), 6.68* (dd, 1H, *J* = 7.5, 1.4 Hz), 6.77 (dd, 1H, *J* = 7.4, 1.4 Hz), 6.94* (dd, 1H, *J* = 8.1, 1.4 Hz), 6.94 (dd, 1H, *J* = 8.0, 1.4 Hz), 7.26* (t, 1H, *J* = 7.7 Hz), 7.27 (t, 1H, *J* = 7.7 Hz), 7.54-7.59 (m, 2H), 8.06* (AA'XX', 2H, *J*_{AX} = 8.6 Hz, *J*_{AA'/XX'} = 2.2 Hz), 8.07 (AA'XX', 2H, *J*_{AX} = 8.7 Hz, *J*_{AA'/XX'} = 2.3 Hz), 9.20-9.35 (exchangeable bs, 1H). ¹³C-NMR (acetone-*d*₆; asterisk denotes isomer peaks) δ (ppm): 28.84, 29.10*, 29.34, 41.26, 41.33*, 43.83, 43.98*, 46.54, 47.09*, 83.29, 83.58*, 115.23, 118.74*, 118.98, 129.78 (2C), 130.53*, 130.70, 130.95* (2C), 130.97 (2C), 135.45*, 135.48, 139.53, 139.57*, 145.66, 145.80*, 157.77, 157.95*, 169.32*, 169.53, 201.25. HPLC analysis: retention time = 11.702 min; peak area, 95% (254 nm). Elemental analysis for C₁₉H₁₇ClINO₃, calculated: % C, 48.58; % H, 3.65; % N, 2.98; found: % C, 48.90; % H, 4.01; % N, 2.59.

(1-(2-Bromo-3-hydroxybenzoyl)piperidin-4-yl)(4-chlorophenyl)methanone (10b). Light yellow solid; 43% yield from **43b**, eluent *n*-hexane/EtOAc 1:1. ¹H-NMR (acetone-*d*₆; asterisk denotes isomer peaks) δ (ppm): 1.52-1.87 (bm, 4H), 3.04 (tt, 1H, *J* = 13.0, 3.6 Hz), 3.16-3.34 (bm, 1H), 3.43-3.55 (bm, 1H), 3.73-3.84 (bm, 1H), 4.63-4.72 (bm, 1H), 6.74* (dd, 1H, *J* = 7.4, 1.5 Hz), 6.84 (dd, 1H, *J* = 7.4, 1.5 Hz), 7.01* (dd, 1H, *J* = 8.1, 1.4 Hz), 7.02 (dd, 1H, *J* = 8.1, 1.5 Hz), 7.25* (t, 1H, *J* = 7.1 Hz), 7.27 (t, 1H, *J* = 7.4 Hz), 7.54-7.59 (m, 2H), 8.06* (AA'XX', 2H, *J*_{AX} = 8.6 Hz, *J*_{AA'/XX'} = 2.2 Hz),

8.07 (AA'XX', 2H, $J_{AX} = 8.6$ Hz, $J_{AA'/XX'} = 2.0$ Hz), 9.07* (exchangeable bs, 1H), 9.10 (exchangeable bs, 1H). ^{13}C -NMR (acetone- d_6 ; asterisk denotes isomer peaks) δ (ppm): 29.04, 29.14*, 32.28, 41.16, 41.27*, 43.86, 43.97*, 46.35, 47.00*, 107.40*, 107.60, 116.79*, 116.83, 119.12*, 119.33, 129.64*, 129.78, 129.80 (2C), 130.98 (2C), 135.48, 135.51*, 139.55, 139.59*, 141.36, 141.48*, 155.20, 155.33*, 167.34, 167.59*, 201.24. HPLC analysis: retention time = 11.589 min; peak area, 98% (254 nm). Elemental analysis for $\text{C}_{19}\text{H}_{17}\text{BrClNO}_3$, calculated: % C, 53.99; % H, 4.05; % N, 3.31; found: % C, 54.15; % H, 3.88; % N, 3.03.

(1-(2-Chloro-3-hydroxybenzoyl)piperidin-4-yl)(4-chlorophenyl)methanone (10c). White solid; 74% yield from **31**, eluent *n*-hexane/EtOAc 1:1. ^1H -NMR (DMSO- d_6 ; asterisk denotes isomer peaks) δ (ppm): 1.34-1.62 (bm, 2H), 1.66-1.77 (bm, 1H), 1.85-1.95 (bm, 1H), 2.93-3.03 (m, 1H), 3.09-3.25 (bm, 2H), 3.66-3.80 (bm, 1H), 4.46-4.58 (bm, 1H), 6.72 (dd, 1H, $J = 7.5, 1.4$ Hz), 6.76* (dd, 1H, $J = 7.5, 1.5$ Hz), 6.95-7.05 (m, 1H), 7.19 (t, 1H, $J = 7.8$ Hz), 7.61 (AA'XX', 2H, $J_{AX} = 8.7$ Hz, $J_{AA'/XX'} = 2.3$ Hz), 8.02 (AA'XX', 2H, $J_{AX} = 8.7$ Hz, $J_{AA'/XX'} = 2.2$ Hz), 10.43 (exchangeable s, 1H). ^{13}C -NMR (DMSO- d_6 ; asterisk denotes isomer peaks) δ (ppm): 28.03, 28.17*, 28.45, 40.21, 42.28, 42.34*, 45.15, 45.83*, 115.86, 115.95*, 116.35*, 116.41, 117.33*, 117.36, 128.09*, 128.19, 128.93 (2C), 130.16 (2C), 134.04, 137.37*, 137.49, 138.18, 153.32, 153.39*, 165.46, 165.68*, 200.78, 200.83*. HPLC analysis: retention time = 11.513 min; peak area, 98% (254 nm). Elemental analysis for $\text{C}_{19}\text{H}_{17}\text{Cl}_2\text{NO}_3$, calculated: % C, 60.33; % H, 4.53; % N, 3.70; found: % C, 60.57; % H, 4.90; % N, 3.96.

(4-(4-Chlorobenzoyl)piperidin-1-yl)(2-fluoro-3-hydroxyphenyl)methanone (10d). White solid; 23% yield from 2-fluoro-3-hydroxybenzoic acid **27b** and **30**, eluent $\text{CHCl}_3/\text{MeOH}$ 99:1. ^1H -NMR (DMSO- d_6) δ (ppm): 1.38-1.56 (bm, 2H), 1.69-1.80 (bm, 1H), 1.86-1.95 (bm, 1H), 2.94-3.05 (m, 1H), 3.15-3.27 (bm, 1H), 3.42-3.51 (m, 1H), 3.69-3.80 (m, 1H), 4.47-4.56 (m, 1H), 6.69-6.76 (m, 1H), 6.99 (td, 1H, $J = 8.2, 1.9$ Hz), 7.04 (t, 1H, $J = 7.8$ Hz), 7.61 (AA'XX', 2H, $J_{AX} = 8.7$ Hz, $J_{AA'/XX'} = 2.2$ Hz), 8.02 (AA'XX', 2H, $J_{AX} = 8.6$ Hz, $J_{AA'/XX'} = 2.1$ Hz), 10.01 (exchangeable bs, 1H). ^{13}C -NMR (DMSO- d_6) δ (ppm): 28.11, 28.46, 40.49, 42.28, 45.82, 117.42 (d, $J = 2.3$ Hz), 118.33 (d, $J =$

2.9 Hz), 124.84 (d, $J = 4.1$ Hz), 125.32 (d, $J = 15.6$ Hz), 128.94 (2C), 130.18 (2C), 134.07, 138.18, 145.03 (d, $J = 11.9$ Hz), 146.72 (d, $J = 242.5$ Hz), 163.94, 200.80. HPLC analysis: retention time = 11.417 min; peak area, 96% (254 nm). Elemental analysis for $C_{19}H_{17}ClFNO_3$, calculated: % C, 63.08; % H, 4.74; % N, 3.87; found: % C, 62.69; % H, 5.10; % N, 4.13.

(4-(4-Chlorobenzoyl)piperidin-1-yl)(5-hydroxy-2-iodophenyl)methanone (11a). Amber solid; 24% yield from **43c**, eluent *n*-hexane/EtOAc 1:1. 1H -NMR (acetone- d_6 ; asterisk denotes isomer peaks) δ (ppm): 1.54-2.03 (bm, 4H), 2.97-3.08 (m, 1H), 3.17-3.35 (m, 1H), 3.44-3.55 (m, 1H), 3.74-3.85 (m, 1H), 4.62-4.69 (m, 1H), 6.69 (dd, 1H, $J = 8.6, 3.0$ Hz), 6.72* (d, 1H, $J = 2.7$ Hz), 6.81 (d, 1H, $J = 3.0$ Hz), 7.54-7.59 (m, 2H), 7.64 (d, 1H, $J = 8.6$ Hz), 7.66* (d, 1H, $J = 8.4$ Hz), 8.03-8.10 (m, 2H), 8.86 (exchangeable s, 1H). ^{13}C -NMR (acetone- d_6 ; asterisk denotes isomer peaks) δ (ppm): 28.87*, 29.13, 39.71, 41.27, 43.85, 43.98*, 46.57, 47.08*, 79.45, 79.66*, 115.20*, 115.43, 118.64*, 118.75, 129.81 (2C), 130.98 (2C), 131.01* (2C), 135.46, 135.49*, 139.56*, 139.61, 140.72, 140.95*, 144.86, 145.03*, 158.74*, 158.86, 168.82*, 168.94, 201.25. HPLC analysis: retention time = 12.107 min; peak area, 95% (254 nm). Elemental analysis for $C_{19}H_{17}ClINO_3$, calculated: % C, 48.58; % H, 3.65; % N, 2.98; found: % C, 48.86; % H, 3.90; % N, 2.69.

(1-(2-Bromo-5-hydroxybenzoyl)piperidin-4-yl)(4-chlorophenyl)methanone (11b). White solid; 69% yield from **32**, eluent *n*-hexane/EtOAc 1:1. 1H -NMR (acetone- d_6 ; asterisk denotes isomer peaks) δ (ppm): 1.53-2.01 (m, 4H), 2.98-3.08 (m, 1H), 3.19-3.35 (m, 1H), 3.47-3.56 (m, 1H), 3.73-3.85 (m, 1H), 4.61-4.70 (m, 1H), 6.75* (d, 1H, $J = 3.0$ Hz), 6.81 (d, 1H, $J = 3.0$ Hz), 6.82-6.85 (m, 1H), 7.42* (d, 1H, $J = 8.9$ Hz), 7.43 (d, 1H, $J = 8.7$ Hz), 7.54-7.59 (m, 2H), 8.05* (AA'XX', 2H, $J_{AX} = 8.6$ Hz, $J_{AA'/XX'} = 2.3$ Hz), 8.07 (AA'XX', 2H, $J_{AX} = 8.7$ Hz, $J_{AA'/XX'} = 2.5$ Hz), 8.86 (exchangeable s, 1H). ^{13}C -NMR (DMSO- d_6 ; asterisk denotes isomer peaks) δ (ppm): 27.96*, 28.09, 28.19*, 28.36, 40.23, 42.28, 42.37*, 45.29*, 45.88, 106.45*, 106.51, 114.30, 114.33*, 117.62*, 117.76, 128.98 (2C), 130.21* (2C), 130.22 (2C), 133.31*, 133.45, 134.04*, 134.06, 138.21*, 138.24, 138.81*, 138.97, 157.03*, 157.10, 166.04*, 166.21, 200.82, 200.85*. HPLC analysis: retention time = 11.946 min;

1
2
3 peak area, 95% (254 nm). Elemental analysis for $C_{19}H_{17}BrClNO_3$, calculated: % C, 53.99; % H, 4.05;
4
5 % N, 3.31; found: % C, 54.35; % H, 4.26; % N, 3.58.

6
7 **(1-(2-Chloro-5-hydroxybenzoyl)piperidin-4-yl)(4-chlorophenyl)methanone (11c)**. Light grey
8
9 solid; 88% yield from **37a**, eluent *n*-hexane/EtOAc 55:45. 1H -NMR (DMSO- d_6 ; asterisk denotes
10
11 isomer peaks) δ (ppm): 1.38-1.65 (m, 2H), 1.69-1.78 (m, 1H), 1.86-1.94 (m, 1H), 2.93-3.04 (m, 1H),
12
13 3.10-3.27 (m, 1H), 3.35-3.40 (m, 1H), 3.65-3.81 (m, 1H), 4.45-4.55 (m, 1H), 6.65* (d, 1H, $J = 2.9$
14
15 Hz), 6.71 (d, 1H, $J = 2.9$ Hz), 6.80* (dd, 1H, $J = 8.7, 2.8$ Hz), 6.81 (dd, 1H, $J = 8.8, 2.9$ Hz), 7.27 (d,
16
17 1H, $J = 8.8$ Hz), 7.28* (d, 1H, $J = 8.7$ Hz), 7.58-7.64 (m, 2H), 7.99-8.05 (m, 2H), 9.94 (exchangeable
18
19 bs, 1H). ^{13}C -NMR (DMSO- d_6 ; asterisk denotes isomer peaks) δ (ppm): 28.02, 28.07*, 28.21*, 28.40,
20
21 40.23, 42.25, 42.30*, 45.22*, 45.83, 114.04, 117.21*, 117.37, 118.26, 118.30*, 128.94 (2C), 130.17
22
23 (2C), 130.24, 130.33*, 134.02, 134.05*, 136.60, 136.77*, 138.18*, 138.21, 156.50*, 156.55, 165.21*,
24
25 165.39, 200.78, 200.82*. HPLC analysis: retention time = 11.868 min; peak area, 99% (254 nm).
26
27 Elemental analysis for $C_{19}H_{17}Cl_2NO_3$, calculated: % C, 60.33; % H, 4.53; % N, 3.70; found: % C,
28
29 60.50; % H, 4.80; % N, 3.50.

30
31 **(4-(4-Chlorobenzoyl)piperidin-1-yl)(2-fluoro-5-hydroxyphenyl)methanone (11d)**. Light grey
32
33 solid; 85% yield from **37b**, eluent *n*-hexane/EtOAc 1:1. 1H -NMR (DMSO- d_6) δ (ppm): 1.38-1.53
34
35 (bm, 2H), 1.71-1.80 (bm, 1H), 1.85-1.94 (bm, 1H), 2.93-3.04 (m, 1H), 3.14-3.28 (bm, 1H), 3.44-3.53
36
37 (bm, 1H), 3.69-3.80 (m, 1H), 4.45-4.54 (m, 1H), 6.64-6.70 (m, 1H), 6.80 (ddd, 1H, $J = 8.9, 4.3, 3.1$
38
39 Hz), 7.08 (t, 1H, $J = 9.1$ Hz), 7.61 (AA'XX', 2H, $J_{AX} = 8.7$ Hz, $J_{AA'/XX'} = 2.2$ Hz), 8.02 (AA'XX',
40
41 2H, $J_{AX} = 8.7$ Hz, $J_{AA'/XX'} = 2.2$ Hz), 9.64 (exchangeable s, 1H). ^{13}C -NMR (DMSO- d_6) δ (ppm):
42
43 28.11, 28.45, 40.53, 42.26, 45.82, 113.94 (d, $J = 3.7$ Hz), 116.40 (d, $J = 23.0$ Hz), 117.21 (d, $J = 7.7$
44
45 Hz), 124.64 (d, $J = 20.3$ Hz), 128.95 (2C), 130.19 (2C), 134.06, 138.20, 150.71 (d, $J = 235.3$ Hz),
46
47 153.74 (d, $J = 2.0$ Hz), 163.80, 200.81. HPLC analysis: retention time = 11.575 min; peak area, 98%
48
49 (254 nm). Elemental analysis for $C_{19}H_{17}ClFNO_3$, calculated: % C, 63.08; % H, 4.74; % N, 3.87;
50
51 found: % C, 62.70; % H, 5.09; % N, 4.22.

1
2
3 **(4-(4-Chlorobenzoyl)piperidin-1-yl)(3-hydroxy-5-iodophenyl)methanone (12a)**. Off-white solid;
4
5 84% yield from **43d**, eluent *n*-hexane/EtOAc 6:4. ¹H-NMR (acetone-*d*₆) δ (ppm): 1.60-1.72 (m, 2H),
6
7 1.84-2.00 (bm, 2H), 2.96-3.38 (bm, 2H), 3.79 (tt, 1H, *J* = 11.2, 3.7 Hz), 4.42-4.67 (bm, 2H), 6.89 (dd,
8
9 1H, *J* = 2.3, 1.3 Hz), 7.24 (t, 1H, *J* = 1.4 Hz), 7.29 (dd, 1H, *J* = 2.3, 1.5 Hz), 7.57 (AA'XX', 2H, *J*_{AX}
10
11 = 8.8 Hz, *J*_{AA'/XX'} = 2.2 Hz), 8.06 (AA'XX', 2H, *J*_{AX} = 8.8 Hz, *J*_{AA'/XX'} = 2.2 Hz), 8.95 (exchangeable
12
13 s, 1H). ¹³C-NMR (acetone-*d*₆) δ (ppm): 43.94, 94.60, 114.38, 126.08, 127.57, 129.83 (2C), 131.00
14
15 (2C), 135.56, 139.62, 140.86, 159.04, 168.30, 201.27. HPLC analysis: retention time = 12.419 min;
16
17 peak area, 99% (254 nm). Elemental analysis for C₁₉H₁₇ClINO₃, calculated: % C, 48.58; % H, 3.65;
18
19 % N, 2.98; found: % C, 48.90; % H, 3.99; % N, 3.16.
20
21
22

23 **(1-(3-Bromo-5-hydroxybenzoyl)piperidin-4-yl)(4-chlorophenyl)methanone (12b)**. Light grey
24
25 solid; 40% yield from **33a**, eluent *n*-hexane/EtOAc 6:4. ¹H-NMR (acetone-*d*₆) δ (ppm): 1.60-1.72 (m,
26
27 2H), 1.84-2.00 (bm, 2H), 2.96-3.40 (bm, 2H), 3.69-3.93 (bm, 1H), 3.79 (tt, 1H, *J* = 11.1, 3.7 Hz),
28
29 4.41-4.70 (bm, 1H), 6.87 (dd, 1H, *J* = 2.2, 1.4 Hz), 7.05 (t, 1H, *J* = 1.5 Hz), 7.09 (t, 1H, *J* = 2.0 Hz),
30
31 7.57 (AA'XX', 2H, *J*_{AX} = 8.8 Hz, *J*_{AA'/XX'} = 2.3 Hz), 8.06 (AA'XX', 2H, *J*_{AX} = 8.7 Hz, *J*_{AA'/XX'} = 2.2
32
33 Hz), 9.04 (exchangeable s, 1H). ¹³C-NMR (acetone-*d*₆) δ (ppm): 43.93, 113.82, 120.10, 121.56,
34
35 123.12, 129.83 (2C), 131.00 (2C), 135.55, 139.62, 140.79, 159.35, 168.50, 201.26. HPLC analysis:
36
37 retention time = 12.281 min; peak area, 97% (254 nm). Elemental analysis for C₁₉H₁₇BrClNO₃,
38
39 calculated: % C, 53.99; % H, 4.05; % N, 3.31; found: % C, 54.22; % H, 4.37; % N, 3.64.
40
41
42

43 **(1-(3-Chloro-5-hydroxybenzoyl)piperidin-4-yl)(4-chlorophenyl)methanone (12c)**. Light yellow
44
45 solid; 78% yield from **33b**, eluent *n*-hexane/EtOAc 6:4. ¹H-NMR (DMSO-*d*₆) δ (ppm): 1.42-1.56 (m,
46
47 2H), 1.70-1.95 (bm, 2H), 2.90-3.05 (bm, 1H), 3.10-3.26 (bm, 1H), 3.52-3.67 (bm, 1H), 3.74 (tt, 1H,
48
49 *J* = 11.3, 3.5 Hz), 4.35-4.52 (bm, 1H), 6.70 (dd, 1H, *J* = 2.2, 1.3 Hz), 6.81-6.88 (m, 2H), 7.62
50
51 (AA'XX', 2H, *J*_{AX} = 8.7 Hz, *J*_{AA'/XX'} = 2.2 Hz), 8.02 (AA'XX', 2H, *J*_{AX} = 8.8 Hz, *J*_{AA'/XX'} = 2.3 Hz),
52
53 10.22 (exchangeable bs, 1H). ¹³C-NMR (DMSO-*d*₆) δ (ppm): 42.40, 112.33, 116.11, 116.89, 129.00
54
55 (2C), 130.24 (2C), 133.71, 134.12, 138.22, 139.05, 158.48, 167.38, 200.89. HPLC analysis: retention
56
57
58
59
60

1
2
3 time = 12.152 min; peak area, 98% (254 nm). Elemental analysis for $C_{19}H_{17}Cl_2NO_3$, calculated: % C,
4 60.33; % H, 4.53; % N, 3.70; found: % C, 60.01; % H, 4.14; % N, 3.95.

7 **(4-(4-Chlorobenzoyl)piperidin-1-yl)(3-fluoro-5-hydroxyphenyl)methanone (12d)**. White solid;
8
9 77% yield from **33c**, eluent *n*-hexane/EtOAc 6:4. 1H -NMR (DMSO- d_6) δ (ppm): 1.43-1.58 (m, 2H),
11 1.65-1.95 (bm, 2H), 2.85-3.30 (bm, 2H), 3.50-3.69 (bm, 1H), 3.74 (tt, 1H, $J = 11.2, 3.4$ Hz), 4.32-
13 4.57 (bm, 1H), 6.57-6.65 (m, 3H), 7.61 (AA'XX', 2H, $J_{AX} = 8.8$ Hz, $J_{AA'/XX'} = 2.3$ Hz), 8.02
15 (AA'XX', 2H, $J_{AX} = 8.8$ Hz, $J_{AA'/XX'} = 2.2$ Hz), 10.17 (exchangeable s, 1H). ^{13}C -NMR (DMSO- d_6)
17 δ (ppm): 42.37, 103.37 (d, $J = 23.7$ Hz), 103.40 (d, $J = 23.2$ Hz), 109.71 (d, $J = 2.6$ Hz), 128.95 (2C),
19 130.19 (2C), 134.08, 138.18, 138.85 (d, $J = 9.5$ Hz), 159.02 (d, $J = 11.8$ Hz), 162.7 (d, $J = 243.65$
21 Hz), 167.59 (d, $J = 3.0$ Hz), 200.85. HPLC analysis: retention time = 11.749 min; peak area, 98%
23 (254 nm). Elemental analysis for $C_{19}H_{17}ClFNO_3$, calculated: % C, 63.08; % H, 4.74; % N, 3.87;
25 found: % C, 62.70; % H, 5.10; % N, 4.22.

30 **(4-(4-Chlorobenzoyl)piperidin-1-yl)(3-hydroxy-4-iodophenyl)methanone (13a)**. White solid;
31
32 33% yield from **37c**, eluent *n*-hexane/EtOAc 1:1. 1H -NMR (acetone- d_6) δ (ppm): 1.59-1.71 (m, 2H),
33 1.82-2.01 (bm, 2H), 2.91-3.38 (bm, 2H), 3.71-3.97 (bm, 1H), 3.80 (tt, 1H, $J = 11.3, 3.7$ Hz), 4.45-
35 4.71 (bm, 1H), 6.71 (dd, 1H, $J = 8.0, 1.9$ Hz), 7.00 (d, 1H, $J = 1.8$ Hz), 7.57 (AA'XX', 2H, $J_{AX} = 8.8$
37 Hz, $J_{AA'/XX'} = 2.3$ Hz), 7.79 (d, 1H, $J = 8.0$ Hz), 8.07 (AA'XX', 2H, $J_{AX} = 8.8$ Hz, $J_{AA'/XX'} = 2.2$ Hz),
39 9.41 (exchangeable bm, 1H). ^{13}C -NMR (DMSO- d_6) δ (ppm): 42.38, 85.94, 112.99, 119.15, 128.99
41 (2C), 130.23 (2C), 134.08, 137.39, 138.21, 138.94, 156.59, 168.12, 200.92. HPLC analysis: retention
43 time = 12.430 min; peak area, 97% (254 nm). Elemental analysis for $C_{19}H_{17}ClINO_3$, calculated: % C,
45 48.58; % H, 3.65; % N, 2.98; found: % C, 48.25; % H, 3.30; % N, 2.66.

51 **(1-(4-Bromo-3-hydroxybenzoyl)piperidin-4-yl)(4-chlorophenyl)methanone (13b)**. White solid;
52
53 70% yield from **33d**, eluent *n*-hexane/EtOAc 1:1. 1H -NMR (acetone- d_6) δ (ppm): 1.59-1.72 (m, 2H),
54 1.80-2.01 (bm, 2H), 2.93-3.35 (bm, 2H), 3.73-3.97 (bm, 1H), 3.80 (tt, 1H, $J = 11.2, 3.7$ Hz), 4.40-
56 4.68 (bm, 1H), 6.85 (dd, 1H, $J = 8.2, 1.8$ Hz), 7.06 (d, 1H, $J = 1.8$ Hz), 7.53-7.60 (m, 3H), 8.06
58 (AA'XX', 2H, $J_{AX} = 8.6$ Hz, $J_{AA'/XX'} = 2.2$ Hz), 9.16 (exchangeable bs, 1H). ^{13}C -NMR (acetone- d_6)
60

1
2
3 δ (ppm): 43.98, 111.46, 115.84, 120.34, 129.84 (2C), 131.01 (2C), 134.00, 135.55, 138.40, 139.63,
4
5 154.93, 169.18, 201.32. HPLC analysis: retention time = 12.168 min; peak area, 98% (254 nm).
6
7 Elemental analysis for $C_{19}H_{17}BrClNO_3$, calculated: % C, 53.99; % H, 4.05; % N, 3.31; found: % C,
8
9 54.22; % H, 4.27; % N, 3.65.

10
11
12 **(1-(4-Chloro-3-hydroxybenzoyl)piperidin-4-yl)(4-chlorophenyl)methanone (13c)**. Off-white
13
14 solid; 81% yield from **33e**, eluent *n*-hexane/EtOAc 1:1. 1H -NMR (acetone- d_6) δ (ppm): 1.60-1.71 (m,
15
16 2H), 1.85-2.00 (bm, 2H), 2.95-3.36 (bm, 2H), 3.73-4.00 (bm, 1H), 3.80 (tt, 1H, $J = 11.3, 3.7$ Hz),
17
18 4.40-4.70 (bm, 1H), 6.92 (dd, 1H, $J = 8.1, 1.9$ Hz), 7.07 (d, 1H, $J = 1.8$ Hz), 7.40 (d, 1H, $J = 8.1$ Hz),
19
20 7.57 (AA'XX', 2H, $J_{AX} = 8.8$ Hz, $J_{AA'/XX'} = 2.3$ Hz), 8.07 (AA'XX', 2H, $J_{AX} = 8.8$ Hz, $J_{AA'/XX'} = 2.2$
21
22 Hz), 9.10 (exchangeable s, 1H). ^{13}C -NMR (acetone- d_6) δ (ppm): 43.96, 116.23, 119.97, 122.21,
23
24 129.83 (2C), 130.82, 131.00 (2C), 135.54, 137.64, 139.62, 153.86, 169.20, 201.30. HPLC analysis:
25
26 retention time = 12.014 min; peak area, 98% (254 nm). Elemental analysis for $C_{19}H_{17}Cl_2NO_3$,
27
28 calculated: % C, 60.33; % H, 4.53; % N, 3.70; found: % C, 60.54; % H, 4.13; % N, 3.45.

29
30
31
32 **(4-(4-Chlorobenzoyl)piperidin-1-yl)(4-fluoro-3-hydroxyphenyl)methanone (13d)**. Yellow solid;
33
34 65% yield from **33f**, eluent *n*-hexane/EtOAc 6:4. 1H -NMR (DMSO- d_6) δ (ppm): 1.42-1.55 (m, 2H),
35
36 1.65-1.96 (bm, 2H), 2.87-3.27 (bm, 2H), 3.50-3.80 (bm, 1H), 3.74 (tt, 1H, $J = 11.2, 3.5$ Hz), 4.31-
37
38 4.55 (bm, 1H), 6.81 (ddd, 1H, $J = 8.3, 4.3, 2.1$ Hz), 6.96 (dd, 1H, $J = 8.5, 2.0$ Hz), 7.18 (dd, 1H, $J =$
39
40 11.3, 8.3 Hz), 7.62 (AA'XX', 2H, $J_{AX} = 8.7$ Hz, $J_{AA'/XX'} = 2.2$ Hz), 8.01 (AA'XX', 2H, $J_{AX} = 8.8$ Hz,
41
42 $J_{AA'/XX'} = 2.3$ Hz), 10.16 (exchangeable bs, 1H). ^{13}C -NMR (DMSO- d_6) δ (ppm): 42.42, 116.14 (d, J
43
44 = 18.6 Hz), 116.37 (d, $J = 3.5$ Hz), 118.02 (d, $J = 7.1$ Hz), 128.99 (2C), 130.23 (2C), 132.68 (d, $J =$
45
46 3.7 Hz), 134.09, 138.20, 144.84 (d, $J = 12.5$ Hz), 151.44 (d, $J = 243.8$ Hz), 168.18, 200.93. HPLC
47
48 analysis: retention time = 11.528 min; peak area, 97% (254 nm). Elemental analysis for
49
50 $C_{19}H_{17}ClFNO_3$, calculated: % C, 63.08; % H, 4.74; % N, 3.87; found: % C, 62.90; % H, 5.10; % N,
51
52 3.48.

53
54
55
56
57
58 **(4-Benzoylpiperidin-1-yl)(3-hydroxyphenyl)methanone (14)**. Off-white solid; 70% yield from
59
60 **49a**, eluent *n*-hexane/EtOAc 3:7. 1H -NMR (DMSO- d_6) δ (ppm): 1.43-1.56 (m, 2H), 1.68-1.95 (bm,

2H), 2.90-3.27 (bm, 2H), 3.59-3.72 (bm, 1H), 3.76 (tt, 1H, $J = 11.2, 3.4$ Hz), 4.37-4.54 (bm, 1H), 6.72-6.75 (m, 1H), 6.77 (dt, 1H, $J = 7.8, 1.3$ Hz), 6.81 (ddd, 1H, $J = 8.2, 2.5, 1.2$ Hz), 7.23 (t, 1H, $J = 7.8$ Hz), 7.51-7.58 (m, 2H), 7.65 (tt, 1H, $J = 7.4, 1.5$ Hz), 7.98-8.03 (m, 2H), 9.67 (exchangeable s, 1H). ^{13}C -NMR (DMSO- d_6) δ (ppm): 42.40, 113.38, 116.30, 117.08, 128.26 (2C), 128.88 (2C), 129.61, 133.28, 135.45, 137.49, 157.27, 168.93, 201.92. HPLC analysis: retention time = 10.185 min; peak area, 98% (254 nm). Elemental analysis for $\text{C}_{19}\text{H}_{19}\text{NO}_3$, calculated: % C, 73.77; % H, 6.19; % N, 4.53; found: % C, 73.43; % H, 6.54; % N, 4.22.

(1-(3-Hydroxybenzoyl)piperidin-4-yl)(*p*-tolyl)methanone (15). White solid; 86% yield from **49b**, eluent *n*-hexane/EtOAc 3:7. ^1H -NMR (DMSO- d_6) δ (ppm): 1.42-1.55 (m, 2H), 1.67-1.92 (bm, 2H), 2.38 (s, 3H), 2.90-3.27 (bm, 2H), 3.58-3.68 (bm, 1H), 3.72 (tt, 1H, $J = 11.2, 3.5$ Hz), 4.38-4.53 (bm, 1H), 6.72-6.75 (m, 1H), 6.77 (dt, 1H, $J = 7.5, 1.2$ Hz), 6.81 (ddd, 1H, $J = 8.2, 2.5, 1.0$ Hz), 7.23 (t, 1H, $J = 7.8$ Hz), 7.32-7.37 (m, 2H), 7.89-7.93 (m, 2H), 9.66 (exchangeable s, 1H). ^{13}C -NMR (DMSO- d_6) δ (ppm): 21.15, 42.27, 113.37, 116.29, 117.07, 128.40 (2C), 129.42 (2C), 129.62, 132.93, 137.51, 143.68, 157.27, 168.92, 201.41. HPLC analysis: retention time = 10.930 min; peak area, 99% (254 nm). Elemental analysis for $\text{C}_{20}\text{H}_{21}\text{NO}_3$, calculated: % C, 74.28; % H, 6.55; % N, 4.33; found: % C, 73.91; % H, 6.87; % N, 3.97.

(4-(4-Ethylbenzoyl)piperidin-1-yl)(3-hydroxyphenyl)methanone (16). White solid; 87% yield from **49c**, eluent *n*-hexane/EtOAc 4:6. ^1H -NMR (DMSO- d_6) δ (ppm): 1.20 (t, 3H, $J = 7.6$ Hz), 1.42-1.55 (m, 2H), 1.65-1.95 (bm, 2H), 2.68 (q, 2H, $J = 7.6$ Hz), 2.85-3.26 (bm, 2H), 3.55-3.76 (bm, 1H), 3.73 (tt, 1H, $J = 11.4, 3.6$ Hz), 4.35-4.55 (bm, 1H), 6.72-6.75 (m, 1H), 6.77 (dt, 1H, $J = 7.5, 1.2$ Hz), 6.81 (ddd, 1H, $J = 8.2, 2.5, 1.0$ Hz), 7.23 (t, 1H, $J = 7.8$ Hz), 7.38 (d, 2H, $J = 8.4$ Hz), 7.93 (d, 2H, $J = 8.4$ Hz), 9.65 (exchangeable s, 1H). ^{13}C -NMR (DMSO- d_6) δ (ppm): 15.17, 28.15, 42.27, 113.36, 116.28, 117.06, 128.24 (2C), 128.48 (2C), 129.59, 133.17, 137.49, 149.69, 157.25, 168.91, 201.41. HPLC analysis: retention time = 11.544 min; peak area, 97% (254 nm). Elemental analysis for $\text{C}_{21}\text{H}_{23}\text{NO}_3$, calculated: % C, 74.75; % H, 6.87; % N, 4.15; found: % C, 74.44; % H, 7.20; % N, 4.55.

(1-(3-Hydroxybenzoyl)piperidin-4-yl)(4-propylphenyl)methanone (17). White solid; 86% yield from **49d**, eluent *n*-hexane/EtOAc 4:6. ¹H-NMR (CDCl₃) δ (ppm): 0.95 (t, 3H, *J* = 7.4 Hz), 1.67 (sext, 2H, *J* = 7.5 Hz), 1.74-2.08 (bm, 4H), 2.65 (t, 2H, *J* = 7.6 Hz), 2.99-3.23 (bm, 2H), 3.48-3.59 (m, 1H), 3.80-3.99 (bm, 1H), 4.57-4.75 (bm, 1H), 6.83-6.91 (m, 2H), 6.93-6.97 (m, 1H), 7.23 (t, 1H, *J* = 7.9 Hz), 7.28 (d, 2H, *J* = 8.4 Hz), 7.87 (d, 2H, *J* = 8.3 Hz). ¹³C-NMR (DMSO-*d*₆) δ (ppm): 13.57, 23.71, 37.11, 42.25, 113.35, 116.26, 117.04, 128.37 (2C), 128.78 (2C), 129.57, 133.18, 137.48, 148.10, 157.25, 168.89, 201.39. HPLC analysis: retention time = 12.121 min; peak area, 99% (254 nm). Elemental analysis for C₂₂H₂₅NO₃, calculated: % C, 75.19; % H, 7.17; % N, 3.99; found: % C, 75.38; % H, 6.78; % N, 3.62.

(1-(3-Hydroxybenzoyl)piperidin-4-yl)(4-isopropylphenyl)methanone (18). White solid; 77% yield from **49e**, eluent *n*-hexane/EtOAc 4:6. ¹H-NMR (DMSO-*d*₆) δ (ppm): 1.22 (d, 6H, *J* = 6.9 Hz), 1.40-1.56 (m, 2H), 1.63-1.96 (bm, 2H), 2.97 (sept, 1H, *J* = 6.9 Hz), 3.00-3.25 (bm, 2H), 3.58-3.78 (bm, 1H), 3.73 (tt, 1H, *J* = 11.1, 3.7 Hz), 4.36-4.54 (bm, 1H), 6.72-6.75 (m, 1H), 6.77 (dt, 1H, *J* = 7.5, 1.2 Hz), 6.81 (ddd, 1H, *J* = 8.2, 2.5, 1.0 Hz), 7.23 (t, 1H, *J* = 7.9 Hz), 7.41 (d, 2H, *J* = 8.2 Hz), 7.94 (d, 2H, *J* = 8.4 Hz), 9.66 (exchangeable s, 1H). ¹³C-NMR (DMSO-*d*₆) δ (ppm): 23.45 (2C), 33.46, 42.24, 113.35, 116.26, 117.03, 126.77 (2C), 128.49 (2C), 129.57, 133.31, 137.47, 154.15, 157.24, 168.90, 201.37. HPLC analysis: retention time = 12.009 min; peak area, 99% (254 nm). Elemental analysis for C₂₂H₂₅NO₃, calculated: % C, 75.19; % H, 7.17; % N, 3.99; found: % C, 75.46; % H, 7.48; % N, 4.17.

(4-(4-Butylbenzoyl)piperidin-1-yl)(3-hydroxyphenyl)methanone (19). White solid; 82% yield from **49f**, eluent *n*-hexane/EtOAc 4:6. ¹H-NMR (DMSO-*d*₆) δ (ppm): 0.89 (t, 3H, *J* = 7.3 Hz), 1.30 (sext, 2H, *J* = 7.4 Hz), 1.41-1.52 (m, 2H), 1.57 (quint, 2H, *J* = 7.6 Hz), 1.65-1.93 (bm, 2H), 2.65 (t, 2H, *J* = 7.6 Hz), 2.88-3.06 (bm, 1H), 3.08-3.27 (bm, 1H), 3.56-3.80 (bm, 1H), 3.73 (tt, 1H, *J* = 11.3, 3.7 Hz), 4.36-4.54 (bm, 1H), 6.72-6.75 (m, 1H), 6.77 (dt, 1H, *J* = 7.4, 1.2 Hz), 6.81 (ddd, 1H, *J* = 8.2, 2.5, 1.0 Hz), 7.23 (t, 1H, *J* = 7.8 Hz), 7.26 (d, 2H, *J* = 8.4 Hz), 7.92 (d, 2H, *J* = 8.4 Hz), 9.66 (exchangeable s, 1H). ¹³C-NMR (DMSO-*d*₆) δ (ppm): 13.71, 21.72, 32.71, 34.75, 42.55, 113.36,

1
2
3 116.27, 117.04, 128.39 (2C), 128.73 (2C), 129.57, 133.13, 137.48, 148.33, 157.26, 168.90, 201.37.

4
5 HPLC analysis: retention time = 12.648 min; peak area, 99% (254 nm). Elemental analysis for
6
7 $C_{23}H_{27}NO_3$, calculated: % C, 75.59; % H, 7.45; % N, 3.83; found: % C, 75.80; % H, 7.07; % N, 3.44.

8
9 **(4-(4-Hydroxybenzoyl)piperidin-1-yl)(3-hydroxyphenyl)methanone (20)**. Beige solid; 40% yield

10
11 from **49g**, eluent *n*-hexane/EtOAc 4:6. 1H -NMR (DMSO- d_6) δ (ppm): 1.40-1.58 (m, 2H), 1.60-1.93

12
13 (bm, 2H), 2.85-3.25 (bm, 2H), 3.55-3.75 (m, 2H), 4.35-4.56 (bm, 1H), 6.72-6.75 (m, 1H), 6.77 (dt,

14
15 1H, $J = 7.6, 1.2$ Hz), 6.81 (ddd, 1H, $J = 8.2, 2.5, 1.0$ Hz), 6.86 (AA'XX', 2H, $J_{AX} = 8.8$ Hz, $J_{AA'/XX'}$

16
17 = 2.3 Hz), 7.23 (t, 1H, $J = 7.8$ Hz), 7.89 (AA'XX', 2H, $J_{AX} = 8.8$ Hz, $J_{AA'/XX'} = 2.4$ Hz), 9.63

18
19 (exchangeable bs, 1H), 10.36 (exchangeable bs, 1H). ^{13}C -NMR (DMSO- d_6) δ (ppm): 41.85, 113.35,

20
21 115.36 (2C), 116.26, 117.04, 126.88, 129.58, 130.81 (2C), 137.51, 157.24, 162.12, 168.89, 199.92.

22
23 HPLC analysis: retention time = 4.718 min; peak area, 99% (254 nm). Elemental analysis for

24
25 $C_{19}H_{19}NO_4$, calculated: % C, 70.14; % H, 5.89; % N, 4.31; found: % C, 70.30; % H, 6.15; % N, 3.99.

26
27 **(2,3-Dihydrobenzo[b][1,4]dioxin-6-yl)(1-(3-hydroxybenzoyl)piperidin-4-yl)methanone (21)**.

28
29 Off-white solid; 50% yield from **49h**, eluent *n*-hexane/EtOAc 2:8. 1H -NMR (DMSO- d_6) δ (ppm):

30
31 1.40-1.53 (bm, 2H), 1.63-1.90 (bm, 2H), 2.90-3.03 (bm, 1H), 3.10-3.23 (bm, 2H), 3.68 (tt, 1H, $J =$

32
33 10.2, 3.7 Hz), 4.27-4.35 (m, 4H), 4.40-4.51 (bm, 1H), 6.71-6.74 (m, 1H), 6.76 (dt, 1H, $J = 7.8, 1.2$

34
35 Hz), 6.81 (ddd, 1H, $J = 8.1, 2.4, 0.9$ Hz), 6.98 (d, 1H, $J = 8.4$ Hz), 7.22 (t, 1H, $J = 7.9$ Hz), 7.50 (d,

36
37 1H, $J = 2.0$ Hz), 7.54 (dd, 1H, $J = 8.5, 2.1$ Hz), 9.67 (exchangeable bs, 1H). ^{13}C -NMR (DMSO- d_6) δ

38
39 (ppm): 41.93, 63.90, 64.52, 113.32, 116.24, 117.03, 117.21, 122.23, 128.93, 129.57, 137.48, 143.33,

40
41 147.93, 157.22 (2C), 168.87, 200.13. HPLC analysis: retention time = 10.153 min; peak area, 95%

42
43 (254 nm). Elemental analysis for $C_{21}H_{21}NO_5$, calculated: % C, 68.65; % H, 5.76; % N, 3.81; found:

44
45 % C, 69.05; % H, 5.37; % N, 4.20.

46
47 **(1-(3-Hydroxybenzoyl)piperidin-4-yl)(4-morpholinophenyl)methanone (22)**. Off-white solid;

48
49 27% yield from **56**, eluent *n*-hexane/EtOAc 35:65. 1H -NMR (DMSO- d_6) δ (ppm): 1.41-1.55 (m, 2H),

50
51 1.60-1.90 (bm, 2H), 2.85-3.24 (bm, 2H), 3.26-3.32 (m, 4H), 3.59-3.70 (m, 2H), 3.70-3.77 (m, 4H),

52
53 4.38-4.54 (bm, 1H), 6.72-6.75 (m, 1H), 6.77 (dt, 1H, $J = 7.7, 1.2$ Hz), 6.81 (ddd, 1H, $J = 8.2, 2.5, 1.0$

Hz), 6.96-7.03 (m, 2H), 7.23 (t, 1H, $J = 7.9$ Hz), 7.85-7.91 (m, 2H), 9.67 (exchangeable s, 1H). ^{13}C -NMR (DMSO- d_6) δ (ppm): 41.68, 46.75 (2C), 65.84 (2C), 113.12 (2C), 113.35, 116.26, 117.05, 125.24, 129.61, 130.15 (2C), 137.54, 154.09, 157.26, 168.89, 199.57. HPLC analysis: retention time = 9.805 min; peak area, 98% (254 nm). Elemental analysis for $\text{C}_{23}\text{H}_{26}\text{N}_2\text{O}_4$, calculated: % C, 70.03; % H, 6.64; % N, 7.10; found: % C, 70.40; % H, 7.01; % N, 6.78.

(1-(2-Fluoro-5-hydroxybenzoyl)piperidin-4-yl)(4-isopropylphenyl)methanone (23). Light yellow solid; 81% yield from **57**, eluent *n*-hexane/EtOAc 6:4. ^1H -NMR (DMSO- d_6) δ (ppm): 1.22 (d, 6H, $J = 6.9$ Hz), 1.38-1.54 (bm, 2H), 1.69-1.79 (bm, 1H), 1.84-1.94 (bm, 1H), 2.90-3.06 (m, 2H), 3.14-3.29 (bm, 1H), 3.43-3.53 (m, 1H), 3.67-3.80 (m, 1H), 4.45-4.54 (m, 1H), 6.64-6.70 (m, 1H), 6.80 (ddd, 1H, $J = 9.0, 4.2, 3.1$ Hz), 7.08 (t, 1H, $J = 9.1$ Hz), 7.41 (d, 2H, $J = 8.3$ Hz), 7.94 (d, 2H, $J = 8.4$ Hz), 9.64 (exchangeable s, 1H). ^{13}C -NMR (DMSO- d_6) δ (ppm): 23.45 (2C), 28.28, 28.59, 33.46, 40.58, 42.10, 45.89, 113.94 (d, $J = 3.7$ Hz), 116.40 (d, $J = 23.2$ Hz), 117.19 (d, $J = 7.8$ Hz), 124.68 (d, $J = 20.1$ Hz), 126.77 (2C), 128.50 (2C), 133.30, 150.71 (d, $J = 235.2$ Hz), 153.73 (d, $J = 1.5$ Hz), 154.18, 163.79, 201.30. HPLC analysis: retention time = 12.274 min; peak area, 99% (254 nm). Elemental analysis for $\text{C}_{22}\text{H}_{24}\text{FNO}_3$, calculated: % C, 71.53; % H, 6.55; % N, 3.79; found: % C, 71.23; % H, 6.82; % N, 3.48.

(4-(4-Butylbenzoyl)piperidin-1-yl)(2-fluoro-5-hydroxyphenyl)methanone (24). Off-white solid; 87% yield from **58**, eluent *n*-hexane/EtOAc 55:45. ^1H -NMR (DMSO- d_6) δ (ppm): 0.90 (t, 3H, $J = 7.4$ Hz), 1.30 (sext, 2H, $J = 7.5$ Hz), 1.39-1.53 (bm, 2H), 1.57 (quint, 2H, $J = 7.6$ Hz), 1.69-1.79 (bm, 1H), 1.84-1.94 (bm, 1H), 2.65 (t, 2H, $J = 7.8$ Hz), 2.93-3.05 (m, 1H), 3.15-3.28 (bm, 1H), 3.43-3.54 (m, 1H), 3.67-3.79 (m, 1H), 4.45-4.55 (m, 1H), 6.64-6.70 (m, 1H), 6.80 (ddd, 1H, $J = 8.9, 4.3, 3.1$ Hz), 7.08 (t, 1H, $J = 9.0$ Hz), 7.36 (d, 2H, $J = 8.3$ Hz), 7.92 (d, 2H, $J = 8.4$ Hz), 9.64 (exchangeable bs, 1H). ^{13}C -NMR (DMSO- d_6) δ (ppm): 13.67, 21.68, 28.27, 28.59, 32.66, 34.71, 40.57, 42.08, 45.86, 113.92 (d, $J = 3.5$ Hz), 116.38 (d, $J = 23.1$ Hz), 117.17 (d, $J = 7.6$ Hz), 124.66 (d, $J = 20.1$ Hz), 128.37 (2C), 128.71 (2C), 133.10, 148.33, 150.70 (d, $J = 235.2$ Hz), 153.72 (d, $J = 1.4$ Hz), 163.77, 201.29. HPLC analysis: retention time = 12.889 min; peak area, 98% (254 nm). Elemental analysis for

$C_{23}H_{26}FNO_3$, calculated: % C, 72.04; % H, 6.83; % N, 3.65; found: % C, 72.28; % H, 7.19; % N, 3.86.

(1-(4-Fluoro-3-hydroxybenzoyl)piperidin-4-yl)(4-isopropylphenyl)methanone (25). White solid; 17% yield from **59**, eluent *n*-hexane/EtOAc 65:35. 1H -NMR (DMSO- d_6) δ (ppm): 1.22 (d, 6H, $J = 6.9$ Hz), 1.43-1.57 (m, 2H), 1.70-1.92 (bm, 2H), 2.97 (sept, 1H, $J = 6.9$ Hz), 2.90-3.25 (bm, 2H), 3.65-3.80 (bm, 1H), 3.72 (tt, 1H, $J = 11.4, 3.5$ Hz), 4.24-4.60 (bm, 1H), 6.81 (ddd, 1H, $J = 8.3, 4.3, 2.1$ Hz), 6.96 (dd, 1H, $J = 8.5, 2.1$ Hz), 7.18 (dd, 1H, $J = 11.3, 8.3$ Hz), 7.41 (d, 2H, $J = 8.2$ Hz), 7.94 (d, 2H, $J = 8.4$ Hz), 10.12 (exchangeable bs, 1H). ^{13}C -NMR (DMSO- d_6) δ (ppm): 23.44 (2C), 33.44, 42.22, 116.05 (d, $J = 18.9$ Hz), 116.34 (d, $J = 3.3$ Hz), 117.97 (d, $J = 7.0$ Hz), 126.75 (2C), 128.48 (2C), 132.69 (d, $J = 3.7$ Hz), 133.31, 144.81 (d, $J = 12.5$ Hz), 151.41 (d, $J = 243.6$ Hz), 154.14, 168.15, 201.37. HPLC analysis: retention time = 12.239 min; peak area, 99% (254 nm). Elemental analysis for $C_{22}H_{24}FNO_3$, calculated: % C, 71.53; % H, 6.55; % N, 3.79; found: % C, 71.84; % H, 6.20; % N, 3.45.

(4-(4-Butylbenzoyl)piperidin-1-yl)(4-fluoro-3-hydroxyphenyl)methanone (26). White solid; 55% yield from **60**, eluent *n*-hexane/EtOAc 6:4. 1H -NMR (DMSO- d_6) δ (ppm): 0.89 (t, 3H, $J = 7.4$ Hz), 1.30 (sext, 2H, $J = 7.4$ Hz), 1.44-1.55 (m, 2H), 1.57 (quint, 2H, $J = 7.6$ Hz), 1.70-1.90 (bm, 2H), 2.65 (t, 2H, $J = 7.7$ Hz), 2.83-3.37 (bm, 2H), 3.54-3.81 (bm, 1H), 3.72 (tt, 1H, $J = 11.3, 3.5$ Hz), 4.20-4.60 (bm, 1H), 6.81 (ddd, 1H, $J = 8.3, 4.3, 2.1$ Hz), 6.96 (dd, 1H, $J = 8.5, 2.1$ Hz), 7.18 (dd, 1H, $J = 11.1, 8.3$ Hz), 7.35 (d, 2H, $J = 8.4$ Hz), 7.92 (d, 2H, $J = 8.4$ Hz), 10.11 (exchangeable bs, 1H). ^{13}C -NMR (DMSO- d_6) δ (ppm): 13.70, 21.72, 32.70, 34.75, 42.25, 116.11 (d, $J = 18.7$ Hz), 116.38 (d, $J = 3.3$ Hz), 118.00 (d, $J = 6.9$ Hz), 128.39 (2C), 128.73 (2C), 132.72 (d, $J = 3.6$ Hz), 133.17, 144.85 (d, $J = 12.4$ Hz), 148.33, 151.45 (d, $J = 243.5$ Hz), 169.18, 201.39. HPLC analysis: retention time = 12.863 min; peak area, 98% (254 nm). Elemental analysis for $C_{23}H_{26}FNO_3$, calculated: % C, 72.04; % H, 6.83; % N, 3.65; found: % C, 72.16; % H, 7.03; % N, 3.29.

(1-(2-Chloro-3-methoxybenzoyl)piperidin-4-yl)(4-chlorophenyl)methanone (31). 59% yield from 2-chloro-3-methoxybenzoic acid **27a** and **30**. 1H -NMR (CDCl₃; asterisk denotes isomer peaks)

1
2
3 δ (ppm): 1.65-2.10 (m, 4H), 3.02-3.30 (m, 2H), 3.40-3.65 (m, 2H), 3.94* (s, 3H), 3.95 (s, 3H), 4.68-
4
5 4.85 (m, 1H), 6.88 (dd, 1H, $J = 7.6, 1.4$ Hz), 6.92-7.00 (m, 1H), 7.27-7.34 (m, 1H), 7.45-7.51 (m,
6
7 2H), 7.89* (AA'XX', 2H, $J_{AX} = 8.7$ Hz, $J_{AA'/XX'} = 2.3$ Hz), 7.90 (AA'XX', 2H, $J_{AX} = 8.8$ Hz, $J_{AA'/XX'}$
8
9 = 2.3 Hz).

10
11
12 **(1-(2-Bromo-5-methoxybenzoyl)piperidin-4-yl)(4-chlorophenyl)methanone (32)**. 72% yield
13
14 from 2-bromo-5-methoxybenzoic acid **28** and **30**. ¹H-NMR (CDCl₃; asterisk denotes isomer peaks) δ
15
16 (ppm): 1.66-2.09 (m, 4H), 3.02-3.14 (m, 1H), 3.21-3.30 (m, 1H), 3.41-3.63 (m, 2H), 3.79* (s, 3H),
17
18 3.80 (s, 3H), 4.67-4.78 (bm, 1H), 6.76-6.83 (m, 2H), 7.41-7.48 (m, 3H), 7.85-7.90 (m, 2H).

19
20
21 **(1-(3-Bromo-5-methoxybenzoyl)piperidin-4-yl)(4-chlorophenyl)methanone (33a)**. 70% yield
22
23 from 3-bromo-5-methoxybenzoic acid **29a** and **30**. ¹H-NMR (CDCl₃) δ (ppm): 1.72-2.09 (bm, 4H),
24
25 2.97-3.26 (bm, 2H), 3.44-3.54 (m, 1H), 3.73-3.95 (bm, 1H), 3.81 (s, 3H), 4.50-4.75 (bm, 1H), 6.86
26
27 (dd, 1H, $J = 2.2, 1.4$ Hz), 7.08-7.12 (m, 2H), 7.46 (AA'XX', 2H, $J_{AX} = 8.6$ Hz, $J_{AA'/XX'} = 2.2$ Hz),
28
29 7.88 (AA'XX', 2H, $J_{AX} = 8.6$ Hz, $J_{AA'/XX'} = 2.2$ Hz).

30
31
32 **(1-(3-Chloro-5-methoxybenzoyl)piperidin-4-yl)(4-chlorophenyl)methanone (33b)**. 65% yield
33
34 from 3-chloro-5-methoxybenzoic acid **29b** and **30**. ¹H-NMR (CDCl₃) δ (ppm): 1.70-2.08 (bm, 4H),
35
36 2.93-3.25 (bm, 2H), 3.44-3.55 (m, 1H), 3.75-3.95 (bm, 1H), 3.82 (s, 3H), 4.55-4.75 (bm, 1H), 6.82
37
38 (dd, 1H, $J = 2.3, 1.3$ Hz), 6.92-6.97 (m, 2H), 7.46 (AA'XX', 2H, $J_{AX} = 8.7$ Hz, $J_{AA'/XX'} = 2.2$ Hz),
39
40 7.89 (AA'XX', 2H, $J_{AX} = 8.6$ Hz, $J_{AA'/XX'} = 2.1$ Hz).

41
42
43 **(4-(4-Chlorobenzoyl)piperidin-1-yl)(3-fluoro-5-methoxyphenyl)methanone (33c)**. 67% yield
44
45 from 5-fluoro-3-methoxybenzoic acid **29c** and **30**. ¹H-NMR (CDCl₃) δ (ppm): 1.72-3.05 (bm, 4H),
46
47 2.96-3.23 (bm, 2H), 3.44-3.54 (m, 1H), 3.74-3.93 (bm, 1H), 3.82 (s, 3H), 4.52-4.75 (bm, 1H), 6.63-
48
49 6.71 (m, 2H), 6.71-6.75 (m, 1H), 7.46 (AA'XX', 2H, $J_{AX} = 8.8$ Hz, $J_{AA'/XX'} = 2.2$ Hz), 7.89 (AA'XX',
50
51 2H, $J_{AX} = 8.7$ Hz, $J_{AA'/XX'} = 2.2$ Hz).

52
53
54 **(1-(4-Bromo-3-methoxybenzoyl)piperidin-4-yl)(4-chlorophenyl)methanone (33d)**. 77% yield
55
56 from 4-bromo-3-methoxybenzoic acid **29d** and **30**. ¹H-NMR (CDCl₃) δ (ppm): 1.72-2.03 (bm, 4H),
57
58 3.01-3.22 (bm, 2H), 3.46-3.55 (m, 1H), 3.76-4.00 (bm, 1H), 3.92 (s, 3H), 4.54-4.75 (bm, 1H), 6.85
59
60

(dd, 1H, $J = 8.0, 1.8$ Hz), 6.97 (d, 1H, $J = 1.8$ Hz), 7.47 (AA'XX', 2H, $J_{AX} = 8.7$ Hz, $J_{AA'/XX'} = 2.2$ Hz), 7.56 (d, 1H, $J = 8.0$ Hz), 7.89 (AA'XX', 2H, $J_{AX} = 8.5$ Hz, $J_{AA'/XX'} = 2.2$ Hz).

(1-(4-Chloro-3-methoxybenzoyl)piperidin-4-yl)(4-chlorophenyl)methanone (33e). 63% yield from 4-chloro-3-methoxybenzoic acid **29e** and **30**. $^1\text{H-NMR}$ (CDCl_3) δ (ppm): 1.72-2.03 (bm, 4H), 2.98-3.23 (bm, 2H), 3.46-3.55 (m, 1H), 3.75-3.95 (bm, 1H), 3.93 (s, 3H), 4.51-4.76 (bm, 1H), 6.92 (dd, 1H, $J = 8.0, 1.8$ Hz), 7.01 (d, 1H, $J = 1.8$ Hz), 7.38 (d, 1H, $J = 8.0$ Hz), 7.46 (AA'XX', 2H, $J_{AX} = 8.8$ Hz, $J_{AA'/XX'} = 2.2$ Hz), 7.89 (AA'XX', 2H, $J_{AX} = 8.7$ Hz, $J_{AA'/XX'} = 2.2$ Hz).

(4-(4-Chlorobenzoyl)piperidin-1-yl)(4-fluoro-3-methoxyphenyl)methanone (33f). 73% yield from 4-fluoro-3-methoxybenzoic acid **29f** and **30**. $^1\text{H-NMR}$ (CDCl_3) δ (ppm): 1.72-2.07 (bm, 4H), 2.99-3.22 (bm, 2H), 3.45-3.55 (m, 1H), 3.81-4.02 (bm, 1H), 3.93 (s, 3H), 4.44-4.83 (bm, 1H), 6.94 (ddd, 1H, $J = 8.2, 4.3, 2.0$ Hz), 7.07 (dd, 1H, $J = 8.0, 2.0$ Hz), 7.09 (dd, 1H, $J = 11.0, 8.2$ Hz), 7.47 (AA'XX', 2H, $J_{AX} = 8.6$ Hz, $J_{AA'/XX'} = 2.2$ Hz), 7.89 (AA'XX', 2H, $J_{AX} = 8.7$ Hz, $J_{AA'/XX'} = 2.2$ Hz).

Methyl 2-chloro-5-methoxybenzoate (35a). 79% yield from 2-chloro-5-hydroxybenzoic acid **34a**. $^1\text{H-NMR}$ (CDCl_3) δ (ppm): 3.82 (s, 3H), 3.93 (s, 3H), 6.96 (dd, 1H, $J = 8.9, 3.1$ Hz), 7.33 (d, 1H, $J = 3.2$ Hz), 7.34 (d, 1H, $J = 8.7$ Hz).

Methyl 2-fluoro-5-methoxybenzoate (35b). 93% yield from 2-fluoro-5-hydroxybenzoic acid **34b**. $^1\text{H-NMR}$ (CDCl_3) δ (ppm): 3.82 (s, 3H), 3.93 (s, 3H), 7.02-7.07 (m, 2H), 7.38-7.42 (m, 1H).

Methyl 4-iodo-3-methoxybenzoate (35c). 99% yield from 3-hydroxy-4-iodobenzoic acid **34c**. $^1\text{H-NMR}$ (CDCl_3) δ (ppm): 3.92 (s, 3H), 3.94 (s, 3H), 7.37 (dd, 1H, $J = 8.1, 1.8$ Hz), 7.45 (d, 1H, $J = 1.8$ Hz), 7.85 (d, 1H, $J = 8.0$ Hz).

2-Chloro-5-methoxybenzoic acid (36a). 99% yield from **35a**. $^1\text{H-NMR}$ (acetone- d_6) δ (ppm): 3.86 (s, 3H), 7.11 (dd, 1H, $J = 8.9, 3.1$ Hz), 7.40 (d, 1H, $J = 3.1$ Hz), 7.42 (d, 1H, $J = 8.9$ Hz).

2-Fluoro-5-methoxybenzoic acid (36b). 99% yield from **35b**. $^1\text{H-NMR}$ (CDCl_3) δ (ppm): 3.84 (s, 3H), 7.15-7.20 (m, 2H), 7.40-7.44 (m, 1H).

4-Iodo-3-methoxybenzoic acid (36c). 95% yield from **35c**. $^1\text{H-NMR}$ (CDCl_3) δ (ppm): 3.96 (s, 3H), 7.45 (dd, 1H, $J = 8.0, 1.8$ Hz), 7.50 (d, 1H, $J = 1.8$ Hz), 7.90 (d, 1H, $J = 8.0$ Hz).

(1-(2-Chloro-5-methoxybenzoyl)piperidin-4-yl)(4-chlorophenyl)methanone (37a). 54% yield from **36a** and **30**. ¹H-NMR (CDCl₃; asterisk denotes isomer peaks) δ (ppm): 1.64-2.07 (m, 4H), 3.02-3.15 (m, 1H), 3.20-3.30 (m, 1H), 3.39-3.65 (bm, 2H), 3.80* (s, 3H), 3.81 (s, 3H), 4.65-4.78 (m, 1H), 6.78-6.89 (m, 2H), 7.24-7.32 (m, 1H), 7.43-7.49 (m, 2H), 7.85-7.91 (m, 2H).

(4-(4-Chlorobenzoyl)piperidin-1-yl)(2-fluoro-5-methoxyphenyl)methanone (37b). 39% yield from **36b** and **30**. ¹H-NMR (CDCl₃) δ (ppm): 1.74-1.88 (bm, 3H), 1.97-2.06 (m, 1H), 3.02-3.12 (m, 1H), 3.13-3.30 (bm, 1H), 3.42-3.54 (bm, 1H), 3.66-3.75 (m, 1H), 3.80 (s, 3H), 4.66-4.76 (m, 1H), 6.85-6.93 (m, 2H), 7.01 (td, 1H, *J* = 8.6, 0.7 Hz), 7.46 (AA'XX', 2H, *J*_{AX} = 8.7 Hz, *J*_{AA'/XX'} = 2.2 Hz), 7.88 (AA'XX', 2H, *J*_{AX} = 8.7 Hz, *J*_{AA'/XX'} = 2.2 Hz).

(4-(4-Chlorobenzoyl)piperidin-1-yl)(4-iodo-3-methoxyphenyl)methanone (37c). 75% yield from **36c** and **30**. ¹H-NMR (CDCl₃) δ (ppm): 1.72-2.08 (bm, 4H), 2.97-3.24 (bm, 2H), 3.45-3.55 (bm, 1H), 3.77-4.02 (bm, 1H), 3.91 (s, 3H), 4.55-4.76 (bm, 1H), 6.73 (dd, 1H, *J* = 7.9, 1.7 Hz), 6.88 (d, 1H, *J* = 1.6 Hz), 7.47 (AA'XX', 2H, *J*_{AX} = 8.7 Hz, *J*_{AA'/XX'} = 2.2 Hz), 7.80 (d, 1H, *J* = 7.9 Hz), 7.89 (AA'XX', 2H, *J*_{AX} = 8.7 Hz, *J*_{AA'/XX'} = 2.1 Hz).

Methyl 2-amino-3-methoxybenzoate (39a). 69% yield from 2-amino-3-methoxybenzoic acid **38a**. ¹H-NMR (CDCl₃) δ (ppm): 3.87 (s, 3H), 3.88 (s, 3H), 4.90-5.45 (bs, 2H), 6.63 (t, 1H, *J* = 8.0 Hz), 6.88 (dd, 1H, *J* = 7.9, 1.3 Hz), 7.49 (dd, 1H, *J* = 8.2, 1.4 Hz).

Methyl 3-amino-5-methoxybenzoate (39b). 97% yield from 3-amino-5-methoxybenzoic acid **38b**. ¹H-NMR (CDCl₃) δ (ppm): 3.80 (s, 3H), 3.88 (s, 3H), 6.41 (t, 1H, *J* = 2.2 Hz), 6.96-6.99 (m, 2H).

Methyl 2-iodo-3-methoxybenzoate (41a). 40% yield from **39a**. ¹H-NMR (CDCl₃) δ (ppm): 3.91 (s, 3H), 3.94 (s, 3H), 6.92 (dd, 1H, *J* = 8.2, 1.2 Hz), 7.22 (dd, 1H, *J* = 7.7, 1.4 Hz), 7.34 (t, 1H, *J* = 7.9 Hz).

Synthesis of methyl 2-bromo-3-methoxybenzoate (41b). To a solution of **39a** (190 mg, 1 equiv) in a mixture of water (0.8 mL) and 1,4-dioxane (0.8 mL) was added dropwise 48% hydrobromic acid (0.5 mL) at room temperature and stirred for 30 min. After cooling the mixture to -5 °C, a solution of sodium nitrite (1.08 equiv) in water (0.2 mL) was added dropwise and then the reaction mixture was

1
2
3 stirred for 30 min at the same temperature. Then a fresh solution of copper (I) bromide (1.49 equiv)
4 in 48% hydrobromic acid (0.3 mL) was added quickly, the reaction mixture was warmed slowly to
5 room temperature, then heated at 110 °C for 5 h. After cooling, the mixture was diluted with water
6 and extracted with ethyl acetate. The combined organic layer was washed with water, saturated
7 NaHCO₃ solution and brine, dried over Na₂SO₄, filtered, and evaporated in vacuo. The residue was
8 purified by flash column chromatography (silica gel) to afford bromide **41b** (50% yield). ¹H-NMR
9 (CDCl₃) δ (ppm): 3.92 (s, 3H), 3.93 (s, 3H), 7.01 (dd, 1H, *J* = 8.0, 1.6 Hz), 7.26 (dd, 1H, *J* = 7.7, 1.7
10 Hz), 7.32 (t, 1H, *J* = 7.9 Hz).

11
12 **Methyl 2-iodo-5-methoxybenzoate (41c)**. 78% yield from **40**. ¹H-NMR (CDCl₃) δ (ppm): 3.82 (s,
13 3H), 3.93 (s, 3H), 6.75 (dd, 1H, *J* = 8.7, 3.1 Hz), 7.34 (d, 1H, *J* = 3.1 Hz), 7.83 (d, 1H, *J* = 8.7 Hz).

14
15 **Methyl 3-iodo-5-methoxybenzoate (41d)**. 25% yield from **39b**. ¹H-NMR (CDCl₃) δ (ppm): 3.83 (s,
16 3H), 3.91 (s, 3H), 7.43 (dd, 1H, *J* = 2.5, 1.5 Hz), 7.51 (dd, 1H, *J* = 2.5, 1.3 Hz), 7.96 (t, 1H, *J* = 1.4
17 Hz).

18
19 **2-Iodo-3-methoxybenzoic acid (42a)**. 99% yield from **41a**. ¹H-NMR (CDCl₃) δ (ppm): 3.92 (s, 3H),
20 6.97 (dd, 1H, *J* = 8.1, 1.4 Hz), 7.37 (t, 1H, *J* = 7.9 Hz), 7.44 (dd, 1H, *J* = 7.7, 1.3 Hz).

21
22 **2-Bromo-3-methoxybenzoic acid (42b)**. 95% yield from **41b**. ¹H-NMR (CDCl₃) δ (ppm): 3.94 (s,
23 3H), 7.07 (dd, 1H, *J* = 8.2, 1.4 Hz), 7.36 (t, 1H, *J* = 8.0 Hz), 7.49 (dd, 1H, *J* = 7.8, 1.5 Hz).

24
25 **2-Iodo-5-methoxybenzoic acid (42c)**. 64% yield from **41c**. ¹H-NMR (CDCl₃) δ (ppm): 3.84 (s, 3H),
26 6.80 (dd, 1H, *J* = 8.7, 3.1 Hz), 7.55 (d, 1H, *J* = 3.1 Hz), 7.89 (d, 1H, *J* = 8.7 Hz).

27
28 **3-Iodo-5-methoxybenzoic acid (42d)**. 99% yield from **41d**. ¹H-NMR (acetone-*d*₆) δ (ppm): 3.88 (s,
29 3H), 7.53-7.56 (m, 2H), 7.93 (t, 1H, *J* = 1.4 Hz).

30
31 **(4-(4-Chlorobenzoyl)piperidin-1-yl)(2-iodo-3-methoxyphenyl)methanone (43a)**. 60% yield from
32 **42a** and **30**. ¹H-NMR (CDCl₃; asterisk denotes isomer peaks) δ (ppm): 1.65 -1.84 (m, 2H), 1.87-2.14
33 (m, 2H), 3.02-3.14 (m, 1H), 3.18-3.26 (m, 1H), 3.42-3.59 (m, 2H), 3.90* (s, 3H), 3.90 (s, 3H), 4.68-
34 4.80 (m, 1H), 6.77-6.82 (m, 1H), 6.84 (dd, 1H, *J* = 7.5, 1.3 Hz), 7.34* (t, 1H, *J* = 7.6 Hz), 7.36 (t, 1H,
35 *J* = 7.7 Hz), 7.43-7.48 (m, 2H), 7.85-7.90 (m, 2H).

(1-(2-Bromo-3-methoxybenzoyl)piperidin-4-yl)(4-chlorophenyl)methanone (43b). 57% yield from **42b** and **30**. ¹H-NMR (CDCl₃; asterisk denotes isomer peaks) δ (ppm): 1.65-2.07 (m, 4H), 3.01-3.26 (m, 2H), 3.40-3.60 (m, 2H), 3.91* (s, 3H), 3.92 (s, 3H), 4.67-4.81 (m, 1H), 6.83* (dd, 1H, *J* = 7.6, 1.3 Hz), 6.87-6.92 (m, 2H), 7.32* (t, 1H, *J* = 7.4 Hz), 7.34 (t, 1H, *J* = 7.9 Hz), 7.43-7.48 (m, 2H), 7.84-7.90 (m, 2H).

(4-(4-Chlorobenzoyl)piperidin-1-yl)(2-iodo-5-methoxyphenyl)methanone (43c). 43% yield from **42c** and **30**. ¹H-NMR (CDCl₃; asterisk denotes isomer peaks) δ (ppm): 1.65-2.14 (bm, 4H), 3.02-3.14 (bm, 1H), 3.21-3.29 (bm, 1H), 3.44-3.62 (bm, 2H), 3.80* (s, 3H), 3.83 (s, 3H), 4.66-4.78 (bm, 1H), 6.67* (dd, 1H, *J* = 8.8, 2.9 Hz), 6.67 (dd, 1H, *J* = 8.7, 3.0 Hz), 6.74* (d, 1H, *J* = 3.0 Hz), 6.79 (d, 1H, *J* = 3.0 Hz), 7.43-7.49 (m, 2H), 7.66 (d, 1H, *J* = 8.8 Hz), 7.69* (d, 1H, *J* = 8.7 Hz), 7.86-7.91 (m, 2H).

(4-(4-Chlorobenzoyl)piperidin-1-yl)(3-iodo-5-methoxyphenyl)methanone (43d). 50% yield from **42d** and **30**. ¹H-NMR (CDCl₃) δ (ppm): 1.72-2.08 (bm, 4H), 2.96-3.24 (bm, 2H), 3.44-3.54 (bm, 1H), 3.76-3.93 (bm, 1H), 3.80 (s, 3H), 4.53-4.74 (bm, 1H), 6.89 (dd, 1H, *J* = 2.3, 1.4 Hz), 7.27-7.31 (m, 2H), 7.46 (AA'XX', 2H, *J*_{AX} = 8.7 Hz, *J*_{AA'/XX'} = 2.2 Hz), 7.89 (AA'XX', 2H, *J*_{AX} = 8.7 Hz, *J*_{AA'/XX'} = 2.2 Hz).

Synthesis of 1-acetylpiperidine-4-carboxylic acid (45). Isonipectic acid **44** (2 g) and pyridine (1.25 mL) were added to 3 mL of Ac₂O at room temperature. The reaction mixture was stirred at 140 °C for 2 h and then cooled down to room temperature. The excess Ac₂O was evaporated under vacuum and then 20 mL EtOAc/diethyl ether (1:1, v:v) was added to the residue. The resulting white solid was filtered and washed with 60 mL EtOAc/diethyl ether (1:1, v:v) to give pure compound **45** (85% yield). ¹H-NMR (CDCl₃) δ (ppm): 1.60-1.77 (m, 2H), 1.93-2.02 (m, 2H), 2.10 (s, 3H), 2.59 (tt, 1H, *J* = 10.6, 4.0 Hz), 2.80-2.91 (m, 1H), 3.10-3.22 (m, 1H), 3.74-3.84 (m, 1H), 4.35-4.46 (m, 1H).

1-(4-Benzoylpiperidin-1-yl)ethanone (46a). 72% yield from **45** and benzene. ¹H-NMR (CDCl₃) δ (ppm): 1.55-2.00 (bm, 4H), 2.13 (s, 3H), 2.73-3.00 (bm, 1H), 3.08-3.37 (bm, 1H), 3.51 (tt, 1H, *J* =

10.7, 4.0 Hz), 3.80-4.05 (bm, 1H), 4.36-4.67 (bm, 1H), 7.46-7.52 (m, 2H), 7.59 (tt, 1H, $J = 7.4, 1.5$ Hz), 7.92-7.96 (m, 2H).

1-(4-(4-Methylbenzoyl)piperidin-1-yl)ethanone (46b). 56% yield from **45** and toluene. $^1\text{H-NMR}$ (CDCl_3) δ (ppm): 1.57-1.74 (bm, 1H), 1.77-1.95 (bm, 3H), 2.11 (s, 3H), 2.42 (s, 3H), 2.77-2.88 (bm, 1H), 3.16-3.27 (bm, 1H), 3.47 (tt, 1H, $J = 10.8, 4.0$ Hz), 3.84-3.94 (bm, 1H), 4.52-4.60 (bm, 1H), 7.26-7.30 (m, 2H), 7.84 (AA'XX', 2H, $J_{\text{AX}} = 8.2$ Hz, $J_{\text{AA'}/\text{XX'}} = 1.9$ Hz).

1-(4-(4-Ethylbenzoyl)piperidin-1-yl)ethanone (46c). 76% yield from **45** and ethylbenzene. $^1\text{H-NMR}$ (CDCl_3) δ (ppm): 1.27 (t, 3H, $J = 7.6$ Hz), 1.56-1.96 (bm, 4H), 2.12 (s, 3H), 2.72 (q, 2H, $J = 7.7$ Hz), 2.76-2.90 (bm, 1H), 3.15-3.29 (bm, 1H), 3.48 (tt, 1H, $J = 10.7, 4.0$ Hz), 3.85-3.95 (bm, 1H), 4.50-4.62 (bm, 1H), 7.31 (d, 2H, $J = 8.2$ Hz), 7.87 (d, 2H, $J = 8.3$ Hz).

1-(4-(4-Propylbenzoyl)piperidin-1-yl)ethanone (46d). 50% yield from **45** and *n*-propylbenzene. $^1\text{H-NMR}$ (CDCl_3) δ (ppm): 0.95 (t, 3H, $J = 7.4$ Hz), 1.67 (sext, 2H, $J = 7.5$ Hz), 1.73-1.96 (bm, 4H), 2.11 (s, 3H), 2.65 (t, 2H, $J = 7.6$ Hz), 2.76-2.91 (bm, 1H), 3.15-3.28 (bm, 1H), 3.48 (tt, 1H, $J = 10.7, 4.0$ Hz), 3.84-3.96 (bm, 1H), 4.50-4.63 (bm, 1H), 7.28 (d, 2H, $J = 8.4$ Hz), 7.86 (AA'XX', 2H, $J_{\text{AX}} = 8.3$ Hz, $J_{\text{AA'}/\text{XX'}} = 1.8$ Hz).

1-(4-(4-Isopropylbenzoyl)piperidin-1-yl)ethanone (46e). 57% yield from **45** and cumene. $^1\text{H-NMR}$ (CDCl_3) δ (ppm): 1.27 (d, 6H, $J = 6.9$ Hz), 1.71-1.95 (bm, 4H), 2.12 (s, 3H), 2.76-2.92 (bm, 1H), 2.97 (sept, 1H, $J = 6.8$ Hz), 3.15-3.29 (bm, 1H), 3.48 (tt, 1H, $J = 10.7, 4.1$ Hz), 3.83-3.98 (bm, 1H), 4.49-4.62 (bm, 1H), 7.33 (d, 2H, $J = 8.2$ Hz), 7.88 (AA'XX', 2H, $J_{\text{AX}} = 8.4$ Hz, $J_{\text{AA'}/\text{XX'}} = 1.8$ Hz).

1-(4-(4-Butylbenzoyl)piperidin-1-yl)ethanone (46f). 50% yield from **45** and *n*-butylbenzene. $^1\text{H-NMR}$ (CDCl_3) δ (ppm): 0.93 (t, 3H, $J = 7.4$ Hz), 1.36 (sext, 2H, $J = 7.4$ Hz), 1.62 (quint, 2H, $J = 7.6$ Hz), 1.59-1.97 (bm, 4H), 2.11 (s, 3H), 2.67 (t, 2H, $J = 7.7$ Hz), 2.75-2.90 (bm, 1H), 3.15-3.28 (bm, 1H), 3.48 (tt, 1H, $J = 10.7, 4.0$ Hz), 3.83-3.97 (bm, 1H), 4.50-4.63 (bm, 1H), 7.28 (d, 2H, $J = 8.4$ Hz), 7.86 (d, 2H, $J = 8.3$ Hz).

1-(4-(4-Methoxybenzoyl)piperidin-1-yl)ethanone (46g). 43% yield from **45** and anisole. $^1\text{H-NMR}$ (CDCl_3) δ (ppm): 1.57-1.96 (bm, 4H), 2.11 (s, 3H), 2.74-2.89 (m, 1H), 3.14-3.28 (m, 1H), 3.45 (tt,

1
2
3 1H, $J = 10.6, 4.1$ Hz), 3.83-3.98 (bm, 1H), 3.87 (s, 3H), 4.52-4.63 (m, 1H), 6.95 (AA'XX', 2H, $J_{AX} = 9.0$ Hz, $J_{AA'/XX'} = 2.5$ Hz), 7.93 (AA'XX', 2H, $J_{AX} = 9.0$ Hz, $J_{AA'/XX'} = 2.5$ Hz).

7 **1-(4-(2,3-Dihydrobenzo[b][1,4]dioxine-6-carbonyl)piperidin-1-yl)ethanone (46h)**. 53% yield
8 from **45** and benzo-1,4-dioxane. ¹H-NMR (CDCl₃) δ (ppm): 1.58-1.94 (bm, 4H), 2.13 (s, 3H), 2.76-
9 2.93 (bm, 1H), 3.08-3.30 (bm, 1H), 3.36-3.45 (m, 1H), 3.84-4.00 (bm, 1H), 4.27-4.35 (m, 4H), 4.46-
10 4.64 (bm, 1H), 6.92 (d, 1H, $J = 8.8$ Hz), 7.46-7.51 (m, 2H).

16 **Phenyl(piperidin-4-yl)methanone (47a)**. 80% yield from **46a**. ¹H-NMR (CDCl₃) δ (ppm): 1.66-1.98
17 (m, 4H), 2.47-2.65 (bm, 2H), 2.79-2.90 (m, 1H), 3.20-3.30 (m, 1H), 3.44 (tt, 1H, $J = 10.6, 3.7$ Hz),
18 7.43-7.50 (m, 2H), 7.57 (tt, 1H, $J = 7.4, 1.7$ Hz), 7.90-7.96 (m, 2H).

23 **Piperidin-4-yl(*p*-tolyl)methanone (47b)**. 66% yield from **46b**. ¹H-NMR (CDCl₃) δ (ppm): 1.64-1.77
24 (m, 2H), 1.81-1.93 (m, 2H), 2.42 (s, 3H), 2.74-2.84 (m, 2H), 3.16-3.25 (m, 2H), 3.39 (tt, 1H, $J = 11.1,$
25 3.7 Hz), 7.24-7.28 (m, 2H), 7.82-7.86 (m, 2H).

30 **(4-Ethylphenyl)(piperidin-4-yl)methanone (47c)**. 91% yield from **46c**. ¹H-NMR (CDCl₃) δ (ppm):
31 1.26 (t, 3H, $J = 7.6$ Hz), 1.63-1.75 (m, 2H), 1.81-1.94 (bm, 2H), 2.71 (q, 2H, $J = 7.6$ Hz), 2.78 (td,
32 2H, $J = 12.3, 2.8$ Hz), 3.19 (dt, 2H, $J = 12.6, 3.4$ Hz), 3.39 (tt, 1H, $J = 11.3, 3.7$ Hz), 7.29 (d, 2H, $J =$
33 8.4 Hz), 7.87 (d, 2H, $J = 8.3$ Hz).

38 **Piperidin-4-yl(4-propylphenyl)methanone (47d)**. 94% yield from **46d**. ¹H-NMR (CDCl₃) δ (ppm):
39 0.94 (t, 3H, $J = 7.3$ Hz), 1.66 (sext, 2H, $J = 7.5$ Hz), 1.79-1.90 (bm, 4H), 2.64 (t, 2H, $J = 7.6$ Hz),
40 2.77 (td, 2H, $J = 12.3, 2.6$ Hz), 3.19 (dt, 2H, $J = 12.6, 3.4$ Hz), 3.38 (tt, 1H, $J = 11.3, 3.7$ Hz), 7.26
41 (d, 2H, $J = 8.4$ Hz), 7.86 (AA'XX', 2H, $J_{AX} = 8.3$ Hz, $J_{AA'/XX'} = 1.8$ Hz).

46 **(4-Isopropylphenyl)(piperidin-4-yl)methanone (47e)**. 94% yield from **46e**. ¹H-NMR (CDCl₃) δ
47 (ppm): 1.27 (d, 6H, $J = 6.9$ Hz), 1.63-1.74 (m, 2H), 1.80-1.89 (bm, 2H), 2.77 (td, 2H, $J = 12.3, 2.6$
48 Hz), 2.96 (sept, 1H, $J = 6.9$ Hz), 3.19 (dt, 2H, $J = 12.5, 3.4$ Hz), 3.39 (tt, 1H, $J = 11.3, 3.7$ Hz), 7.31
49 (d, 2H, $J = 8.2$ Hz), 7.88 (AA'XX', 2H, $J_{AX} = 8.4$ Hz, $J_{AA'/XX'} = 1.8$ Hz).

54 **(4-Butylphenyl)(piperidin-4-yl)methanone (47f)**. 94% yield from **46f**. ¹H-NMR (CDCl₃) δ (ppm):
55 0.93 (t, 3H, $J = 7.3$ Hz), 1.36 (sext, 2H, $J = 7.4$ Hz), 1.61 (quint, 2H, $J = 7.6$ Hz), 1.66-1.75 (m, 2H),
56 60

1
2
3 1.80-1.95 (m, 2H), 2.66 (t, 2H, $J = 7.7$ Hz), 2.77 (td, 2H, $J = 12.2, 2.6$ Hz), 3.19 (dt, 2H, $J = 12.5, 3.3$
4 Hz), 3.83 (tt, 1H, $J = 11.2, 3.6$ Hz), 7.27 (d, 2H, $J = 8.2$ Hz), 7.86 (d, 2H, $J = 8.3$ Hz).

7 **(4-Methoxyphenyl)(piperidin-4-yl)methanone (47g)**. 81% yield from **46g**. $^1\text{H-NMR}$ (CDCl_3) δ
8 (ppm): 1.64-1.78 (m, 2H), 1.79-1.90 (m, 2H), 2.78 (td, 2H, $J = 12.2, 2.8$ Hz), 3.20 (dt, 2H, $J = 12.7,$
9 3.5 Hz), 3.36 (tt, 1H, $J = 11.3, 3.7$ Hz), 3.87 (s, 3H), 6.94 (AA'XX', 2H, $J_{\text{AX}} = 9.0$ Hz, $J_{\text{AA}'/\text{XX}'} = 2.5$
10 Hz), 7.93 (AA'XX', 2H, $J_{\text{AX}} = 9.0$ Hz, $J_{\text{AA}'/\text{XX}'} = 2.5$ Hz).

13 **(2,3-Dihydrobenzo[b][1,4]dioxin-6-yl)(piperidin-4-yl)methanone (47h)**. 95% yield from **46h**. $^1\text{H-}$
14 NMR (CDCl_3) δ (ppm): 1.63-1.97 (m, 4H), 2.30-2.56 (bm, 2H), 2.72-2.95 (bm, 1H), 3.13-3.39 (bm,
15 2H), 4.23-4.38 (m, 4H), 6.91 (d, 1H, $J = 8.8$ Hz), 7.44-7.52 (m, 2H).

18 **(4-Benzoylpiperidin-1-yl)(3-methoxyphenyl)methanone (49a)**. 34% yield from **47a** and **48**. $^1\text{H-}$
19 NMR (CDCl_3) δ (ppm): 1.74-2.10 (bm, 4H), 2.98-3.22 (bm, 2H), 3.50-3.60 (bm, 1H), 3.78-3.95 (bm,
20 1H), 3.83 (s, 3H), 4.60-4.80 (bm, 1H), 6.92-6.99 (m, 3H), 7.31 (dd, 1H, $J = 9.0, 7.5$ Hz), 7.46-7.52
21 (m, 2H), 7.59 (tt, 1H, $J = 7.4, 1.5$ Hz), 7.92-7.98 (m, 2H).

24 **(1-(3-Methoxybenzoyl)piperidin-4-yl)(*p*-tolyl)methanone (49b)**. 37% yield from **47b** and **48**. $^1\text{H-}$
25 NMR (CDCl_3) δ (ppm): 1.73-2.08 (bm, 4H), 2.42 (s, 3H), 2.97-3.21 (bm, 2H), 3.47-3.57 (bm, 1H),
26 3.83 (s, 3H), 3.83-3.95 (bm, 1H), 4.60-4.76 (bm, 1H), 6.92-6.99 (m, 3H), 7.26-7.34 (m, 3H), 7.83-
27 7.87 (m, 2H).

30 **(4-(4-Ethylbenzoyl)piperidin-1-yl)(3-methoxyphenyl)methanone (49c)**. 94% yield from **47c** and
31 **48**. $^1\text{H-NMR}$ (CDCl_3) δ (ppm): 1.26 (t, 3H, $J = 7.6$ Hz), 1.73-2.07 (bm, 4H), 2.71 (q, 2H, $J = 7.6$ Hz),
32 2.96-3.24 (bm, 2H), 3.48-3.59 (bm, 1H), 3.78-3.95 (bm, 1H), 3.83 (s, 3H), 4.60-4.77 (bm, 1H), 6.92-
33 6.99 (m, 3H), 7.28-7.34 (m, 3H), 7.88 (AA'XX', 2H, $J_{\text{AX}} = 8.4$ Hz, $J_{\text{AA}'/\text{XX}'} = 1.8$ Hz).

36 **(1-(3-Methoxybenzoyl)piperidin-4-yl)(4-propylphenyl)methanone (49d)**. 89% yield from **47d**
37 and **48**. $^1\text{H-NMR}$ (CDCl_3) δ (ppm): 0.95 (t, 3H, $J = 7.3$ Hz), 1.67 (sext, 2H, $J = 7.4$ Hz), 1.73-1.87
38 (bm, 4H), 2.65 (t, 2H, $J = 7.6$ Hz), 2.97-3.20 (bm, 2H), 3.47-3.58 (m, 1H), 3.72-4.00 (bm, 1H), 3.82
39 (s, 3H), 4.58-4.79 (bm, 1H), 6.92-7.00 (m, 3H), 7.27-7.33 (m, 3H), 7.87 (d, 2H, $J = 8.2$ Hz).

(4-(4-Isopropylbenzoyl)piperidin-1-yl)(3-methoxyphenyl)methanone (49e). 92% yield from **47e** and **48**. ¹H-NMR (CDCl₃) δ (ppm): 1.27 (d, 6H, *J* = 6.9 Hz), 1.74-2.09 (bm, 4H), 2.97 (sept, 1H, *J* = 6.9 Hz), 2.99-3.21 (bm, 2H), 3.48-3.59 (m, 1H), 3.77-3.97 (bm, 1H), 3.83 (s, 3H), 4.58-4.77 (bm, 1H), 6.92-6.99 (m, 3H), 7.28-7.36 (m, 3H), 7.99 (d, 2H, *J* = 8.4 Hz).

(4-(4-Butylbenzoyl)piperidin-1-yl)(3-methoxyphenyl)methanone (49f). 97% yield from **47f** and **48**. ¹H-NMR (CDCl₃) δ (ppm): 0.93 (t, 3H, *J* = 7.3 Hz), 1.36 (sext, 2H, *J* = 7.3 Hz), 1.54-1.67 (m, 2H), 1.73-1.87 (m, 3H), 1.91-2.08 (bm, 1H), 2.67 (t, 2H, *J* = 7.8 Hz), 2.96-3.24 (bm, 2H), 3.47-3.58 (m, 1H), 3.74-3.97 (bm, 1H), 3.83 (s, 3H), 4.59-4.79 (bm, 1H), 6.92-7.00 (m, 3H), 7.26-7.34 (m, 3H), 7.87 (d, 2H, *J* = 8.3 Hz).

(4-(4-Methoxybenzoyl)piperidin-1-yl)(3-methoxyphenyl)methanone (49g). 33% yield from **47g** and **48**. ¹H-NMR (CDCl₃) δ (ppm): 1.70-2.10 (bm, 4H), 2.94-3.23 (bm, 2H), 3.44-3.56 (bm, 1H), 3.77-3.96 (bm, 1H), 3.82 (s, 3H), 3.88 (s, 3H), 4.59-4.80 (bm, 1H), 6.91-7.00 (m, 5H), 7.27-7.34 (m, 1H), 7.94 (AA'XX', 2H, *J*_{AX} = 8.9 Hz, *J*_{AA'/XX'} = 2.4 Hz).

(2,3-Dihydrobenzo[b][1,4]dioxin-6-yl)(1-(3-methoxybenzoyl)piperidin-4-yl)methanone (49h). 71% yield from **47h** and **48**. ¹H-NMR (CDCl₃) δ (ppm): 1.71-2.06 (bm, 4H), 2.96-3.20 (bm, 2H), 3.41-3.51 (m, 1H), 3.78-3.92 (bm, 1H), 3.83 (s, 3H), 4.27-4.35 (m, 4H), 4.60-4.76 (bm, 1H), 6.91-6.98 (m, 4H), 7.31 (dd, 1H, *J* = 8.0, 7.5 Hz), 7.48-7.52 (m, 2H).

Synthesis of ethyl piperidine-4-carboxylate (50). Isonipecotic acid **44** (500 mg, 1 equiv) was dissolved in absolute ethanol (19.4 mL). The solution was cooled to 0 °C and SOCl₂ (4 eq) was added dropwise. The mixture was heated at 90 °C for 3 h, then the mixture was cooled to room temperature and the solvent was evaporated in vacuo. The residue was dissolved in EtOAc and washed with a 10% aqueous solution of NaOH and with brine. The organic layer was dried and evaporated. The residue furnished the pure ethyl ester **50** (74% yield). ¹H-NMR (CDCl₃) δ (ppm): 1.25 (t, 3H, *J* = 7.1 Hz), 1.54-1.66 (m, 2H), 1.83-1.91 (m, 2H), 2.40 (tt, 1H, *J* = 11.3, 3.9 Hz), 2.62 (td, 2H, *J* = 12.0, 2.5 Hz), 3.08 (dt, 2H, *J* = 12.7, 3.8 Hz), 4.13 (q, 2H, *J* = 7.1 Hz).

Synthesis of ethyl 1-benzoylpiperidine-4-carboxylate (51). Benzoyl chloride (1 equiv) was added dropwise with stirring to a cooled solution of ethyl isonipecotate **50** (700 mg, 1 equiv) and triethylamine (1.5 equiv) in 7 mL CH₂Cl₂. Following the addition, the reaction mixture was stirred overnight, then treated with water and stirred for an additional 10 min. The mixture was diluted with CH₂Cl₂ and the layers were separated, the organic extract was washed 0.5 M HCl and with saturated sodium bicarbonate solution. After drying over anhydrous sodium sulfate, the solution was concentrated and then the residue was purified by flash column chromatography to give compound **51** (93% yield). ¹H-NMR (CDCl₃) δ (ppm): 1.26 (t, 3H, *J* = 7.1 Hz), 1.60-2.13 (bm, 4H), 2.57 (tt, 1H, *J* = 10.8, 4.1 Hz), 2.96-3.14 (bm, 2H), 3.61-3.86 (bm, 1H), 4.16 (q, 2H, *J* = 7.1 Hz), 4.40-4.65 (bm, 1H), 7.35-7.44 (m, 5H).

Synthesis of 1-benzoylpiperidine-4-carboxylic acid (52). The ester **51** (1.1 g, 1 equiv) was redissolved in 70% aqueous ethanol (4.4 mL). Then ground NaOH pellets (2.5 equiv) were added into the above solution. The reaction mixture was stirred overnight, evaporated, diluted with water, then followed by addition of 1 N HCl and extraction with EtOAc. The organic phase was dried over anhydrous sodium sulfate, filtered and concentrated to give carboxylic acid **52** (99% yield). ¹H-NMR (CDCl₃) δ (ppm): 1.60-2.15 (bm, 4H), 2.63 (tt, 1H, *J* = 10.6, 4.1 Hz), 3.00-3.16 (m, 2H), 3.64-3.87 (bm, 1H), 4.40-4.64 (bm, 1H), 7.36-7.43 (m, 5H).

(1-Benzoylpiperidin-4-yl)(4-bromophenyl)methanone (53). 43% yield from **52** and bromobenzene. ¹H-NMR (CDCl₃) δ (ppm): 1.70-2.07 (bm, 4H), 2.96-3.23 (bm, 2H), 3.43-3.54 (m, 1H), 3.76-3.98 (bm, 1H), 4.58-4.79 (bm, 1H), 7.41 (s, 5H), 7.63 (AA'XX', 2H, *J*_{AX} = 8.7 Hz, *J*_{AA'/XX'} = 2.1 Hz), 7.81 (AA'XX', 2H, *J*_{AX} = 8.6 Hz, *J*_{AA'/XX'} = 2.1 Hz).

Synthesis of (1-benzoylpiperidin-4-yl)(4-morpholinophenyl)methanone (54). A solution of Pd₂dba₃ (0.02 equiv), XPhos (0.08 equiv), K₃PO₄ (1.4 equiv), morpholine (1.2 equiv) and compound **53** (150 mg, 1 equiv) in toluene (0.8 mL) was stirred at 100 °C under argon in a sealed vial for 20 h. The reaction mixture was allowed to cool to room temperature, then filtered through a small pad of Celite, washed with ethyl acetate and concentrated under vacuum. The obtained crude residue was

1
2
3 purified by flash column chromatography to give intermediate **54** (63% yield). $^1\text{H-NMR}$ (CDCl_3) δ
4 (ppm): 1.70-2.10 (m, 4H), 2.95-3.20 (bm, 2H), 3.26-3.37 (m, 4H), 3.44-3.54 (m, 1H), 3.78-4.95 (m,
5 5H), 4.60-4.80 (bm, 1H), 6.88 (AA'XX', 2H, $J_{\text{AX}} = 9.1$ Hz, $J_{\text{AA'}/\text{XX'}} = 2.3$ Hz), 7.41 (s, 5H), 7.90
6
7 (AA'XX', 2H, $J_{\text{AX}} = 9.1$ Hz, $J_{\text{AA'}/\text{XX'}} = 2.4$ Hz).

8
9
10
11
12 **(4-Morpholinophenyl)(piperidin-4-yl)methanone (55)**. 72% yield from **54**. $^1\text{H-NMR}$ (CDCl_3) δ
13 (ppm): 1.60-1.74 (m, 2H), 1.76-1.86 (m, 2H), 2.76 (td, 2H, $J = 12.2, 2.7$ Hz), 3.18 (dt, 2H, $J = 12.5,$
14 3.2 Hz), 3.26-3.40 (m, 5H), 3.82-3.90 (m, 4H), 6.88 (AA'XX', 2H, $J_{\text{AX}} = 9.1$ Hz, $J_{\text{AA'}/\text{XX'}} = 2.4$ Hz),
15 7.90 (AA'XX', 2H, $J_{\text{AX}} = 9.0$ Hz, $J_{\text{AA'}/\text{XX'}} = 2.4$ Hz).

16
17
18
19
20
21 **(1-(3-Methoxybenzoyl)piperidin-4-yl)(4-morpholinophenyl)methanone (56)**. 99% yield from **55**
22 and **48**. $^1\text{H-NMR}$ (CDCl_3) δ (ppm): 1.70-2.08 (m, 4H), 2.94-3.21 (bm, 2H), 3.28-3.35 (m, 4H), 3.43-
23 3.54 (bm, 1H), 3.83 (s, 3H), 3.84-3.90 (m, 5H), 4.61-4.77 (bm, 1H), 6.85-6.91 (m, 2H), 6.92-6.99 (m,
24 3H), 7.31 (dd, 1H, $J = 9.0, 7.5$ Hz), 7.87-7.93 (m, 2H).

25
26
27
28
29
30
31 **(1-(2-Fluoro-5-methoxybenzoyl)piperidin-4-yl)(4-isopropylphenyl)methanone (57)**. Yellow
32 solid; 93% yield from **47e** and **36b**, eluent *n*-hexane/EtOAc 7:3. $^1\text{H-NMR}$ (CDCl_3) δ (ppm): 1.28 (d,
33 6H, $J = 6.9$ Hz), 1.76-1.88 (bm, 3H), 1.98-2.06 (bm, 1H), 2.97 (sept, 1H, $J = 7.0$ Hz), 3.03-3.13 (m,
34 1H), 3.14-3.30 (bm, 1H), 3.46-3.58 (bm, 1H), 3.65-3.75 (m, 1H), 3.80 (s, 3H), 4.66-4.75 (m, 1H),
35 6.85-6.92 (m, 2H), 6.97-7.04 (m, 1H), 7.33 (d, 2H, $J = 8.2$ Hz), 7.88 (AA'XX', 2H, $J_{\text{AX}} = 8.4$ Hz,
36 $J_{\text{AA'}/\text{XX'}} = 1.9$ Hz). $^{13}\text{C-NMR}$ (CDCl_3) δ (ppm): 23.78 (2C), 28.70, 28.76, 34.39, 41.58, 43.22, 46.66,
37 56.02, 113.06, 116.68 (d, $J = 23.7$ Hz), 117.14, 124.66 (d, $J = 19.9$ Hz), 127.04 (2C), 128.67 (2C),
38 133.65, 152.49 (d, $J = 240.3$ Hz), 155.00, 156.15 (d, $J = 2.0$ Hz), 165.18, 201.33. HPLC analysis:
39 retention time = 13.261 min; peak area, 99% (254 nm). Elemental analysis for $\text{C}_{23}\text{H}_{26}\text{FNO}_3$,
40 calculated: % C, 72.04; % H, 6.83; % N, 3.65; found: % C, 71.68; % H, 7.14; % N, 4.01.

41
42
43
44
45
46
47
48
49
50
51
52
53 **(4-(4-Butylbenzoyl)piperidin-1-yl)(2-fluoro-5-methoxyphenyl)methanone (58)**. 86% yield from
54 **47f** and **36b**. $^1\text{H-NMR}$ (CDCl_3) δ (ppm): 0.93 (t, 3H, $J = 7.3$ Hz), 1.36 (sext, 2H, $J = 7.4$ Hz), 1.62
55 (quint, 2H, $J = 7.6$ Hz), 1.73-1.88 (bm, 3H), 1.97-2.07 (bm, 1H), 2.67 (t, 2H, $J = 7.7$ Hz), 3.03-3.13
56
57
58
59
60

(m, 1H), 3.14-3.30 (bm, 1H), 3.45-3.58 (bm, 1H), 3.66-3.75 (m, 1H), 3.80 (s, 3H), 4.66-4.75 (m, 1H), 6.85-6.93 (m, 2H), 6.96-7.04 (m, 1H), 7.29 (d, 2H, $J = 8.3$ Hz), 7.86 (d, 2H, $J = 8.3$ Hz).

(1-(4-Fluoro-3-methoxybenzoyl)piperidin-4-yl)(4-isopropylphenyl)methanone (59). 89% yield from **47e** and **29f**. $^1\text{H-NMR}$ (CDCl_3) δ (ppm): 1.28 (d, 6H, $J = 6.9$ Hz), 1.74-2.00 (bm, 4H), 2.98 (sept, 1H, $J = 6.9$ Hz), 3.04-3.21 (bm, 2H), 3.49-3.59 (m, 1H), 3.81-3.99 (bm, 1H), 3.91 (s, 3H), 4.50-4.75 (bm, 1H), 6.94 (ddd, 1H, $J = 8.2, 4.4, 2.0$ Hz), 7.05-7.12 (m, 2H), 7.34 (d, 2H, $J = 8.2$ Hz), 7.89 (d, 2H, $J = 8.4$ Hz).

(4-(4-Butylbenzoyl)piperidin-1-yl)(4-fluoro-3-methoxyphenyl)methanone (60). 89% yield from **47f** and **29f**. $^1\text{H-NMR}$ (CDCl_3) δ (ppm): 0.94 (t, 3H, $J = 7.3$ Hz), 1.36 (sext, 2H, $J = 7.4$ Hz), 1.62 (quint, 2H, $J = 7.6$ Hz), 1.74-2.07 (bm, 4H), 2.68 (t, 2H, $J = 7.7$ Hz), 3.02-3.20 (bm, 2H), 3.49-3.59 (m, 1H), 3.80-4.00 (bm, 1H), 3.92 (s, 3H), 4.40-4.80 (bm, 1H), 6.94 (ddd, 1H, $J = 8.2, 4.3, 2.0$ Hz), 7.05-7.13 (m, 2H), 7.29 (d, 2H, $J = 8.4$ Hz), 7.87 (d, 2H, $J = 8.3$ Hz).

2. Docking Calculations. The X-ray structure of MAGL (pdb code 3PE6⁴⁵) was downloaded from the Protein Data Bank.⁴⁶ Hydrogen atoms were added to the ligand-protein complex, which was then minimized using Amber16 software⁴⁷ and ff14SB force field at 300 K. By using TIP3P explicit solvent model, a 10 Å water cap was generated around the complex, which was thus placed at the center of a rectangular parallelepiped box of explicit water molecules. Sodium ions were then added for the neutralization of the system. The system was subjected to two steps of energy minimization. In the first step, the coordinates of the protein were restrained using a harmonic potential of 500 kcal/mol·Å², thus minimizing only the position of the solvent molecules. During the second step, the whole system was minimized through 5000 steps of steepest descent followed by conjugate gradient (CG), until a convergence of 0.05 kcal/Å·mol. Maestro⁴⁸ was employed to build the ligands, while MacroModel⁴⁹ was used for their minimization in water environment performed with the CG method until a convergence value of 0.05 kcal/Å·mol, MMFFs force field and a distance-dependent dielectric constant of 1.0. AUTODOCK 4.0 software⁵⁰ was employed for molecular docking. The identification of the torsion angles in the ligands, the addition of the solvent model and the determination of protein

1
2
3 and ligand atomic charges was carried out using Autodock Tools. Kollmann charges were assigned
4
5 to the protein and Gasteiger charges to the ligand. The docking site used for calculations was defined
6
7 as a box of 82, 40, and 30 points in the x, y, and z directions centered on the center of mass of the
8
9 reference inhibitor ZYH. A grid spacing of 0.375 Å and a distance-dependent function of the
10
11 dielectric constant were used for the energetic map calculations. The compounds were subjected to a
12
13 robust docking procedure by applying 200 runs of Autodock search, using the Lamarckian Genetic
14
15 Algorithm with 10 000 000 steps of energy evaluations.⁵¹ The number of individuals in the initial
16
17 population was set to 500 and a maximum of 10 000 000 generations were simulated during each
18
19 docking run. Cluster analysis was performed on the results using an RMS tolerance of 2.0 Å.
20
21

22
23 Chemicalize was used for prediction of log*P* and p*K*_a properties, Nov, 2018, <https://chemicalize.com/>
24
25 developed by ChemAxon (<http://www.chemaxon.com>).
26
27

28 **3. MD Simulations.** Molecular dynamic simulations were performed using AMBER, version 16⁴⁷
29
30 and were carried out using the ff14SB force field at 300 K. General Amber force field (GAFF)
31
32 parameters were assigned to the ligands, while partial charges were calculated using the AM1-BCC
33
34 method using the Antechamber suite of AMBER 16. By using TIP3P explicit solvent model, a 20 Å
35
36 water cap was generated around the complexes, which were thus placed at the center of a rectangular
37
38 parallelepiped box of explicit water molecules. Sodium ions were then added for the neutralization
39
40 of the systems. Prior to MD simulations, two steps of energy minimization were performed with the
41
42 same procedure described above. The minimized structures of the complexes were used as the starting
43
44 conformations for the MD simulations, which were run using Particle Mesh Ewald (PME)
45
46 electrostatics and periodic boundary conditions. The time step of the simulations was 2.0 fs with a
47
48 cutoff of 10 Å for the nonbonded interaction, while SHAKE was employed to keep all bonds
49
50 involving hydrogen atoms rigid. An initial MD step of 1.0 ns with constant-volume periodic boundary
51
52 conditions was performed: in this step, the temperature of the system was raised from 0 to 300 K.
53
54 Subsequently, a second step of constant pressure periodic boundary MD was run for 100 ns, keeping
55
56 the temperature of the system at the constant value of 300 K with Langevin thermostat. A harmonic
57
58
59
60

1
2
3 potential of 10 kcal/mol•Å² was applied on all α carbons of the protein during both MD steps. The
4
5 final structure of **23**-MAGL complex corresponded to the average of the last 80.0 ns of MD
6
7 minimized by the CG method until a convergence of 0.05 kcal/mol•Å². The average structure was
8
9 obtained using the Cpptraj program⁵² implemented in AMBER 16.

11
12 **4. Binding Energy Evaluation.** The ligand-protein binding affinity of the four ligand-protein
13
14 complexes and the pairwise per-residue free energy decomposition of **23**-MAGL complex were
15
16 calculated with AMBER 16 using the MM-GBSA method. The trajectories corresponding to the last
17
18 80 ns of MD simulation were used for the evaluation, which was performed on a total of 400 MD
19
20 frames (one every 200 ps). MOLSURF program and the MM-PBSA module of AMBER 16 were
21
22 used to calculate nonpolar and polar energies, respectively, while SANDER module estimated van
23
24 der Waals, electrostatic and internal contributions. The ligand's entropy was not taken into account
25
26 in the calculation.
27
28

30
31 **5. MAGL inhibition assay.** Human recombinant MAGL, **2** and 4-nitrophenylacetate (4-NPA)
32
33 substrate were purchased from Cayman Chemical. The IC₅₀ values were generated in 96-well
34
35 microtiter plates. The MAGL reaction was carried out at room temperature, at a final volume of 200
36
37 μL in 10 mM Tris buffer, pH 7.2, containing 1 mM EDTA and BSA 0.1 mg/mL. A total of 150 μL
38
39 of 4-NPA 133.3 μM was added to 10 μL of DMSO containing the suitable amount of compound. The
40
41 reaction was initiated by the addition of 40 μL of MAGL (11 ng/well) in such a way that the assay
42
43 was linear over 30 min. After the reaction had proceeded for 30 min, absorbance values were then
44
45 measured by using a Victor X3 Microplates Reader (PerkinElmer®) at 405 nm.⁵³ Two reactions were
46
47 also run: one reaction containing no compounds and the second one containing neither compound nor
48
49 MAGL. IC₅₀ values were derived from experimental data using the Sigmoidal dose–response fitting
50
51 of GraphPad Prism software. Final values were obtained from duplicates of three independent
52
53 experiments. To remove possible false positive results, for each compound concentration a blank
54
55 analysis was carried out, and the final absorbance results were obtained deducting the absorbance
56
57 produced by the presence of all the components except MAGL in the same conditions. In the enzyme
58
59
60

1
2
3 kinetics experiments, compound **23** was tested in the presence of scalar concentrations of 4-NPA. It
4 was added in scalar amounts (concentration range = 1–0.125 μM) to a reaction mixture containing
5 scalar concentrations of 4-NPA (15–1400 μM). Finally, MAGL solution was added (11 ng/well). The
6
7
8
9
10
11
12
13
14
15
16
17
18
19
20
21
22
23
24
25
26
27
28
29
30
31
32
33
34
35
36
37
38
39
40
41
42
43
44
45
46
47
48
49
50
51
52
53
54
55
56
57
58
59
60
MAGL activity was measured by recording the increase in 4-nitrophenol absorbance using the Victor
X3 Microplates Reader (PerkinElmer®). The experimental data were analyzed by non-linear
regression analysis with GraphPad Prism software, using a second order polynomial regression
analysis, and by applying the mixed-model inhibition fit.

6. MAGL preincubation assay. The MAGL reaction was conducted in the same conditions reported
above. A total of 150 μL of MAGL (11 ng/well) was added to 10 μL of DMSO containing the
appropriate amount of compound. After 0 min, 30 min, and 60 min of incubation time the reaction
was initiated by the addition of 40 μL of 4-NPA 500 μM . The enzyme activity was then measured
according to the procedure described above. Final values were obtained from triplicates of two
independent experiments.

7. MAGL dilution assay. The enzyme (880 ng in 75 μL of Tris buffer, pH 7.2) was incubated during
60 min at room temperature with 5 μL of compound **23** (concentration of 4 μM in the mixture)
dissolved in DMSO. The MAGL-inhibitor mixture was then diluted 40-fold with the buffer. After 15
min of incubation, the reaction was initiated on a 160 μL aliquot by the addition of 40 μL of 4-NPA
500 μM and the enzyme activity was measured according to the procedure described above. Final
values were obtained from triplicates of two independent experiments.

8. Enzyme Activity Assays. Enzyme activity assays were performed as previously described using
cell homogenates of U937 cells (FAAH) and HEK-293 cells stably transfected with ABHD6 and
ABHD12 (ABHD6 and ABHD12), and intact U937 cells (MAGL).⁶ Briefly, FAAH activity was
determined using U937 cell homogenates (1.0×10^6 cells per sample) which were diluted in 200 μL
of Tris-HCl 10 mM, EDTA 1 mM, pH 8 containing 0.1% fatty acid-free BSA and pre-incubated with
the compounds at different concentrations for 15 min at 37 °C. Then, 100 nM of AEA containing 1
nM of [ethanolamine-1-³H]AEA were added to the homogenates and incubated for 15 min at 37 °C.

1
2
3 The reaction was stopped by the addition of 400 μL of ice-cold $\text{CHCl}_3\text{:MeOH}$ (1:1) and samples were
4
5 vortexed and rapidly centrifuged at $16000\times g$ for 10 min at $4\text{ }^\circ\text{C}$. The upper aqueous phase was
6
7 collected in scintillation tubes and mixed with 3 mL of Ultima Gold scintillation liquid (PerkinElmer
8
9 Life Sciences). The radioactivity was measured for tritium content by liquid scintillation
10
11 spectroscopy. *hABHD6* and *hABHD12* activity assays were performed using cell homogenates from
12
13 *hABHD6* and *hABHD12* stably transfected HEK293 cells. Compounds at the screening concentration
14
15 of $10\text{ }\mu\text{M}$ were pre-incubated with $40\text{ }\mu\text{g}$ of cell homogenate for 30 min at $37\text{ }^\circ\text{C}$ in assay buffer (Tris
16
17 1 mM , EDTA 10 mM plus fatty acid-free 0.1% BSA, pH 7.6). WWL70 $10\text{ }\mu\text{M}$ or THL $20\text{ }\mu\text{M}$ were
18
19 used as positive controls, while DMSO as vehicle control. Then, $10\text{ }\mu\text{M}$ of 2-OG was added and
20
21 incubated for 5 min at $37\text{ }^\circ\text{C}$. The reaction was stopped by the addition of $400\text{ }\mu\text{L}$ of ice-cold
22
23 $\text{CHCl}_3\text{:MeOH}$ (1:1) and samples were vortexed and centrifuged ($16000\times g$, 10 min, $4\text{ }^\circ\text{C}$). Aliquots
24
25 ($200\text{ }\mu\text{L}$) of the aqueous phase were assayed for tritium content by liquid scintillation spectroscopy.
26
27 Blank values were recovered from tubes containing no enzyme, whereas basal 2-OG hydrolysis
28
29 occurring in non-transfected HEK293 cells was subtracted. For MAGL activity assay 1.0×10^6 of
30
31 intact U937 cells were suspended in $400\text{ }\mu\text{L}$ of assay buffer (Tris-HCl 10 mM , EDTA 1 mM plus
32
33 fatty acid-free 0.1% BSA, pH 8) in plastic tubes and incubated with different concentrations of the
34
35 screening compounds at $37\text{ }^\circ\text{C}$ (co-incubation). Then, $10\text{ }\mu\text{M}$ of nonradioactive (2-OG) and a small
36
37 tracer (0.5 nM) of $[1,2,3\text{-}^3\text{H}]2\text{-OG}$ was added and cells were incubated for 5 min at $37\text{ }^\circ\text{C}$ with
38
39 shaking. The reaction was stopped by the addition of $800\text{ }\mu\text{L}$ of a methanol chloroform ice-cold
40
41 mixture 1:1 (v/v) and, after vigorous vortexing, aqueous and organic phases were separated by
42
43 centrifugation at $10000\times g$, for 10 min, at $4\text{ }^\circ\text{C}$. Aliquots ($400\text{ }\mu\text{L}$) of both the aqueous and organic
44
45 phases were transferred in scintillation tubes and mixed with 3 mL of Ultima Gold scintillation liquid.
46
47 The radioactivity associated with the $[^3\text{H}]$ glycerol formation for the aqueous phase and $[^3\text{H}]2\text{-OG}$ for
48
49 the organic phase was measured for tritium content by liquid scintillation spectroscopy. Compounds
50
51 were tested in two independent experiments, each performed in triplicates.
52
53
54
55
56
57
58
59
60

1
2
3 **9. MAGL activity assay in mouse brain membrane preparations.** The assay was performed
4
5 similarly to the MAGL assay in U937 cells (see paragraph above). Briefly, 100 µg of mouse brain
6
7 membranes were used per each sample and diluted in 245 µL of assay buffer (Tris-HCl 10 mM,
8
9 EDTA 1 mM plus fatty acid-free 0.1% BSA, pH 8). In each tube, the FAAH inhibitor **URB597** (1
10
11 µM) was added in order to avoid possible 2-OG hydrolysis by FAAH. The samples were incubated
12
13 with DMSO (15 min), **JZL184** 1 µM (30 min) or compound **23** (15 min) at different concentrations
14
15 (0.01-30 µM) at 37 °C under shaking (400 rpm). Afterwards, the 2-OG mix (final concentration of 2-
16
17 OG 10 µM with 1 nM tracer of [1,2,3-³H]2-OG) was added to each sample and the reaction was
18
19 stopped after 2 min of incubation at 37 °C by adding 500 µL of ice-cold chloroform-methanol solution
20
21 (1:1, v/v) and placing the tubes on ice. As blank, the 2-OG mixture was added in the assay buffer
22
23 without mouse brain membranes and the chloroform-methanol solution was added. The tubes were
24
25 centrifuged for 10 min at 10'000 rpm at 4 °C. For all samples, an aliquot (400 µL) of the aqueous
26
27 phase was transferred in a scintillation tube and mixed with 3 mL of Ultima Gold scintillation liquid
28
29 and shaken for 5 min. The radioactivity associated with the [³H]glycerol formation for the aqueous
30
31 phase was measured for tritium content by liquid scintillation spectroscopy.

32
33 **10. CB1 and CB2 binding assay.** Binding assay to cannabinoid receptor 1 and 2 (CB1 and CB2)
34
35 were performed as previously described.⁶ Briefly, clean membranes expressing *hCB1* or *hCB2* were
36
37 re-suspended in binding buffer (50 mM Tris-HCl, 2.5 mM EDTA, 5 mM MgCl₂, 0.5% fatty acid-free
38
39 bovine serum albumin (BSA), pH 7.4) and incubated with vehicle or compounds and 0.5 nM of
40
41 [³H]CP55,940 for 90 min at 30 °C. Non-specific binding was determined in the presence of 10 µM
42
43 of WIN55,512. After incubation, membranes were filtered through a pre-soaked 96-well microplate
44
45 bonded with GF/B filters under vacuum and washed twelve times with 150 µL of ice-cold binding
46
47 buffer. The radioactivity was measured and the results expressed as [³H]CP55,940 binding.
48
49 Compounds were tested, at a screening concentration of 10 µM, in two independent experiments,
50
51 each performed in triplicates.
52
53
54
55
56
57
58
59
60

1
2
3 **11. Competitive Activity-Based Protein Profiling (ABPP).** Activity-based protein profiling
4 (ABPP) experiments were performed using mouse brain membrane preparations at a final
5 concentration of 2 mg/mL in PBS. Sample preparations was performed as previously described.⁶
6
7 Samples (19.5 μ L) were preincubated with either DMSO (vehicle control), URB597 (4 μ M), JZL184
8 (1 μ M), WWL70 (10 μ M) or compound **23** (different concentrations) for 25 minutes at 25 °C under
9 shaking and then added with TAMRA-FP probe (125 nM final concentration) and incubated for 5
10 minutes at 25 °C under shaking. URB597, JZL184, and WWL70 were used as positive controls for
11 FAAH, MAGL, and ABHD6 inhibition, respectively. The reaction was stopped by adding of 10 μ L
12 of 3x Laemmli buffer and the samples kept for 3 min at room temperature, boiled for 10 min at 90
13 °C, cooled down to room temperature and centrifuged at 10'000 g for 1 min. The samples were loaded
14 on a 11% SDS-PAGE gel and resolved by electrophoresis at 120 V for 180 min. The gel was scanned
15 with a Typhoon FLA 9500 using TAMRA settings at excitation wavelength of 542 nm and emission
16 light wavelength 568 nm. After coomassie staining and destaining, the gels were scanned in Cy5
17 settings. The gels were analyzed using the software ImageJ and the quantification of band intensity
18 was performed by normalizing the values obtained for FAAH (band 1), MAGL (bands 3 and 4) and
19 ABHD6 (band 5) with the reference band (2). The intensities were compared to DMSO sample, which
20 reflects 100% of enzyme activity respectively and thus no inhibition of the enzymes. Data are an
21 average of three independent gels.
22
23
24
25
26
27
28
29
30
31
32
33
34
35
36
37
38
39
40
41
42
43

44 **12. Cell viability assay.** Human breast MDA-MB-231, colorectal HCT116 and ovarian CAOV3,
45 OVCAR3 and SKOV3 cancer cells (from ATCC) were maintained at 37 °C in a humidified
46 atmosphere containing 5% CO₂ according to the supplier. Cells (5×10^2) were plated in 96-well
47 culture plates. The day after seeding, vehicle or compounds were added at different concentrations to
48 the medium. Compounds were added to the cell culture at a concentration ranging from 200 to 0.02
49 μ M. Cell viability was measured after 96 h according to the supplier (CellTiter-Glo® luminescence
50 assay, Promega G7571) with a Tecan M1000 PRO instrument. IC₅₀ values were calculated from
51
52
53
54
55
56
57
58
59
60

1
2
3 logistical dose response curves. Averages were obtained from two independent experiments, each
4 performed in triplicates, and error bars are standard deviations.
5
6

7 **13. LC-MS/MS quantification of AEA, 2-AG, arachidonic acid and prostaglandins *in vivo* after**

8 **the administration of compound 23.** Male, 8-10 weeks old C57BL6 mice were provided by Janvier
9 Labs (St Berthevin, France) and housed in groups of five per cage in a selected pathogen-free unit
10 under controlled 12-h light/12-h dark cycle, ambient temperature 21 °C ± 1 °C humidity 40% to 50%
11 with free access to standard rodent chow and water in accordance with the Swiss Federal guidelines.
12 The mice were acclimatized to the animal house for 1 week before the experiment and trained to i.p.
13 injections for 4 days (with sterile saline solution). For the experiments, mice were injected
14 intraperitoneal (i.p.) with compound **23** at the dose of 50 mg/kg or vehicle (DMSO). The animals
15 were sacrificed 1 h post-injection for the vehicle group and 1 h or 2 h post-injection for compound
16 **23**. Brain and plasma were collected immediately after death, rinsed in ice-cold PBS and snap-frozen
17 using dry ice. Samples extraction was performed as previously described.⁶ Briefly, brain or plasma
18 were weighed and transferred to extraction tubes containing three steel beads and 0.1 M formic acid
19 for mechanic homogenization. Afterwards, the homogenates were rapidly transferred into glass tubes
20 containing 1.5 mL of ethyl acetate:hexane (9:1) 0.1% formic acid solution and spiked with internal
21 standards. The samples were vortexed strongly for 30 s, sonicated in cold ultrasound bath for 10 min.
22 In order to separate the phases, samples were centrifuged at 3000 rpm for 10 min at 4 °C and kept for
23 1 h at -20 °C to freeze the aqueous phase. The upper organic phase was transferred in plastic tubes,
24 evaporated and the extracted samples reconstituted in 100 µL of ACN:H₂O (8:2). 10 µL of the
25 solution were injected in the LC-MS/MS system (5500 QTrap, AbSciex with Exion UHPLC).
26
27
28
29
30
31
32
33
34
35
36
37
38
39
40
41
42
43
44
45
46
47
48
49

50
51 **14. LC-MS/MS conditions.** A hybrid triple quadrupole 5500 QTRAP mass spectrometer (AB Sciex)
52 was used with a Exion UHPLC. The column for the UHPLC was a Reprisil-PUR C18 column (3 µm
53 particle size; 2 × 50 mm, Dr. A. Maisch HPLC GmbH, Ammerbuch-Entringen, Germany) kept at 40
54 °C with a mobile phase flow rate of 0.3 mL/min using a gradient with increasing organic solvent. As
55 mobile phase a composition mixture for the negative and positive mode has been used as followed:
56
57
58
59
60

1
2
3 Negative Mode: Water, 2 mM ammonium acetate and 0.1% formic acid and acetonitrile 0.1% formic
4 acid. Positive Mode: Water, 2 mM ammonium acetate and methanol, 2 mM ammonium acetate.
5
6

7
8 As previously published,⁶ the following MRM transitions were monitored and used for quantification
9
10 of the analytes: PGE2, m/z 351→271, PGD2 351→189.1 (internal standard PGE2-d4 355→319),
11
12 arachidonic acid (AA) 303→59 (internal standard AA-d8 311→59), 2-AG, m/z 379→203 (internal
13
14 standard 2-AG-d5 384→287), AEA 348→62 (internal standard AEA-d4 352→66). Calibration was
15
16 prepared by using eleven points calibrations in the appropriate matrix. To ensure constant background
17
18 concentrations of the endogenous analytes, bulk tissues were homogenized and used for validation
19
20 experiments (the background was subtracted to spiked concentration levels). For the calibration
21
22 curve, the concentration range as well as the quantity of internal standards were specifically designed
23
24 to quantify the analytes in the biological matrix of interest. For data analysis, the ratio (Peak area
25
26 under the curve analyte/peak area under the curve of internal standard) was calculated and used to
27
28 ensure linearity of the method. The slope, intercept and regression coefficient of each calibration line
29
30 was determined. Analyte amounts were normalized to the tissue weight respectively to the microliter
31
32 of plasma extracted.
33
34
35
36
37
38
39

40 SUPPORTING INFORMATION

41
42 MM-GBSA results for the four ligand-MAGL complexes; calculated log P values for the reported
43
44 compounds; MD simulation and H-bond analysis of **23**; docking results of compounds **13d** into
45
46 MAGL; cytochrome P450 prediction for compound **23**; quantification of arachidonic acid and
47
48 prostaglandin levels in plasma and brain of C57BL6 mice treated with compound **23**; concentration-
49
50 dependent inhibition of 2-OG hydrolysis of compound **23** in mouse brain membrane preparations;
51
52 RP-HPLC traces of final compounds; ¹H and ¹³C-NMR spectra of compounds **11d**, **13b-d**, **15-19**, **23-**
53
54 **26**; Molecular Formula Strings.
55
56
57
58
59
60

ACKNOWLEDGMENTS

We are grateful to the University of Pisa (Progetti di Ricerca di Ateneo, prog. n. PRA-2017-51 and PRA-2018-18) for funding.

ABBREVIATIONS USED

ECS, endocannabinoid system; eCBs, endocannabinoids; MAGL, monoacylglycerol lipase; AEA, anandamide; 2-AG, 2-arachidonoylglycerol; FAAH, fatty acid amide hydrolase; ABHD6, α/β hydrolase-6; ABHD12, α/β hydrolase-12; MD, molecular dynamics; 2-OG, 2-oleoyl glycerol; 4-NPA, 4-nitrophenylacetate; 4-NP, 4-nitrophenol; GAFF, General Amber force field.

AUTHOR INFORMATION

Corresponding Author

*E-mail: tiziano.tuccinardi@unipi.it. Phone: +39-050-2219595.

REFERENCES.

- (1) Matsuda, L. A.; Lolait, S. J.; Brownstein, M. J.; Young, A. C.; Bonner, T. I. Structure of a Cannabinoid Receptor and Functional Expression of the Cloned CDNA. *Nature* **1990**, *346* (6284), 561–564.
- (2) Munro, S.; Thomas, K. L.; Abu-Shaar, M. Molecular Characterization of a Peripheral Receptor for Cannabinoids. *Nature* **1993**, *365* (6441), 61–65.
- (3) Macedonio, G.; Stefanucci, A.; Maccallini, C.; Mirzaie, S.; Novellino, E.; Mollica, A. Hemopressin Peptides as Modulators of the Endocannabinoid System and Their Potential Applications as Therapeutic Tools. *Protein Pept. Lett.* **2016**, *23* (12), 1045–1051.
- (4) Maccarrone, M.; Guzmán, M.; Mackie, K.; Doherty, P.; Harkany, T. Programming of Neural Cells by (Endo)Cannabinoids: From Physiological Rules to Emerging Therapies. *Nat. Rev. Neurosci.* **2014**, *15* (12), 786–801.
- (5) Chicca, A.; Marazzi, J.; Nicolussi, S.; Gertsch, J. Evidence for Bidirectional Endocannabinoid

- 1
2
3 Transport across Cell Membranes. *J. Biol. Chem.* **2012**, *287* (41), 34660–34682.
- 4
5
6 (6) Chicca, A.; Nicolussi, S.; Bartholomäus, R.; Blunder, M.; Aparisi Rey, A.; Petrucci, V.;
7 Reynoso-Moreno, I. del C.; Viveros-Paredes, J. M.; Dalghi Gens, M.; Lutz, B.; Schiöth, H. B.;
8 Soeberdt, M.; Abels, C.; Charles, R.-P.; Altmann, K.-H.; Gertsch, J. Chemical Probes to
9 Potently and Selectively Inhibit Endocannabinoid Cellular Reuptake. *Proc. Natl. Acad. Sci.*
10 **2017**, *114* (25), E5006–E5015.
- 11
12
13
14
15
16 (7) Ahn, K.; McKinney, M. K.; Cravatt, B. F. Enzymatic Pathways That Regulate
17 Endocannabinoid Signaling in the Nervous System. *Chem. Rev.* **2008**, *108* (5), 1687–1707.
- 18
19
20
21 (8) Bisogno, T.; Petrocellis, L.; Marzo, V. Fatty Acid Amide Hydrolase, an Enzyme with Many
22 Bioactive Substrates. Possible Therapeutic Implications. *Curr. Pharm. Des.* **2002**, *8* (7), 533–
23 547.
- 24
25
26
27
28 (9) Lichtman, A. H. Reversible Inhibitors of Fatty Acid Amide Hydrolase That Promote
29 Analgesia: Evidence for an Unprecedented Combination of Potency and Selectivity. *J.*
30 *Pharmacol. Exp. Ther.* **2004**, *311* (2), 441–448.
- 31
32
33
34
35 (10) Mulvihill, M. M.; Nomura, D. K. Therapeutic Potential of Monoacylglycerol Lipase Inhibitors.
36 *Life Sci.* **2013**, *92* (8–9), 492–497.
- 37
38
39
40 (11) Tuo, W.; Leleu-Chavain, N.; Spencer, J.; Sansook, S.; Millet, R.; Chavatte, P. Therapeutic
41 Potential of Fatty Acid Amide Hydrolase, Monoacylglycerol Lipase, and N-Acylethanolamine
42 Acid Amidase Inhibitors. *J. Med. Chem.* **2017**, *60* (1), 4–46.
- 43
44
45
46 (12) Bedse, G.; Bluett, R. J.; Patrick, T. A.; Romness, N. K.; Gaulden, A. D.; Kingsley, P. J.; Plath,
47 N.; Marnett, L. J.; Patel, S. Therapeutic Endocannabinoid Augmentation for Mood and Anxiety
48 Disorders: Comparative Profiling of FAAH, MAGL and Dual Inhibitors. *Transl. Psychiatry*
49 **2018**, *8* (1), 92.
- 50
51
52
53
54
55 (13) Pasquarelli, N.; Engelskirchen, M.; Hanselmann, J.; Endres, S.; Porazik, C.; Bayer, H.; Buck,
56 E.; Karsak, M.; Weydt, P.; Ferger, B.; Witting, A. Evaluation of Monoacylglycerol Lipase as
57 a Therapeutic Target in a Transgenic Mouse Model of ALS. *Neuropharmacology* **2017**, *124*,

1
2
3
4
5
6
7
8
9
10
11
12
13
14
15
16
17
18
19
20
21
22
23
24
25
26
27
28
29
30
31
32
33
34
35
36
37
38
39
40
41
42
43
44
45
46
47
48
49
50
51
52
53
54
55
56
57
58
59
60

157–169.

- (14) Pasquarelli, N.; Porazik, C.; Bayer, H.; Buck, E.; Schildknecht, S.; Weydt, P.; Witting, A.; Ferger, B. Contrasting Effects of Selective MAGL and FAAH Inhibition on Dopamine Depletion and GDNF Expression in a Chronic MPTP Mouse Model of Parkinson's Disease. *Neurochem. Int.* **2017**, *110*, 14–24.
- (15) Dvoracsko, S.; Stefanucci, A.; Novellino, E.; Mollica, A. The Design of Multitarget Ligands for Chronic and Neuropathic Pain. *Future Med. Chem.* **2015**, *7* (18), 2469–2483.
- (16) Monti, L.; Stefanucci, A.; Pieretti, S.; Marzoli, F.; Fidanza, L.; Mollica, A.; Mirzaie, S.; Carradori, S.; De Petrocellis, L.; Schiano Moriello, A.; Benyhe, S.; Zádor, F.; Szűcs, E.; Ötvös, F.; Erdei, A. I.; Samavati, R.; Dvorácskó, S.; Tömböly, C.; Novellino, E. Evaluation of the Analgesic Effect of 4-Anilidopiperidine Scaffold Containing Ureas and Carbamates. *J. Enzyme Inhib. Med. Chem.* **2016**, *31* (6), 1638–1647.
- (17) Stefanucci, A.; Macedonio, G.; Dvorácskó, S.; Tömböly, C.; Mollica, A. Novel Fubinaca/Rimonabant Hybrids as Endocannabinoid System Modulators. *Amino Acids* **2018**, *50* (11), 1595–1605.
- (18) Mollica, A.; Pelliccia, S.; Famigliani, V.; Stefanucci, A.; Macedonio, G.; Chiavaroli, A.; Orlando, G.; Brunetti, L.; Ferrante, C.; Pieretti, S.; Novellino, E.; Benyhe, S.; Zador, F.; Erdei, A.; Szucs, E.; Samavati, R.; Dvorácskó, S.; Tomboly, C.; Ragno, R.; Patsilnakos, A.; Silvestri, R. Exploring the First Rimonabant Analog-Opioid Peptide Hybrid Compound, as Bivalent Ligand for CB1 and Opioid Receptors. *J. Enzyme Inhib. Med. Chem.* **2017**, *32* (1), 444–451.
- (19) Scalvini, L.; Piomelli, D.; Mor, M. Monoglyceride Lipase: Structure and Inhibitors. *Chem. Phys. Lipids* **2016**, *197*, 13–24.
- (20) Granchi, C.; Caligiuri, I.; Minutolo, F.; Rizzolio, F.; Tuccinardi, T. A Patent Review of Monoacylglycerol Lipase (MAGL) Inhibitors (2013-2017). *Expert Opin. Ther. Pat.* **2017**, *27* (12), 1341–1351.
- (21) Butler, C. R.; Beck, E. M.; Harris, A.; Huang, Z.; McAllister, L. A.; am Ende, C. W.; Fennell,

- 1
2
3 K.; Foley, T. L.; Fonseca, K.; Hawrylik, S. J.; Johnson, D. S.; Knafels, J. D.; Mente, S.; Noell,
4 G. S.; Pandit, J.; Phillips, T. B.; Piro, J. R.; Rogers, B. N.; Samad, T. A.; Wang, J.; Wan, S.;
5 Brodney, M. A. Azetidine and Piperidine Carbamates as Efficient, Covalent Inhibitors of
6 Monoacylglycerol Lipase. *J. Med. Chem.* **2017**, *60* (23), 9860–9873.
7
8
9
10
11
12 (22) McAllister, L. A.; Butler, C. R.; Mente, S.; O’Neil, S. V.; Fonseca, K. R.; Piro, J. R.;
13 Cianfrogna, J. A.; Foley, T. L.; Gilbert, A. M.; Harris, A. R.; Helal, C. J.; Johnson, D. S.;
14 Montgomery, J. I.; Nason, D. M.; Noell, S.; Pandit, J.; Rogers, B. N.; Samad, T. A.; Shaffer,
15 C. L.; da Silva, R. G.; Uccello, D. P.; Webb, D.; Brodney, M. A. Discovery of Trifluoromethyl
16 Glycol Carbamates as Potent and Selective Covalent Monoacylglycerol Lipase (MAGL)
17 Inhibitors for Treatment of Neuroinflammation. *J. Med. Chem.* **2018**, *61* (7), 3008–3026.
18
19
20
21
22
23
24
25
26 (23) Schlosburg, J. E.; Blankman, J. L.; Long, J. Z.; Nomura, D. K.; Pan, B.; Kinsey, S. G.; Nguyen,
27 P. T.; Ramesh, D.; Booker, L.; Burston, J. J.; Thomas, E. A.; Selley, D. E.; Sim-Selley, L. J.;
28 Liu, Q. S.; Lichtman, A. H.; Cravatt, B. F. Chronic Monoacylglycerol Lipase Blockade Causes
29 Functional Antagonism of the Endocannabinoid System. *Nat. Neurosci.* **2010**, *13* (9), 1113–
30 1119.
31
32
33
34
35
36
37
38 (24) Long, J. Z.; Li, W.; Booker, L.; Burston, J. J.; Kinsey, S. G.; Schlosburg, J. E.; Pavón, F. J.;
39 Serrano, A. M.; Selley, D. E.; Parsons, L. H.; Lichtman, A. H.; Cravatt, B. F. Selective
40 Blockade of 2-Arachidonoylglycerol Hydrolysis Produces Cannabinoid Behavioral Effects.
41 *Nat. Chem. Biol.* **2009**, *5* (1), 37–44.
42
43
44
45
46
47 (25) Muccioli, G. G.; Labar, G.; Lambert, D. M. CAY10499, a Novel Monoglyceride Lipase
48 Inhibitor Evidenced by an Expeditious MGL Assay. *Chembiochem* **2008**, *9* (16), 2704–2710.
49
50
51
52 (26) King, A. R.; Dotsey, E. Y.; Lodola, A.; Jung, K. M.; Ghomian, A.; Qiu, Y.; Fu, J.; Mor, M.;
53 Piomelli, D. Discovery of Potent and Reversible Monoacylglycerol Lipase Inhibitors. *Chem.*
54 *Biol.* **2009**, *16* (10), 1045–1052.
55
56
57
58 (27) Wang, L.; Wang, G.; Yang, D.; Guo, X.; Xu, Y.; Feng, B.; Kang, J. Euphol Arrests Breast
59 Cancer Cells at the G1 Phase through the Modulation of Cyclin D1, P21 and P27 Expression.
60

1
2
3
4
5
6
7
8
9
10
11
12
13
14
15
16
17
18
19
20
21
22
23
24
25
26
27
28
29
30
31
32
33
34
35
36
37
38
39
40
41
42
43
44
45
46
47
48
49
50
51
52
53
54
55
56
57
58
59
60

Mol. Med. Rep. **2013**, *8* (4), 1279–1285.

- (28) Yousef, B.; Hassan, H.; Zhang, L.-Y.; Jiang, Z.-Z. Anticancer Potential and Molecular Targets of Pristimerin: A Mini- Review. *Curr. Cancer Drug Targets* **2017**, *17* (2), 100–108.
- (29) Chicca, A.; Marazzi, J.; Gertsch, J. The Antinociceptive Triterpene β -Amyrin Inhibits 2-Arachidonoylglycerol (2-AG) Hydrolysis without Directly Targeting Cannabinoid Receptors. *Br. J. Pharmacol.* **2012**, *167* (8), 1596–1608.
- (30) Hernández-Torres, G.; Cipriano, M.; Hedén, E.; Björklund, E.; Canales, A.; Zian, D.; Feliú, A.; Mecha, M.; Guaza, C.; Fowler, C. J.; Ortega-Gutiérrez, S.; López-Rodríguez, M. L. A Reversible and Selective Inhibitor of Monoacylglycerol Lipase Ameliorates Multiple Sclerosis. *Angew. Chemie - Int. Ed.* **2014**, *53* (50), 13765–13770.
- (31) Patel, J. Z.; Ahenkorah, S.; Vaara, M.; Staszewski, M.; Adams, Y.; Laitinen, T.; Navia-Paldanius, D.; Parkkari, T.; Savinainen, J. R.; Walczyński, K.; Laitinen, J. T.; Nevalainen, T. J. Loratadine Analogues as MAGL Inhibitors. *Bioorg. Med. Chem. Lett.* **2015**, *25* (7), 1436–1442.
- (32) Aghazadeh Tabrizi, M.; Baraldi, P. G.; Baraldi, S.; Ruggiero, E.; De Stefano, L.; Rizzolio, F.; Di Cesare Mannelli, L.; Ghelardini, C.; Chicca, A.; Lapillo, M.; Gertsch, J.; Manera, C.; Macchia, M.; Martinelli, A.; Granchi, C.; Minutolo, F.; Tuccinardi, T. Discovery of 1,5-Diphenylpyrazole-3-Carboxamide Derivatives as Potent, Reversible, and Selective Monoacylglycerol Lipase (MAGL) Inhibitors. *J. Med. Chem.* **2018**, *61* (3), 1340–1354.
- (33) Granchi, C.; Rizzolio, F.; Palazzolo, S.; Carmignani, S.; Macchia, M.; Saccomanni, G.; Manera, C.; Martinelli, A.; Minutolo, F.; Tuccinardi, T. Structural Optimization of 4-Chlorobenzoylpiperidine Derivatives for the Development of Potent, Reversible, and Selective Monoacylglycerol Lipase (MAGL) Inhibitors. *J. Med. Chem.* **2016**, *59* (22), 10299–10314.
- (34) Tuccinardi, T.; Granchi, C.; Rizzolio, F.; Caligiuri, I.; Battistello, V.; Toffoli, G.; Minutolo, F.; Macchia, M.; Martinelli, A. Identification and Characterization of a New Reversible MAGL Inhibitor. *Bioorganic Med. Chem.* **2014**, *22* (13), 3285–3291.

- 1
2
3 (35) Chang, J. W.; Niphakis, M. J.; Lum, K. M.; Cognetta, A. B.; Wang, C.; Matthews, M. L.;
4
5 Niessen, S.; Buczynski, M. W.; Parsons, L. H.; Cravatt, B. F. Highly Selective Inhibitors of
6
7 Monoacylglycerol Lipase Bearing a Reactive Group That Is Bioisosteric with
8
9 Endocannabinoid Substrates. *Chem. Biol.* **2012**, *19* (5), 579–588.
- 10
11
12 (36) King, A. R.; Lodola, A.; Carmi, C.; Fu, J.; Mor, M.; Piomelli, D. A Critical Cysteine Residue
13
14 in Monoacylglycerol Lipase Is Targeted by a New Class of Isothiazolinone-Based Enzyme
15
16 Inhibitors. *Br. J. Pharmacol.* **2009**, *157* (6), 974–983.
- 17
18
19 (37) Pan, P.; Sun, H.; Liu, H.; Li, D.; Zhou, W.; Kong, X.; Li, Y.; Yu, H.; Hou, T. In Silico
20
21 Exploration for Novel Type-I Inhibitors of Tie-2/TEK: The Performance of Different Selection
22
23 Strategy in Selecting Virtual Screening Candidates. *Sci. Rep.* **2016**, *6* (1), 37628.
- 24
25
26 (38) Wang, L.; Chen, L.; Yu, M.; Xu, L. H.; Cheng, B.; Lin, Y. S.; Gu, Q.; He, X. H.; Xu, J.
27
28 Discovering New MTOR Inhibitors for Cancer Treatment through Virtual Screening Methods
29
30 and in Vitro Assays. *Sci. Rep.* **2016**, *6* (1), 18987.
- 31
32
33 (39) Shao, C.-Y.; Su, B.-H.; Tu, Y.-S.; Lin, C.; Lin, O. A.; Tseng, Y. J. CypRules: A Rule-Based
34
35 P450 Inhibition Prediction Server. *Bioinformatics* **2015**, *31* (11), 1869–1871.
- 36
37
38 (40) Zaretski, J.; Matlock, M.; Swamidass, S. J. XenoSite: Accurately Predicting CYP-Mediated
39
40 Sites of Metabolism with Neural Networks. *J. Chem. Inf. Model.* **2013**, *53* (12), 3373–3383.
- 41
42
43 (41) Niphakis, M. J.; Cravatt, B. F. Enzyme Inhibitor Discovery by Activity-Based Protein
44
45 Profiling. *Annu. Rev. Biochem.* **2014**, *83* (1), 341–377.
- 46
47
48 (42) Blankman, J. L.; Cravatt, B. F. Chemical Probes of Endocannabinoid Metabolism. *Pharmacol.*
49
50 *Rev.* **2013**, *65* (2), 849–871.
- 51
52
53 (43) Baggelaar, M. P.; Janssen, F. J.; van Esbroeck, A. C. M.; den Dulk, H.; Allarà, M.;
54
55 Hoogendoorn, S.; McGuire, R.; Florea, B. I.; Meeuwenoord, N.; van den Elst, H.; van der
56
57 Marel, G. A.; Brouwer, J.; Di Marzo, V.; Overkleeft, H. S.; van der Stelt, M. Development of
58
59 an Activity-Based Probe and In Silico Design Reveal Highly Selective Inhibitors for
60
61 Diacylglycerol Lipase- α in Brain. *Angew. Chemie Int. Ed.* **2013**, *52* (46), 12081–12085.

- 1
2
3 (44) Bononi, G.; Granchi, C.; Lapillo, M.; Giannotti, M.; Nieri, D.; Fortunato, S.; Boustani, M. El;
4 Caligiuri, I.; Poli, G.; Carlson, K. E.; Kim, S. H.; Macchia, M.; Martinelli, A.; Rizzolio, F.;
5 Chicca, A.; Katzenellenbogen, J. A.; Minutolo, F.; Tuccinardi, T. Discovery of Long-Chain
6 Salicylketoxime Derivatives as Monoacylglycerol Lipase (MAGL) Inhibitors. *Eur. J. Med.*
7 *Chem.* **2018**, *157*, 817–836.
8
9
10
11
12
13
14 (45) Schalk-Hihi, C.; Schubert, C.; Alexander, R.; Bayoumy, S.; Clemente, J. C.; Deckman, I.;
15 DesJarlais, R. L.; Dzordzorme, K. C.; Flores, C. M.; Grasberger, B.; Kranz, J. K.;
16 Lewandowski, F.; Liu, L.; Ma, H.; Maguire, D.; Macielag, M. J.; McDonnell, M. E.;
17 Haarlander, T. M.; Miller, R.; Milligan, C.; Reynolds, C.; Kuo, L. C. Crystal Structure of a
18 Soluble Form of Human Monoglyceride Lipase in Complex with an Inhibitor at 1.35 Å
19 Resolution. *Protein Sci.* **2011**, *20* (4), 670–683.
20
21
22
23
24
25
26
27
28 (46) Berman, H. M. The Protein Data Bank. *Nucleic Acids Res.* **2000**, *28* (1), 235–242.
29
30
31 (47) D.A. Case, V. Babin, J.T. Berryman, R.M. Betz, Q. Cai, D.S. Cerutti, T.E. Cheatham, III, T.A.
32 Darden, R. E.; Duke, H. Gohlke, A.W. Goetz, S. Gusarov, N. Homeyer, P. Janowski, J. Kaus,
33 I. Kolossváry, A. K.; T.S. Lee, S. LeGrand, T. Luchko, R. Luo, B. Madej, K.M. Merz, F.
34 Paesani, D.R. Roe, A. Roitberg, C. S.; R. Salomon-Ferrer, G. Seabra, C.L. Simmerling, W.
35 Smith, J. Swails, R.C. Walker, J. Wang, R.M. Wolf, X.; Kollman, W. and P. A. AMBER.
36 version 16; University of California: San Francisco, CA, 2016.
37
38
39
40
41
42
43
44 (48) *Maestro*, version 9.0; Schrödinger Inc: Portland, OR, 2009.
45
46
47 (49) *Macromodel*, version 9.7; Schrödinger Inc: Portland, OR, 2009
48
49
50 (50) Morris, G. M.; Ruth, H.; Lindstrom, W.; Sanner, M. F.; Belew, R. K.; Goodsell, D. S.; Olson,
51 A. J. AutoDock4 and AutoDockTools4: Automated Docking with Selective Receptor
52 Flexibility. *J. Comput. Chem.* **2009**, *30* (16), 2785–2791.
53
54
55
56 (51) Poli, G.; Gelain, A.; Porta, F.; Asai, A.; Martinelli, A.; Tuccinardi, T. Identification of a New
57 STAT3 Dimerization Inhibitor through a Pharmacophore-Based Virtual Screening Approach.
58 *J. Enzyme Inhib. Med. Chem.* **2016**, *31* (6), 1011–1017.
59
60

- 1
2
3 (52) Roe, D. R.; Cheatham, T. E. PTRAJ and CPPTRAJ: Software for Processing and Analysis of
4 Molecular Dynamics Trajectory Data. *J. Chem. Theory Comput.* **2013**, *9* (7), 3084–3095.
5
6
7 (53) Granchi, C.; Caligiuri, I.; Bertelli, E.; Poli, G.; Rizzolio, F.; Macchia, M.; Martinelli, A.;
8 Minutolo, F.; Tuccinardi, T. Development of Terphenyl-2-Methyloxazol-5(4H)-One
9 Derivatives as Selective Reversible MAGL Inhibitors. *J. Enzyme Inhib. Med. Chem.* **2017**, *32*
10 (1), 1240–1252.
11
12
13
14
15
16
17
18
19
20
21
22
23
24
25
26
27
28
29
30
31
32
33
34
35
36
37
38
39
40
41
42
43
44
45
46
47
48
49
50
51
52
53
54
55
56
57
58
59
60

TABLE OF CONTENTS GRAPHIC

